DEVELOPMENT OF A GEOMETRIC MODELLING APPROACH FOR HUMAN BODY SEGMENT INERTIAL PARAMETER ESTIMATION

by

JENNIFER DURKIN, BSc., MSc.

A Thesis
Submitted to the School of Graduate Studies
in Partial Fulfillment of the Requirements
for the Degree
Doctor of Philosophy

McMaster University

GEOMETRIC MODELLING APPROACH FOR HUMAN BSP ESTIMATION

DOCTOR OF PHILOSOPHY (2003)
(Kinesiology)

McMaster University
Hamilton, Ontario

TITLE: Development of a Geometric Modelling Approach for Human Body Segment Inertial Parameter Estimation

AUTHOR: Jennifer L. Durkin, BSc. (University of Ottawa), MSc. (McMaster University)

SUPERVISOR: Dr. James J. Dowling, Associate Professor

NUMBER OF PAGES: xviii, 164

ABSTRACT

Calculating net joint forces and moments of force in the study of human movement requires accurate human body segment parameter (BSP) information. The purpose of this study was to investigate an approach for developing geometric models based on segment mass distribution (MD) information for BSP estimation. Study 1 investigated the MD properties of the human thigh for four human populations using dual energy x-ray absorptiometry (DEXA). Thigh mass, centre of mass in the longitudinal (CM_x) and mediolateral (CM_y) directions, and moment of inertia about the CM along an anteroposterior axis (I_{CMz}) were determined using DEXA. Thigh MD properties of 20 subjects were used for model generation and the equations were validated on 80 subjects by comparing estimations with DEXA measurements. BSP estimations from 4 other models available in the literature were also examined. Study 2 followed the methodology of Study 1, using the forearm segment. Study 3 advanced on Studies 1 and 2 by adding a sagittal plane dimension to a lower leg model. Forty subjects underwent frontal and sagittal plane DEXA scans and models were validated using a split-half reliability method. The results of all three studies showed that mass and I_{CM} estimates were not significantly better than the other models examined, however CM estimations were often improved. The models in Studies 1 and 2 may have been limited by the 2D nature of the methodology. The use of an elliptical model helped to account for the more posterior location of the CM in the lower leg, however insufficient statistical power may have prevented the detection of significant differences in mass and I_{CM} estimates. The results of this study show promise for future modelling of human body segments. Modelling

according to MD properties allows the assumption of constant density while accounting for inertial changes along the segment length. 3D model validation, greater sample sizes, and the analysis of the remaining segments of the human body may lead us closer to understanding the kinetics of human movement.

To my parents,

Your encouragement and support have made this challenge all the more rewarding.

ACKNOWLEDGEMENTS

This work could not have been completed without the help of several individuals, all of whom deserve many thanks for their contributions. First and foremost, I would like to thank my advisor Dr. Jim Dowling for his friendship and guidance throughout my time at McMaster. Thank you for teaching me the importance of independence in research and for helping me develop the skills necessary to realize my potential. I would also like to thank Dr. David Andrews and Dr. Michael Pierrynowski for taking time out of their busy schedules to provide invaluable insight and direction on this project. Particular appreciation goes to Dr. David Andrews, not only for his friendship, but also for his support and wisdom throughout my graduate career.

My defense would not have been possible without the participation of Dr. David Pearsall, Dr. Patrick Ryan and Dr. Don Dawson. Don, thanks also for being a guinea pig (repeatedly). Many thanks to the Government of Ontario, The Natural Sciences and Engineering Research Council, and the Department of Kinesiology at McMaster University for funding my doctoral degree.

I would like to thank Dr. Joe Blimkie, Dr. Digby Elliott, Dr. Maureen MacDonald and Nick Cipriano for taking the time to answer many career-related questions over the years. Your guidance was greatly appreciated. Of course, I cannot forget my good friends Tara-Lyn Elston and Dave Ditor who have made my time at Mac an enjoyable one. I sincerely value your friendship and look forward to all our future shared giggles and

gripes. Finally, special thanks goes to Stefan Teague who is my best friend and, when times are tough, a good voice of reason. Your positive attitude and strong sense of self are a fraction of the qualities I admire in you.

TABLE OF CONTENTS

Page

Page

LIST OF TABLES

Table **Page**

Table **Page**

Table **Page**

LIST OF FIGURES

Figure **Page**

Figure **Page**

Figure **Page**

CHAPTER 1

INTRODUCTION

1.1 Backround and Rationale

Determining the kinetics of motion is a necessary step in understanding a human movement. These movement characteristics are typically estimated using either inverse dynamics or forward solutions methods. Calculating the net joint forces and moments of force of a movement through inverse dynamics methods requires the measurement of an external force in addition to joint kinematic profiles. Conversely, forward solutions techniques use estimated moments and forces to produce a simulation coincident with the true kinematics of the movement. Each method, however, requires the input of body segment inertial parameters (BSPs), including segment masses, centre of mass locations and moments of inertia.

The accurate determination of human body segment parameters (BSPs) has been a long standing challenge in biomechanics. Several methods for measuring or estimating these properties have been developed, however limitations in these procedures have led to continued efforts at obtaining reliable measures (Cheng et al., 2000; Pearsall and Reid, 1994). Early studies used cadavers to measure body segment volumes, masses, centre of mass locations, and moments of inertia directly from the segmented limbs of specimens (Braune and Fischer, 1889; Chandler et al., 1975; Clauser et al., 1969; Dempster, 1955; Harless, 1860). Cadaver studies provide a great opportunity to directly measure the BSPs of specimens, yet difficulty in obtaining subjects of varying age and gender, as well as

the cost and intricacy of the methods, preclude the analysis of large numbers of subjects. For example, Harless (1860) and Braune and Fischer (1889) examined only two and three male cadavers, respectively. Dempster used 8 male war veterans in his analysis, Clauser et al. (1969) examined 10, and Chandler et al. (1975) dissected only 6 male specimens. These small sample sizes make the extrapolation of results to larger populations difficult and data from the various studies cannot be pooled due to differences in segmentation patterns. Furthermore, cadaver studies offer additional limitations such as fluid and tissue losses during segmentation, differences between properties of living and deceased tissue, and a narrow population representation. For example, Harless (1860) used decapitated specimens, likely causing large losses of fluid and thus altering mass and centre of mass measurements. Braune and Fischer (1889) froze their specimens to prevent fluid losses, however the resulting changes in volume may have altered segment inertial properties (Reid and Jensen, 1990). Dempster (1955) reported average segment density values in his results, but there has been some question as to how much difference exists between cadaveric tissue properties and those of living tissue. Furthermore, many of these studies were comprised solely of male subjects, most of which were elderly and Caucasian (Pearsall and Reid, 1994).

Researchers in the mid 20th century investigated experimental measurement techniques that would allow the direct determination of BSPs in a non-invasive manner on living human subjects. These techniques included water immersion, reaction change, quick release, relaxed oscillation and compound pendulum methods to determine human BSPs (Drillis and Contini, 1966; McConville et al., 1980; Plagenhoef et al., 1983; Young

et al., 1983). Water immersion methods require the application of constant density values to estimate segment masses and centre of mass locations. These density terms are typically obtained from cadaveric data and there has been some debate as to whether significant differences exist from living tissue properties, particularly for trunk density values (Mungiole and Martin, 1990). Furthermore, quick release methods assume that passive tissue of adjacent segments and muscle activation have a negligible effect on moment of inertia estimates (Pearsall and Reid, 1994). These limitations have forced others to seek alternative methods of directly measuring BSPs using medical imaging technology.

Improvements in the science of medical imaging, as well as increases in equipment availability, have lead to greater use of these techniques for directly measuring BSPs on living human subjects. Fuller et al. (1999) and Elia et al. (2000) compared the performance of bioelectric impedance analysis with anthropometric methods in estimating muscle and adipose tissue mass and muscle volume, respectively. Bioelectric impedance analysis was found to predict these parameters better than anthropometric methods, however considerable individual variability was found with both methods.

Zatsiorsky and Seluyanov (1983) used gamma-mass scanning to measure segment inertial properties on 100 young Caucasian males. The technology is based on the attenuation of an incident gamma-radiation beam as it passes through a sample of tissue. The attenuation of the beam provides information regarding the surface density of the mass in its path. Knowing the location of the mass element and the calculated surface density, mass distribution information can be obtained. Zatsiorsky and Seluyanov (1983)

determined segment masses, centre of mass locations and moments of inertia about three axes for 16 body segments. The results were found to be accurate, however the technology is not widely available today. Furthermore, while segment inertial properties were determined about three principal axes, validation of centre of mass and moment of inertia calculations were possible in one plane only. The other two axes were estimated from surface density calculations using a constant density parallelepiped model for each scanned element.

Computed tomography (CT) has also been used to measure BSPs directly on humans (Erdmann, 1997; Pearsall et al., 1996). Axial scanning of biological tissue produces CT data proportional to tissue density on a pixel-by-pixel basis. These tissue densities can then be applied to the digitized pixel volumes to determine segment mass distribution information. Huang (1983) used CT imaging to measure the BSPs of a porcine specimen and a young female child cadaver, while Erdmann (1997) used CT to determine the mass and centre of mass locations of human trunk sections on 15 male patients. Furthermore, Pearsall et al. (1996) used CT imaging to measure trunk segment mass, centre of mass locations and moments of inertia on two male and two female subjects. BSP measurement using CT imaging is considered very accurate and reliable, however, the method is limited by its tediousness and its cost. Furthermore, both gamma-mass scanning and CT imaging require exposing subjects to radiation, albeit in small doses.

Magnetic resonance imaging (MRI) has recently been explored as a method for measuring BSPs directly from humans. MRI is similar to CT imaging in that three-

dimensional mass distribution information can be obtained from axial scans, but has the advantage of obtaining this information without exposing subjects to radiation. MRI was used by Martin et al. (1989) to measure the inertial properties of baboon cadaver segments by obtaining axial scans of the segments, digitizing images to obtain tissue areas and applying estimated tissue densities to determine slice mass distribution properties. Martin et al. (1989) were able to measure mass, centre of mass location and moment of inertia with errors of 6.7, -2.4 and 4.4%, respectively. Mungiole and Martin (1990) later used MRI to measure the BSPs of 12 adult male athletes. Validation of these measurements were not possible, yet previous research (Martin et al. 1989) indicated that the results were very reliable. Similar to CT scanning, however, technology availability is limited, data acquisition is costly and data processing methods are time-consuming. This makes direct measurement of individual subjects using MRI impractical.

Recently, dual energy x-ray absorptiometry (DEXA) has been used by Durkin et al. (2002) to determine the BSPs of human segments. This technology operates much in the same way as gamma-mass scanning. Two collimated beams of alternating intensity (70 KeV/140 KeV) are emitted and passed through a sample of tissue. The attenuation of the high energy beam (140 KeV) is directly proportional to mass, therefore the inertial properties of the scanned material can be determined from the measured mass information and the known areal dimensions of the scanned elements in the chosen scan plane. Durkin et al. (2002) validated DEXA using a homogeneous geometric object as well as a human cadaveric leg specimen and were able to measure mass, centre of mass location and moment of inertia about the centre of mass with under 3.2% error.

Furthermore, the method was rapid and safe, and the technology is widely available in hospitals. The ease with which the method can be applied, accompanied by low operational costs, make the method ideal for direct BSP measurement on individual subjects as well as for developing predictive equations from large databases of subjects. As with other imaging techniques, however, availability of the technology may be limited for some, or scanning of individual subjects may simply not be a practical option. The need for predictive equations for estimating BSPs accurately on a variety of individuals of varying race, gender, age, and activity level therefore remains an important issue in biomechanics.

The development of predictive equations for estimating BSPs on living humans has been the focus of biomechanical studies for decades. These predictive equations generally fall into two categories: regression equations and geometric models. Regression equations for BSP estimation have been generated from a variety of data measurement procedures such as cadaver studies (Barter, 1957; Chandler et al. 1975; Clauser et al. 1969; Dempster, 1955; Hinrichs, 1985) and living subject studies (Drillis and Contini, 1966; Plagenhoef, et al.,, 1983; Young et al. 1983), including those using medical imaging techniques (Durkin and Dowling, 2003; Erdmann, 1997; Zatsiorsky and Seluyanov, 1985; Zatsiorsky et al., 1990). These regression equations are limited by the deficiencies of the methods used to obtain the data, however, and are specific to the population from which they were generated. For instance, the equations generated from cadaveric data are typically based on male specimens, most of which were over 50 years of age (Pearsall and Reid, 1994) and some of which were in fairly emaciated states when

they passed. Dempster (1955) used elderly male war veterans whose ages ranged from 52 to 83 years of age and whose body masses ranged from 49.7 to 72.5 kg. Additionally, only Chandler et al. (1975) provided equations estimating centre of mass locations and moments of inertia about all three segment axes (Cappozzo and Berme, 1990). Other studies limited their experiments to segment volume, mass and centre of mass locations and many assumed symmetry between frontal and sagittal plane properties for centre of mass and moment of inertia values.

Regression equations generated from reliable data measurement methods such as gamma-mass and DEXA allow greater confidence in estimating human BSPs. The equations should not be applied to individuals outside the population from which they were generated, however. For example, Durkin and Dowling (2003) investigated the BSPs of selected human body segments on four populations of different gender and age categories. Using DEXA, segment masses were measured and reported as a percentage of whole body mass and centre of mass locations and radii of gyration were determined and reported as a percentage of segment length. These BSP measurements were compared between the groups and significant differences were found, supporting the need for different sets of regression equations specific to age and gender. Furthermore, while the regression equations were able to account for differences between groups, they did not account for individual differences within groups. This population specificity of regression equations has led some to theorize that geometric models may provide more accurate estimates of human BSPs, accounting for differences in morphology, age, gender, and race (Durkin, 1998; Pavol et al., 2002; Zatsiorsky et al., 1990).

Geometric models have been developed with varying levels of complexity to more accurately account for the differences in morphology between individuals. Hanavan (1964) developed a geometric model of the human body using a series of spheres, ellipsoids, circular cylinders and frusta. Segment masses were estimated using the regression equations of Barter (1957), however Barter (1957) developed his equations using cadaveric data from two different sources, each of which used different segmentation methods. Furthermore, Hanavan's (1964) model assumed constant density throughout each segment and the estimates were validated for whole body mass and inertia estimates only. Jensen (1978) later used photogrammetry to develop a detailed elliptical model of the human body that was meant to account for differences in morphology between individuals regardless of age, gender and race. The method assumed constant density, however, and was validated for segment volume only. Hatze (1980) also developed a geometric model of the human body that could be applied to individuals regardless of age, gender or morphology, and boasted a maximum error of 5%. The mathematical model used detailed anthropometric information and made no assumptions of constant density, yet this procedure has been criticized due to the 242 anthropometric measurements needed to obtain BSP estimates.

Gamma-mass scanning has been used by Zatsiorsky et al. (1990) to develop models of human body segments based on geometric considerations. Body segments were modelled as cylinders and a constant "pseudodensity" factor was applied to account for differences between segment and model shape and density. The models require the input of limb circumferences and lengths and separate coefficients are provided for male

and female populations. The estimates are promoted as being more accurate than those obtained using multiple regression equations developed from the same data set and are advocated as accurate when used on children. The models have been validated solely on young adult males and females, however, and have been validated in the frontal plane only. Durkin (1998) later developed geometric models of selected body segments for individuals from four human populations and validated estimates in the frontal plane using DEXA. Each segment model consisted of a series of geometric solids chosen to more accurately represent the changes in segment shape along the length of the limb. The models performed poorly and it was concluded that assuming constant density while modelling according to segment shape resulted in large errors in BSP estimation.

The use of predictive equations remains a preferred means for obtaining human BSP data in biomechanical analyses of motion. Regression equations are population-specific and may not account for differences between individuals of varying morphology. Furthermore, the assumption of constant density in geometric modelling and its effect on inertial estimates remains questionable. Theoretically, models based on geometric approximations may allow more accurate representation of individuals regardless of age, race, gender and morphology by using anthropometric measures such as limb lengths, circumferences and breadths. An alternative method for designing geometric models that circumvents the problems of a constant density assumption is therefore needed. The method of Hatze (1980) avoids this issue, however the large amount of input data required makes the model impractical. Wei and Jensen (1995) attempted to develop axial density profiles using regression equations, but they were unable to determine whether

inertial estimates were improved. Durkin and Dowling (2003) suggested developing geometric models according to the mass distribution properties of segments rather than segment shape. By modeling segments according to mass distribution, it is possible that errors in moment of inertia estimates will be reduced by more accurately accounting for changes in mass at the proximal and distal ends of the segment. Using medical imaging techniques, the mass distribution properties of segments may be determined allowing the development of geometric models based on the contours of these properties, while still assuming constant segment density.

1.2 Objectives and Project Design

The purpose of this study was to use DEXA to determine the mass distribution properties of selected human body segments for a variety of human populations and to develop geometric models accordingly for the purpose of BSP estimation. The mass distribution properties of the segments were compared between populations for geometric similarity and a geometric model was developed according to the contours of these mass distribution characteristics. The models were then validated against DEXA measurements along with four other popular models available in the literature.

Study 1 involved the analysis of the mass distribution properties of the human thigh segment in the frontal plane. One hundred individuals from four populations separated by age (19-30 Years /55+ Years) and gender (Male/Female) were scanned using DEXA and the thigh segments were digitally sectioned. A geometric model of the thigh was developed on 20 of the 100 subjects and validated on the remaining 80

subjects. Furthermore, estimates from four other popular models in the literature were calculated and compared to DEXA estimates to determine whether BSP estimates on the examined populations were improved. The models examined from the literature included the linear regression equations of Dempster (1955) (via Winter, 1990) based on elderly male cadaveric data, the simple geometric models of Hanavan (1964), and both the multiple regression equations and geometric models of Zatsiorsky et al. (1990) based on young adult male and female data obtained from gamma-mass scanning.

Study 2 involved the analysis of the mass distribution properties of the human forearm and followed the methodology used in Study 1. BSP estimates were calculated and validated in the frontal plane and compared to calculations from four other popular models in the literature.

Study 3 involved the analysis of the human lower leg in a similar manner as Studies 1 and 2, however this study involved the addition of a DEXA scan and model validation in the sagittal plane, enabling the development and validation of an elliptical model for BSP estimation. Twenty participants from four populations were used for model development and the equations were validated on another group of 20 subjects.

The selection of body segments for analysis was determined based on the ease with which the segments could be measured using DEXA. The thigh, forearm and lower leg can be easily sectioned from the body in the frontal plane with minimal overlap with other segments. Furthermore, these segments may be more easily positioned to ensure consistent measurement axes in the frontal and sagittal planes. Additionally, these segments may present more simple mass distribution properties than other areas such as

the trunk, and therefore serve as optimal limbs from which to test this modelling approach.

1.3 Hypotheses

It was hypothesized that the four populations examined would demonstrate geometric similarity in the mass distribution properties of the thigh, forearm and leg segments, enabling the development of one model to predict BSPs for all groups. It was therefore expected that the null hypothesis (H_o) would be accepted and the alternative hypothesis (H^a) would be rejected.

H_o: Males (19-30 Years) = Females (19-30 Years)

Males (19-30 Years)= Males (55+ Years)

Males (19-30 Years) = Females (55+ Years)

Females (19-30 Years) = Males (55+ Years)

Females (19-30 Years) = Females (55+ Years)

Males (55+ Years) = Females (55+ Years)

H_a: Males (19-30 Years) $\neq$ Females (19-30 Years)

Males (19-30 Years) $\neq$ Males (55+ Years)

Males (19-30 Years) $\neq$ Females (55+ Years)

Females (19-30 Years) $\neq$ Males (55+ Years)

Females (19-30 Years) $\neq$ Females (55+ Years)

Males (55+ Years) $\neq$ Females (55+ Years)

It was further hypothesized that geometric models constructed according to the mass distribution properties of the segments would provide significantly less error in BSP estimates than the other four sources evaluated in the respective studies (H_a). It was therefore expected that the null hypothesis (H_o) would be rejected.

H_o: μ = Dempster (1955) via Winter (1990)

μ = Hanavan (1964)

μ = Zatsiorsky et al. (1990)

H_a: μ < Dempster (1955) via Winter (1990)

μ < Hanavan (1964)

μ < Zatsiorsky et a. (1990)

1.4 Thesis Outline

This thesis will comprise three studies written in manuscript format followed by a "Conclusions and Suggestions for Future Research" chapter. Each manuscript is presented in a format suitable for submission to, and publication in, an academic journal. Study 1 has been submitted and is currently under review in the Journal of Biomechanical Engineering and is therefore presented in the required ASME format. The remaining two studies are presented in APA format (2001, 5th Ed.). Due to the independent presentation of each manuscript and the similar content of each study, considerable overlap of introductory material and methodology may be found amongst all chapters of the thesis.

1.5 References

American Psychological Association. (2001). *Publication Manual of the American Psychological Association (5th Ed.).* Washington D.C.: American Psychological Association.

Barter, J.T. (1957). *Estimation of the mass of body segments.* TR-57-260. Ohio: Wright-Patterson Air Force Base.

Braune, W. & Fischer, O. (1889). *The centre of gravity of the human body as related to the German infantryman.* ATI 138 452. Leipzig: National Technical Information Service.

Cappozzo, A. & Berme, N. (1990). Subject-specific segmental inertia parameter determination. In Berme, N. and Cappozzo, A. (Eds.), *Biomechanics of Human Movement: Applications in Rehabilitation, Sports and Ergonomics* (pp. 179-185). Washington, D.C.: Bertec Corporation.

Chandler, R.F., Clauser, J.T., McConville, H.M., Reynolds, H.M. & Young, J.W. (1975). *Investigation of inertial properties of the human body.* AMRL-TR-74-137. Ohio: Aerospace Medical Research Laboratory. Wright-Patterson Air Force Base.

Cheng, C-K., Chen, H-H., Chen, C-S., Lee, C-L. & Chen, C-Y. (2000). Segment inertial properties of Chinese adults determined from magnetic resonance imaging. *Clinical Biomechanics*, 15(8), 559-566.

Clauser, C.E., McConville, J.T. & Young, J.W. (1969). *Weight, volume, and center of mass of segments of the human body.* AMRL-TR-69-70. Ohio: Aerospace Medical Research Laboratory. Wright Patterson Air Force Base.

Dempster, W.T. (1955). *Space requirements of the seated operator.* WADC-TR-55-159. Ohio: Wright Air Development Center, Wright Patterson Air Force Base.

Drillis, R. & Contini, R. (1966). *Body segment parameters.* TR-1166-03. New York, NY: New York University School of Engineering Science.

Durkin, J.L. (1998*). The prediction of body segment parameters using geometric modelling and dual photon absorptiometry.* Masters Thesis. McMaster University, Hamilton, ON.

Durkin, J.L., Dowling, J.J. & Andrews, D.A. (2002). The measurement of body segment inertial parameters using dual energy x-ray absorptiometry. *Journal of Biomechanics*, 35(12), 1575-1580

Durkin, J.L. & Dowling, J.J. (2003). Analysis of body segment parameter differences between four human populations and the estimation errors of four popular mathematical models. *Journal of Biomechanical Engineering*, 125(4), 515-522.

Elia, M., Fuller, N.J., Hardingham, C.R., Graves, M., Screaton, N., Dixon, A.K. & Ward, L.C. (2000). Modeling leg sections by bioelectrical impedance analysis, dual-energy x-ray absorptiometry, and anthropometry: Assissing segmental muscle volume using magnetic resonance imaging as a reference. *Annals of the New York Academy of Sciences*, 904, 298-305.

Erdmann, W.S. (1997). Geometric and inertial data of the trunk in adult males. *Journal of Biomechanics*, 30(7), 679-688.

Fuller, N.J., Hardingham, C.R., Graves, M., Screaton, N., Dixon, A.K., Ward, L.C. & Elia, M. (1999). Predicting composition of leg sections with anthropometry and bioelectrical impedance analysis, using magnetic resonance imaging as reference. *Clinical Science*, 96, 647-657.

Hanavan, E.P. (1964). *A mathematical model of the human body*. AMRL-TR-64-102. Aerospace Medical Research Laboratories, Ohio: Wright-Patterson Air Force Base.

Harless, H. (1860). *Die statischen Momente der menschlichen Gliedmassen. Abhandl Mathematische-Physikalischen Classe Konigl Bayerischen Akad Wissenschaft*, 8, 69-96, 257- 294.

Hatze, H. (1980). A mathematical model for the computational determination of parameter values of anthropomorphic segments. *Journal of Biomechanics*, 13(10), 833-843.

Hinrichs, R.N. (1985). Regression equations to predict segmental moments of inertia from anthropometric measurements: an extension of the data of Chandler *et al. Journal of Biomechanics*, 18(8), 821-932.

Huang, H.K. (1983). Evaluation of cross-sectional geometry and mass density distributions of humans and laboratory animals using computerized tomography. *Journal of Biomechanics*, 16(10), 821:832.

Jensen, R.K. (1978). Estimation of the biomechanical properties of three body types using a photogrammetric method. Journal of Biomechanics, 11(8-9), 349-358.

Martin, P.E., Mungiole, M., Marzke, M.W. & Longhill, J.M. (1989). The use of magnetic resonance imaging for measuring segment inertial properties. *Journal of Biomechanics*, 22(4), 367-376.

McConville, J.T., Churchill, T.D., Kaleps, I., Clauser, C.E. & Cuzzi, J. (1980). *Anthropometric relationships of body and body segment moments of inertia*. AFAMRL-TR-80-119. Ohio: Air Force Aerospace Medical Research Laboratory. Wright-Patterson Air Force Base.

Mungiole, M. & Martin, P.E. (1990). Estimating segment inertial properties: Comparison of magnetic resonance imaging with existing methods. *Journal of Biomechanics*, 23(10), 1039-1046.

Pavol, M.J., Owings, T.M. & Grabiner, M.D. (2002). Body segment inertial parameter estimation for the general population of older adults. *Journal of Biomechanics*, 35, 707-712.

Pearsall, D.J. & Reid, J.G. (1994). The study of human body segment parameters in biomechanics. *Sports Medicine*, 18(2), 126:140.

Pearsall, D.J., Reid, J.G. & Livingston, L.A. (1996). Segmental inertial parameters of the human trunk as determined from computed tomography. *Annals of Biomedical Engineering*, 24(2), 198-210.

Plagenhoef, S., Evans, F.G. & Abdelnour, T. (1983). Anatomical data for analyzing human motion. *Research Quarterly for Exercise and Sport*, 52(4), 169-178.

Reid, J.G. & Jensen, R.K. (1990). Human body segment inertia parameters: A survey and status report. *Exercise and Sport Science Reviews*, 18, 225-241.

Wei, C. & Jensen, R.K. (1995). The application of segment axial density profiles to a human body inertia model. *Journal of Biomechanics*, 28(1), 103-108.

Winter, D.A. (1990). *Biomechanics and motor control of human movement*. (2nd Ed.). New York: John Wiley and Sons, Inc, pp. 51-64.

Young, J.W., Chandler, R.F. & Snow, C.C. (1983). *Anthropometric and mass distribution characteristics of the adult female*. FAA-AM-83-16. Oklahoma: FAA Civil Aeromedical Institute.

Zatsiorsky, V. & Seluyanov, V. (1983). The mass and inertia characteristics of the main segments of the human body. In H. Matsui & K. Kobayashi (Eds.). *Biomechanics V-IIIB*. Champaign, IL: Human Kinetics Publishers Inc., pp. 1152-1159.

Zatsiorsky, V. & Seluyanov, V. (1985). Estimation of the mass and inertia characteristics of the human body by means of best predictive regression equations. In D.A. Winter, R.W. Norman, & R.P. Wells. (Eds.). *Biomechanics IX-B*.. Champaign, IL: Human Kinetics Publishers Inc, pp. 233-239.

Zatsiorsky, V., Seluyanov, V. & Chugunova, L.G. (1990). Methods of determining mass-inertial characteristics of human body segments. In G.G. Chernyi & S.A. Regirer (Eds.). *Contemporary Problems of Biomechanics* (Ch. 11). Boston, MA: CRC Press, pp. 272-291.

CHAPTER 2

USING MASS DISTRIBUTION INFORMATION TO MODEL THE HUMAN THIGH FOR BODY SEGMENT PARAMETER ESTIMATION

2.1 Introduction

An accurate and efficient way of obtaining body segment inertial parameters (BSPs) is required to calculate reliable net joint forces and torques using inverse or forward dynamics methods. Many attempts to measure or estimate these BSPs have been made, yet limitations in the methods available have led to continued efforts in reducing BSP error [1,2]. Early studies used cadavers to measure human BSPs directly, developing regression equations from the data for segment parameter estimation [3-7]. These studies have been criticized, however, for containing small sample sizes limited to elderly Caucasian males. Furthermore, data from individual studies cannot be combined due to differences in segmentation patterns and the validity of using deceased tissue to represent that of living subjects is yet unknown [2]. Methods using living subjects such as stereophotogrammetry [8], water immersion, quick release [9], and oscillation techniques [10] have also been developed but have involved questionable assumptions. For instance, water immersion and stereophotogrammetry assume that segment densities are known and constant throughout.

Mathematical modelling and medical imaging techniques have been used to obtain more accurate BSPs. Hanavan [11] developed a geometric model of the human body, modelling segments as a series of cylinders, frusta and ellipsoids, however a criticism of this model was that it was too simple to accurately depict the inertial properties of human

body segments. Furthermore, the model was evaluated for accuracy in whole body inertial parameter estimation but was not validated segmentally. Jensen [12] used a more detailed elliptical modelling approach with photogrammetry to explain variations in body morphology as well as to develop a method appropriate for use on children. The method explained changes in segment shape, however the model assumed constant segment densities, was validated for segment volume estimations only, and the software developed is not readily available for use. Hatze [13] later developed a more involved geometric model of the human body requiring the input of 242 anthropometric measurements which has resulted in its limited use.

Medical imaging techniques such as MRI, CT imaging, dual energy x-ray absorptiometry (DEXA) and gamma-mass scanning have enabled the accurate measurement of human BSPs. Zatsiorsky and Seluyanov [14] used a gamma-mass scanner to measure the BSPs of 100 young males, however, the technique requires exposing subjects to radiation and the technology is not widely available. This led Zatsiorsky et al. [15] to develop multiple regression equations and geometric models for young male and female subjects. The equations developed have been a common BSP source in the literature, but their applicability to individuals outside a young Caucasian population has been questioned [2]. CT imaging [16,17] and MRI [18-20] have yielded accurate BSP measurements and provide promise for precise BSP measurement, yet both methods are quite costly and time consuming and CT imaging requires exposing subjects to a substantial amount of radiation [19]. The arduousness of these methods has also discouraged the accumulation of large databases of subjects for the development of

predictive models.

Recently, Durkin et al. [1] used dual energy x-ray absorptiometry (DEXA) to measure human BSPs directly on living humans. The procedure is considered rapid, safe and accurate, measuring BSPs with under 3.2% error, however, similar to the gamma-mass scanner, the machine is not widely accessible. This led Durkin and Dowling [21] to develop simple linear regression equations on 100 subjects for selected body segments in the frontal plane. Four groups of individuals (25 per group) separated by gender (male/female) and age (19-30 years / 55+ years) were examined and separate regression equations were developed for each sample for mass, centre of mass location (CM) and moment of inertia about the CM (I_{CM}). Errors for these equations, as well as those from Dempster [6], Zatsiorsky et al. [15] and Hanavan [11] were determined and it was found that no single predictor performed best for a particular segment, population, or BSP. Furthermore, it was found that the linear regression equations could account for differences between groups but did not satisfactorily explain individual differences within groups. It was suggested that multiple regression equations be developed for each population, incorporating a number of anthropometric measurements such as limb lengths and circumferences. Alternatively, it was suggested that geometric models be developed which are more detailed than those developed in the past but which are still easy to use.

There is still a need for a complete anthropometric model of the human body that is accurate yet simple to apply [2]. Multiple regression equations may provide this function, yet different equations need to be developed for each population to accurately represent their differences. Geometric models may circumvent this requirement while also

accounting for individual differences within a group, yet many of the geometric models developed in the past have been too simple to depict the changes in density that occur along the length of the segment [22]. Durkin [23] developed geometric models for selected human body segments using composites of geometric shapes in an attempt to more accurately represent segment volume distribution. A comparison of model estimates with DEXA measurements revealed large errors and suggested that modelling segments according to volume distribution, while assuming constant density, results in poor estimates of human BSPs. Wei and Jensen [24] developed density profiles from axial CT scans to account for such changes but were unable to determine whether the profiles produced more accurate estimates of inertia. One way of alleviating the need for density profiles in geometric models is to model segments according to their mass distribution properties rather than volume. By using DEXA to visualize the mass distribution contours of a segment, a geometric shape can be developed accordingly while still assuming constant density. With this modelling technique, it is possible that CM and I_{CM} estimations could be more accurate than when using a model that mimics the volume distribution of a segment. Furthermore, if it is found that individuals in different populations are geometrically similar in their mass distribution properties for a given segment, it is possible that one model could be used for all individuals, reducing the need for separate equations according to gender, age, race and body type.

Development of a complete anthropometric model of the human body in this manner will require separate detailed analyses of the mass distribution properties of each body segment along with construction and validation of appropriate models. The purpose

of this study is to begin development of this whole body anthropometric model with the thigh segment by: i) examining the mass distribution properties of the thigh segments of 100 volunteers from four different populations using DEXA, ii) developing a geometric model of the thigh based on these mass distribution properties, iii) comparing the accuracy of this model with a selected group of models available in the literature. It is hypothesized that a geometric model of the thigh segment that is based on its mass distribution properties will yield more accurate BSP estimates than the other popular models examined. Furthermore, it is believed that the mass distribution properties of the thigh segment will be similar between the four populations examined and that all four groups can be satisfactorily estimated using one common geometric model.

2.2 Methods

One hundred volunteers were recruited and categorized into four groups (25 per group) according to gender (male/female) and age (19-30 years old, 55+ years old). Average height and weight values for the 5^{th}, 25^{th}, 50^{th}, 75^{th}, and 95^{th} percentiles of Canadian adults were obtained from Demirjian [25] for each gender and age category, resulting in the construction of 25 height/mass cells per group. Subjects were recruited using posters on the McMaster University campus and at the McMaster University Medical Centre. Participants included university students and faculty/staff as well as staff and visitors to the hospital. One individual was matched to each of the 25 height and mass categories, resulting in a subject database comprised of a variety of height and mass combinations within each group. Five subjects from each population were then randomly chosen to

represent a model development group while the remaining subjects were used for model validation (Tables 1 and 2). The heights and mass of each of these groups were similar and were normally distributed (Durkin, 1998).

The participants were asked to change into a hospital gown while keeping undergarments on. Each individual underwent one whole body DEXA scan (QDR-1000/W, Hologic Inc., Bedford, MA, USA) where they were asked to lie supine on the DEXA table with palms facing the bed (forearms pronated). The DEXA scan was acquired, collecting mass data in units of 1.32 X 0.53 cm, after which the participants were asked to stand upright while a series of anthropometric measurements were taken (Table 3). Informed consent was obtained from each volunteer in accordance with approval from the McMaster University Research Ethics Board.

The DEXA scan files were processed using custom software (DXA Digitization Software, Durkin, 1998) as in Durkin et al. [1]. Density images of the scan data were created such that the skeleton could be clearly seen and bony landmarks could be used for digitization purposes (Fig. 1). An image based on mass was also created to ensure that all soft tissue not visible on the density image would be included in the digitized area (Fig. 2). The mass data were then interpolated to 40X the original resolution, increasing the areal resolution of the mass elements to 0.132 x 0.132 cm. The interpolation was performed using a cubic spline algorithm set to follow the data with as little smoothing as possible (Fig. 3).

Table 1. Means (±SD) and ranges of age, whole body mass and height of model development participants in the four population groups.

			Age (years)		Whole Body Mass (kg)		Height (m)	
Group	N	n	Mean (±SD)	Range	Mean (±SD)	Range	Mean (±SD)	Range
Males (19-30 Years)	5	10	22.6 (1.1)	21-24	75.7 (15.3)	59.0-97.7	1.73 (0.10)	1.55-1.80
Females (19-30 Years)	5	10	23.2 (4.0)	19-30	57.8 (10.2)	47.0-70.5	1.63 (0.11)	1.52-1.77
Males (55+ Years)	5	10	67.8 (7.2)	59-76	80.1 (19.7)	59.0-106.0	1.71 (0.06)	1.63-1.80
Females (55+ Years)	5	10	69.2 (9.6)	59-82	62.7 (11.7)	50.9-77.0	1.60 (0.04)	1.55-1.63

N = number of subjects, n = number of thigh segments used in analysis

Table 2. Means (±SD) and ranges of age, whole body mass and height of model validation participants in the four population groups.

			Age (years)		Whole Body Mass (kg)		Height (cm)	
Group	N	n	Mean (±SD)	Range	Mean (±SD)	Range	Mean (±SD)	Range
Males (19-30 Years)	20	40	23.2(2.0)	19-27	71.5(9.3)	55.5-86.0	1.75(0.06)	1.63-1.85
Females (19-30 Years)	20	40	21.7(2.6)	19-28	56.9(6.4)	47.7-70.5	1.64(0.07)	1.53-1.80
Males (55+ Years)	20	30	68.1(7.4)	55-78	84.8(11.7)	67.3-107.7	1.75(0.06)	1.63-1.85
Females (55+ Years)	20	38	66.2(7.5)	56-81	62.8(7.5)	51.0-86.4	1.60(0.05)	1.52-1.70

N = number of subjects, n = number of thigh segments used in analysis

Table 3. Description of the anthropometric measurements used to estimate BSPs with the developed geometric model.

Measurement	Description
Proximal Thigh Circumference (PC)	Circumference about thigh inferior to superior ramus of pubis (proximal limit of medial thigh)
Knee Circumference (KC)	Circumference about knee at distal border of medial and lateral femoral condyles
Inner Thigh Length (IL)	Length between distal border of medial femoral condyle to pubic tubercle of pubic ramus
Outer Thigh Length (OL)	Length between distal border of lateral femoral condyle to tubercle of iliac crest (about 5 cm superior to anterior superior iliac spine)

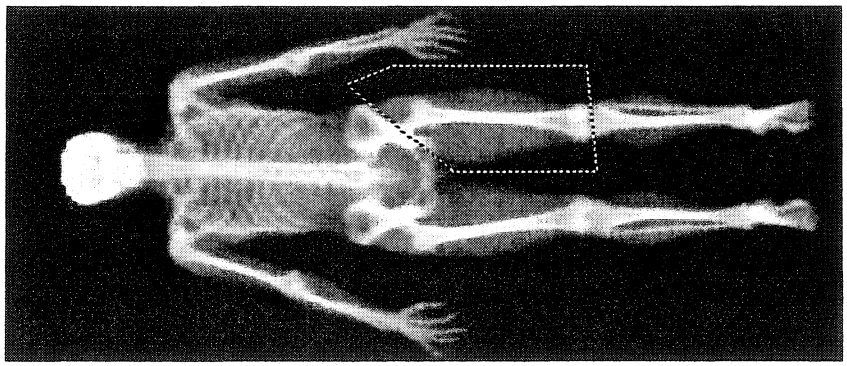

Figure 1. Density image of a young female volunteer produced from DEXA scan information to display bony landmarks. Dashed line represents an example of the digitization method for the thigh segment.

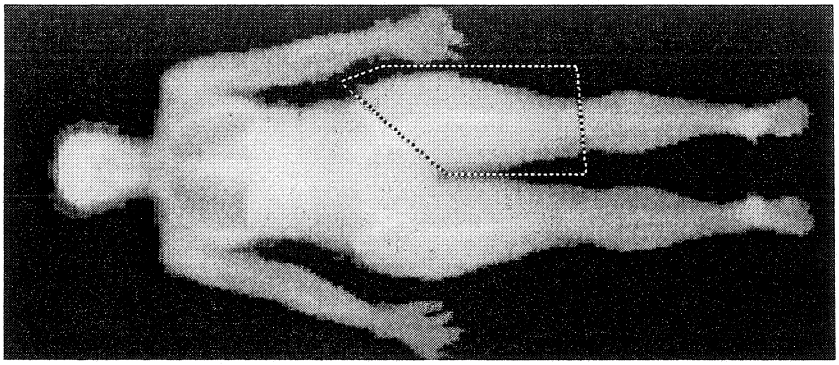

Figure 2. Mass image of a young female volunteer produced from DEXA scan information to display all soft tissue mass, ensuring that all relevant thigh mass is contained within the digitized area (dashed line). Image is produced using raw data dimensions of 1.32 X 0.53 cm.

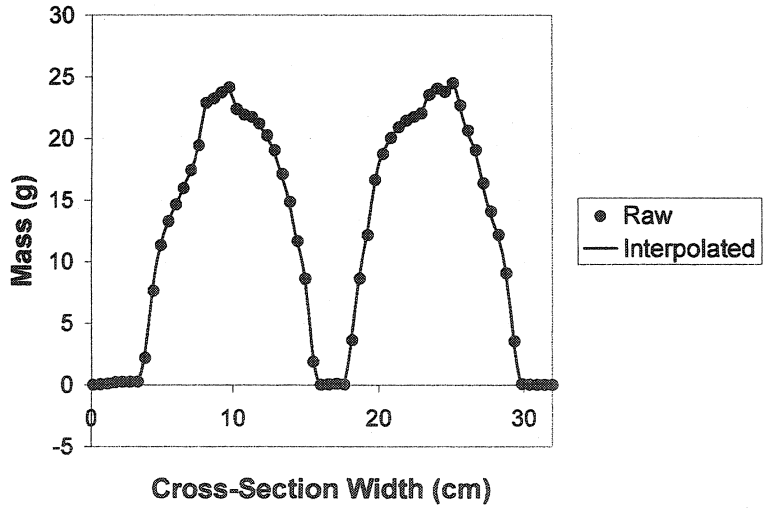

Figure 3. Example of interpolated data points fitting raw DEXA data with very little smoothing. Mass cross-section is through mid-thigh region.

The right and left thighs of each participant were segmented by sectioning at the hip and knee. The thigh was sectioned at the hip by an oblique plane slicing in an anteroposterior direction just lateral to the anterior superior iliac spine and medial to the lateral border of the obturator foramen/medial border of the ramus of the ischium (see Fig. 1). The thigh was sectioned at the knee by a plane slicing anteroposteriorly between

the femoral condyles and tibial plateau. The proximal end point was selected as a point along the segmentation plane of the hip joint, midway through the neck of the femur. The distal end point was selected as a point along the segmentation plane of the knee, midway between the lateral edges of the femoral condyles. Other digitization points were selected to ensure all soft tissue not visible on the density image was enclosed within the digitized area by toggling between the density and mass images.

The digitized information was then processed in several stages. First, the data array was rotated to ensure that the proximal and distal end points represented the longitudinal (x) axis of the segment. Second, thigh mass, centre of mass in the cephalocaudal direction (CM_x), centre of mass in the mediolateral direction (CM_y) and moment of inertia about the centre of mass (I_{CMz}) were calculated as in Durkin, et al. [1]. Third, a sum of the mass elements within the digitized area was created at every 1% segment length interval to create a mass distribution plot of the thigh segments normalized to 100% segment length and 100% segment mass. The mass distribution of the thigh was plotted so that the lateral and medial components of the thigh, identified by the proximal-distal axis, were plotted independently and the area between the two curves represented 100% of the segment mass. The mass distribution plots of the right thighs were then inverted to match those of the left thighs and were treated as independent samples.

Ensemble averages of the mass distribution plots of 5 subjects (10 segments) from each group were performed to yield the mean (±SD) thigh mass distribution for each population (Fig. 4). Geometric similarity was determined by examining the graphs

Figure 4. Ensemble averages of the mass distribution characteristics of the thigh segment for four population groups. The plots represent the amount of mass present every 1% segment length from proximal to distal ends. Positive y-axis represents lateral thigh mass. Negative y-axis represents medial thigh mass. The area between the curves represents 100% of the segment mass. Inside curve represents the mean mass distribution, outside curve represents +1 SD. The negative standard deviation has been omitted.

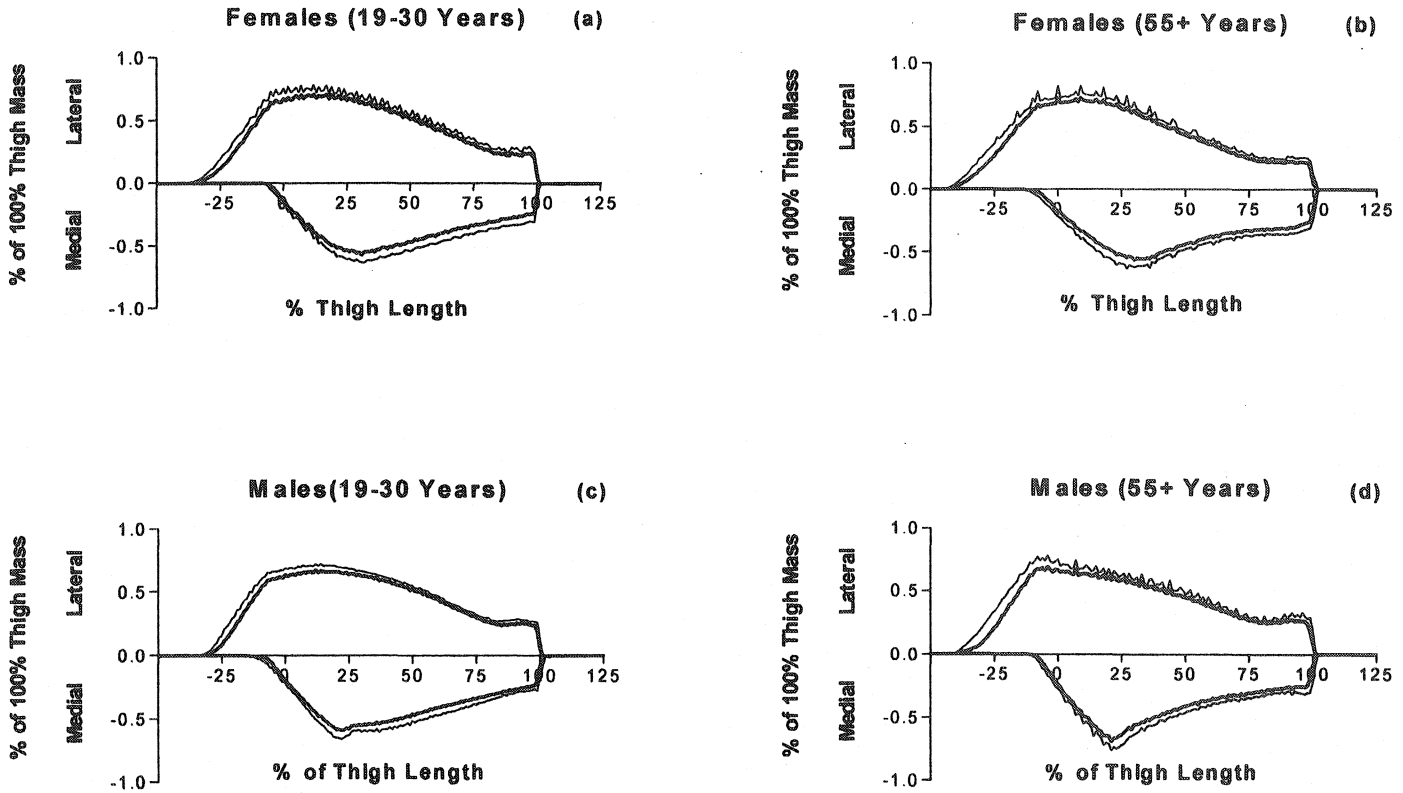

visually and by correlating the mass distribution properties of the groups. Pearson product moment correlation coefficients were determined between each of the groups by correlating the percent of 100% segment mass values (y-axis in Fig. 4) at each 1% of segment length. The ensemble averages were then used for the development of the geometric model to predict thigh BSPs.

2.3 Results

2.3.1 Geometric Model

Visual examination of the mass distribution plots showed that there was a substantial amount of geometric similarity between the groups and the small standard deviations in each ensemble average showed that there was little variability within each sample. Furthermore, Pearson product moment correlation coefficients between the groups were high (Table 4), supporting the use of one model to predict BSPs for all individuals.

Five different geometric models of increasing complexity were developed to represent the mass distribution properties of the thigh segment. Only one model with the lowest error will be presented in this paper. The other models were variations of the one presented here with more simple representations of the proximal segment. One of the models was also adapted to account for gender differences. The geometric model developed was a composite consisting of three geometric shapes joined end to end. The proximal segment was adapted from a right circular cylinder cut on an oblique plane that followed three slopes, the middle segment was that of a decreasing right circular frustum

Table 4. Correlation data comparing mass distribution characteristics between groups including linear regression equations and Pearson Product Moment Correlation coefficients. (a) represents correlations of lateral thigh mass data (positive y-values in Figure 4). (b) represents correlations of medial thigh mass data (negative y-values in Figure 4). YF = Females (19-30 Years), YM = Males (19-30 Years), OF = Females (55+ Years), OM = (Males 55+ Years).

(a)

Groups Correlated	Linear Regression Equation	Pearson r
Males (19-30) vs. Females (19-30)	YF = - 0.007 + 1.033(YM)	0.999
Females (19-30) vs. Females (55+)	OF = 0.021 + 0.936(YF)	0.968
Females (55+) vs. Males (55+)	OM = 0.009 + 0.935(OF)	0.990
Males (55+) vs. Males (19-30)	YM = - 0.009 + 1.032(OM)	0.975
Males (19-30) vs. Females (55+)	OF = 0.022 + 0.963(YM)	0.963
Females (19-30) vs. Males (55+)	OM = 0.024 + 0.891(YF)	0.976

(b

Groups Correlated	Linear Regression Equation	Pearson r
Males (19-30) vs. Females (19-30)	YF = - 0.002 + 0.966(YM)	0.994
Females (19-30) vs. Females (55+)	OF = 0.008 + 0.961(YF)	0.996
Females (55+) vs. Males (55+)	OM = 0.0002 + 1.053(OF)	0.969
Males (55+) vs. Males (19-30)	YM = 0.006 + 0.969(OM)	0.986
Males (19-30) vs. Females (55+)	OF = 0.005 + 0.930(YM)	0.992
Females (19-30) vs. Males (55+)	OM = 0.008 + 1.012(YF)	0.966

and the distal segment was that of a right circular cylinder (Fig. 5). The changing slope pattern of the proximal segment was chosen to better represent the shape of the mass distribution curve as identified in Figure 4. Previous models utilizing one slope created a convex curvature in the model mass distribution plot, resulting in an overestimation of thigh mass at the proximal end. Segment density was assumed to be constant throughout at 0.00105 kg m^{-3} [26] and the mass, CM_x, CM_y and I_{CMz} of the model were determined using the geometric properties of the shapes selected. The length proportions of each model segment were determined by visually inspecting the mass distribution plots and selecting points along the segment length where the slope of the mass distribution curve

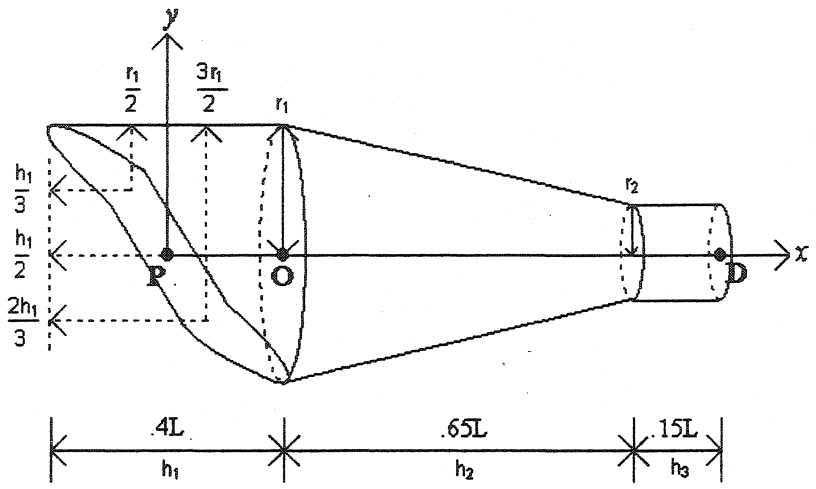

Figure 5. Diagram of the geometric model used to represent the mass distribution characteristics of the thigh segment for four groups of humans. Points P and D represent the proximal and distal segment endpoints, respectively.

appeared to change for all groups.

The volume of the proximal segment (V_1) was found by integrating units with a rectangular cross-section and thicknesses of dy from $-r_1$ to r_1 along the y-axis (Fig. 6).

$$V_1 = \int_{-r_1}^{r_1} (z\,x)dy = \sum_{i=1}^{n} V_i \qquad (1)$$

where r_1 is determined from the proximal thigh circumference (r_1=PC/2π), dy = 0.001 cm, V_i = volume of each rectangular element, $n = 2r_1/dy$, z = width of base of rectangle and depends on the base of a circle with radius r_1:

$$z = 2\left(r_1^2 - y^2\right)^{0.5} \qquad (2)$$

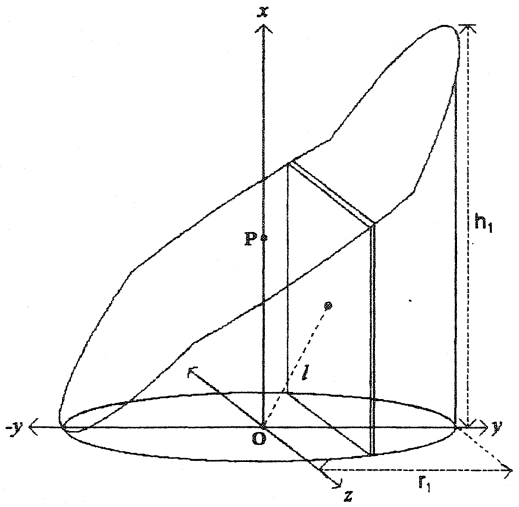

Figure 6. Diagram of the proximal segment of the geometric model illustrating the three slopes of the oblique plane and the elements used to integrate for segment volume.

and x = height of rectangle and depends on the position of the rectangular slice along the y-axis and the slope of the oblique plane. There are three slopes and four conditions that determine the height of x:

$$If\ y<\frac{-r_1}{2},\quad x=\left(\frac{h_1}{3}\right)\left(\frac{2}{r_1}\right)(y+r_1) \qquad (3)$$

$$If\ \frac{-r_1}{2}\le y<0,\quad x=\left(\frac{h_1}{3r_1}\right)\left(\frac{y+r_1}{2}\right)+a_1 \qquad (4)$$

$$a_1=\left(\frac{h_1}{3}\right)\left(\frac{2}{r_1}\right)\left(\frac{r_1}{2}+r_1\right) \qquad (5)$$

$$If\ 0\le y<\frac{r_1}{2},\quad x=\left(\frac{h_1}{3r_1}\times y\right)+a_2 \qquad (6)$$

$$a_2=\left(\frac{h_1}{3r_1}\right)\left(0+\frac{r_1}{2}\right)+a_1 \qquad (7)$$

$$If\ \frac{r_1}{2}\le y\le r_1,\quad x=\left(\frac{2h_1}{3r_1}\right)\left(y-\frac{r_1}{2}\right)+a_3 \qquad (8)$$

$$a_3=\left(\frac{h_1}{3r_1}\right)\left(\frac{r_1}{2}\right)+a_2 \qquad (9)$$

where $h_1 = 0.4(SL)$ and SL = segment length which is calculated as:

$$SL = 0.5(h_o - h_i) + h_i \quad \textbf{(10)}$$

and h_o = outer thigh length, h_i = inner thigh length. The mass (M_1) of the proximal segment was determined by:

$$M_1 = \sum_{i=1}^{n}(m_i) = \sum_{i=1}^{n}(V_i\,\rho) \quad \textbf{(11)}$$

where m_i = mass of the i^{th} element, V_i = volume of the i^{th} element, ρ = density of the solid.

The location of the centre of mass was calculated from a point of origin on the base of the proximal segment (O) (See Figs. 4 and 5):

$$CM_{x1} = \frac{\sum_{i=1}^{n}(x_i\,m_i)}{M_1} \quad \textbf{(12)} \qquad CM_{y1} = \frac{\sum_{i=1}^{n}(y_i\,m_i)}{M_1} \quad \textbf{(13)}$$

where CM_{x1}, CM_{y1} = centre of mass locations of the proximal segment along the x and y axes, respectively, x_i = centre of mass location of the i^{th} element in the x-direction, y_i = centre of mass location of the i^{th} element in the y-direction.

The moment of inertia of the proximal segment was calculated about the z-axis at a point of origin located at the base of the segment (O). I_{O1} was calculated by first determining the moment of inertia of each rectangular unit about its own CM (I_{CMi}) (Eq. 14), using parallel axis theorem to calculate the I_{CMi} about O for each element (I_{Oi}) (Eq. 15) and summing the elements to determine the moment of inertia of the proximal segment about point O (I_{O1}) (Eq. 16).

$$I_{CMi} = \frac{1}{12}\left(m_i\, dy^2\right) \quad \textbf{(14)} \qquad I_{Oi} = I_{CMi} + m_i + l_i^2 \quad \textbf{(15)}$$

$$I_{O1} = \sum_{i=1}^{n} I_{Oi} \quad \textbf{(16)}$$

where l_i = the distance between the CM of the i^{th} element and point O. l_i was determined using the Pythagorean Theorem with CM_{xi} and CM_{yi}:

The second component of the geometric model was that of a decreasing right circular frustum. Volume (V_2) and mass (M_2) were calculated with the formulae:

$$V_2 = \frac{\pi h_2}{3}\left(r_1^2 + r_1 r_2 + r_2^2\right) \quad \textbf{(17)} \qquad M_2 = V_2\ \rho \quad \textbf{(18)}$$

where r_2 = radius determined from the knee circumference ($r_2 = KC/2\pi$) and h_2 = 0.65(SL). The CM_{x2}, CM_{y2} and I_{CMz2} of the right circular frustum were determined as in Hanavan [11] and I_{O2} was subsequently calculated using parallel axis theorem:

$$I_{O2} = I_{CMz2} + M_2 CM_{x2}^{\ 2} \quad \textbf{(19)}$$

The distal segment of the geometric model was that of a right circular cylinder. Volume (V_3) and mass (M_3) were calculated as:

$$V_3 = \pi r_2^2 h_3 \quad \textbf{(20)} \qquad M_3 = V_3\ \rho \quad \textbf{(21)}$$

where h_3 = 0.15(SL).

$CM_{y3} = 0$ and lies on the x-axis and CM_{x3} from point O was determined as:

$$CM_{z3} = \frac{h_3}{2} + h_2 \quad (22)$$

I_{CM3} and I_{O3} were calculated using the formulae:

$$I_{CM3} = \frac{m_3}{12}\left(h_3^2 + 3r_2^2\right) \quad (23) \qquad I_{O3} = I_{CM3} + M_3 CM_{x3}{}^2 \quad (24)$$

The mass of the entire composite (M) was calculated by summing the masses of the individual components:

$$M = M_1 + M_2 + M_3 \quad (25)$$

The centre of mass locations from point O (CM_{xO}, CM_{yO}) were calculated and CM_x was determined as a distance from the proximal end (P):

$$CM_{xO} = \left[\left(CM_{x1}\, m_1\right) + \left(CM_{x2}\, m_2\right) + \left(CM_{x3}\, m_3\right)\right] / M \quad (26)$$

$$CM_x = CM_{xO} + \left(h_1/2\right) \quad (27) \qquad CM_y = CM_{yO} = \left(CM_{y1}\, M_1\right) / M \quad (28)$$

The moment of inertia of the entire composite was calculated by first determining the moment of inertia about point O (I_O) (Eq.29) and then using parallel axis theorem to determine I_{CM} (Eq.30):

$$I_O = I_{O1} + I_{O2} + I_{O3} \quad (29) \qquad I_{CM} = I_O - M\left(CM_{xO} + CM_{yO}\right)^2 \quad (30)$$

2.3.2 Model Accuracy

The accuracy of the model's BSP estimates were determined by comparison of the remaining 80 subjects to DEXA measurements by calculating the root mean squared error (RMSE) for each group. Mass and moment of inertia estimates were evaluated by calculating a % RMSE in units of % DEXA mass and % DEXA moment of inertia, respectively. Centre of mass estimates were evaluated by calculating the RMSE for each group in units of % segment length.

Estimation errors from four other popular sources in the literature were also determined by estimating the BSPs using the respective equations and calculating the RMSEs from the DEXA measurements (Tables 5-8). The four sources selected included Dempster [6] (via Winter [26]), Hanavan [11] and two models by Zatsiorsky et al. [15] including a set of multiple regression equations and a set of predictive equations based on geometric considerations. These models were selected as they were thought to represent a sample of the more popular sources in the literature. Unfortunately, some thigh segments in the elderly groups had to be excluded due to the presence of metallic implants that were not reported prior to scanning (See Table 2), therefore the results are based on unequal sample sizes.

One-way repeated measures analyses of variance (ANOVAs) were performed to determine if significant differences existed between the model errors for each BSP within each group. Tukey HSD post hoc analyses were then performed to determine where these

Table 5. Percent root mean squared errors (RMSE) of BSP estimations from five anthropometric models as compared to DEXA measurements for Males (19-30 years old). Models evaluated include the present geometric model (D), Dempster (1955) (via Winter, 1990)(W), Hanavan (1964) (H) and two models from Zatsiorsky et al. (1990) including a multiple regression model (ZR) and a geometric model (ZG). RMSE values are in units of % DEXA measurements for mass and I_{CM}. RMSE values are in units of % segment length for CM estimations.

	D	W	H	ZR	ZG	F	p
Mass	18.3	28.3	19.9	8.7	9.9	71.1	<0.001
CM_x	3.2	6.1	5.4	9.1	12.7	171.3	<0.001
CM_y	1.3	2.5	2.5	2.5	2.5	98.8	<0.001
I_{CM}	14.7	17.5	22.5	17.2	21.1	3.3	<0.02

Table 6. Percent RMSEs of BSP estimations from five anthropometric models as compared to DEXA measurements for Females (19-30 years old). Models evaluated include the present geometric model (D), Dempster (1955) (via Winter, 1990)(W), Hanavan (1964) (H) and two models from Zatsiorsky et al. (1990) including a multiple regression model (ZR) and a geometric model (ZG). RMSE values are in units of % DEXA measurements for mass and I_{CM}. RMSE values are in units of % segment length for CM estimations.

	D	W	H	ZR	ZG	F	p
Mass	13.4	32.4	20.7	9.0	20.0	103.6	<0.001
CM_x	4.4	7.9	6.7	10.3	14.4	321.1	<0.001
CM_y	1.4	2.5	2.5	2.5	2.5	58.8	<0.001
I_{CM}	12.3	24.4	26.4	13.1	31.4	11.1	<0.001

Table 7. Percent RMSEs of BSP estimations from five anthropometric models as compared to DEXA measurements for Males (55+ years old). Models evaluated include the present geometric model (D), Dempster (1955) (via Winter, 1990)(W), Hanavan (1964) (H) and two models from Zatsiorsky et al. (1990) including a multiple regression model (ZR) and a geometric model (ZG). RMSE values are in units of % DEXA measurements for mass and I_{CM}. RMSE values are in units of % segment length for CM estimations.

	D	W	H	ZR	ZG	F	p
Mass	24.8	23.5	17.1	13.5	12.4	17.0	<0.001
CM_x	9.5	7.7	8.6	13.0	14.2	9.0	<0.001
CM_y	1.4	2.1	2.1	2.1	2.1	8.40	<0.001
I_{CM}	25.5	22.5	27.8	14.3	22.1	7.30	<0.001

Table 8. Percent RMSEs of BSP estimations from five anthropometric models as compared to DEXA measurements for Females (55+ years old). Models evaluated include the present geometric model (D), Dempster (1955) (via Winter, 1990)(W), Hanavan (1964) (H) and two models from Zatsiorsky et al. (1990) including a multiple regression model (ZR) and a geometric model (ZG). RMSE values are in units of % DEXA measurements for mass and I_{CM}. RMSE values are in units of % segment length for CM estimations.

	D	W	H	ZR	ZG	F	p
Mass	16.1	30.4	20.4	17.8	17.8	19.0	<0.001
CM_x	7.1	9.3	9.2	11.1	15.7	110.3	<0.001
CM_y	2.5	3.4	3.4	3.4	3.4	4.69	<0.002
I_{CM}	20.5	28.7	30.3	19.9	26.7	5.81	<0.001

differences lay. The ANOVAs showed significant differences between the models for each BSP within each group (Tables 5-8). The regression equations of Zatsiorsky et al. [15] provided the lowest errors in thigh mass estimation for all groups except for older females where the present model was lower. Tukey HSD post hoc analyses showed the regression equations of Zatsiorsky et al. [15] to be significantly lower in mass estimation error than the present model for both male groups but not for the female groups.

Furthermore, the model developed in this study was the best predictor of thigh CM overall. It was found to produce significantly less error than all other models for CM_x except for Males (55+) where Dempster [6] produced the lowest errors. In this group, the present model, Dempster [6] and Hanavan [11] were not significantly different from each other. The newly developed thigh model was also found to predict CM_y with significantly less error than all other models for all groups. It also provided lower I_{CM} error for the younger groups, although the errors were not significantly different from the regression equations of Zatsiorsky et al. [15]. For the younger males, Hanavan [11] produced I_{CM} errors that were significantly higher than all other models. Zatsiorsky et al. [15] provided the lowest errors in I_{CM} estimation for the older groups when the regression equations were used, however differences were significant from the present model only in the older male group. Overall, the regression equations of Zatsiorsky et al. [15] and the present model produced the lowest errors in BSP estimation, however, where the present model did not provide the most accurate estimations, it closely approximated the errors of the model that was superior. The models that performed the worst for mass and I_{CM}, on average, were Dempster [6] and Hanavan [11], respectively.

2.4 Discussion

The results showed that the geometric model developed in this study performed best for CM estimations and provided the lowest I_{CM} estimation errors for the younger groups, although the I_{CM} errors were not significantly different from the regression equations of Zatisorsky et al. [15]. The results of the post hoc analyses found that no one set of

predictors performed best in all cases for a particular group or BSP and that, often, the present model and the regression equations of Zatsiorsky et al. [15] showed no significant difference in prediction error. Correlating the mass and I_{CM} estimations of the present model with the DEXA measurements showed that the model underestimated mass for all groups (Fig, 7a and Table 9) and that there was variability in I_{CM} values within the groups that the model could not account for (Fig, 7b and Table 10). Furthermore, overlaying the mean mass and I_{CM} distribution properties of the thigh as determined from DEXA with the mean mass and I_{CM} distribution properties predicted by the model for the four groups revealed that mass (Fig. 8a), as well as I_{CM} (Fig. 8b), was underestimated by the model at the proximal end of the thigh. One or more anthropometric parameters other than proximal thigh circumference may provide a more accurate representation of the mass at the proximal end and should be considered in future models. Conversely, mass and I_{CM} were predicted well at the distal end, indicating that knee circumference is a good predictor of distal thigh mass and I_{CM} in the frontal plane.

The segmentation procedures selected in this study were designed to follow identifiable bony landmarks and the segment digitization methods were assumed to be repeatable. While this is a limitation of the study, all data processing was performed by one individual, minimizing inter-digitizer error. The digitization landmarks selected were easily identifiable and it is assumed that the segmentation repeatability was high. The selected segmentation procedure also occasionally resulted in the exclusion of some proximal thigh mass medially and the addition of mass laterally in subjects with steeper iliac crest-to-ischial tuberosity slopes. This may have caused an increase in the DEXA

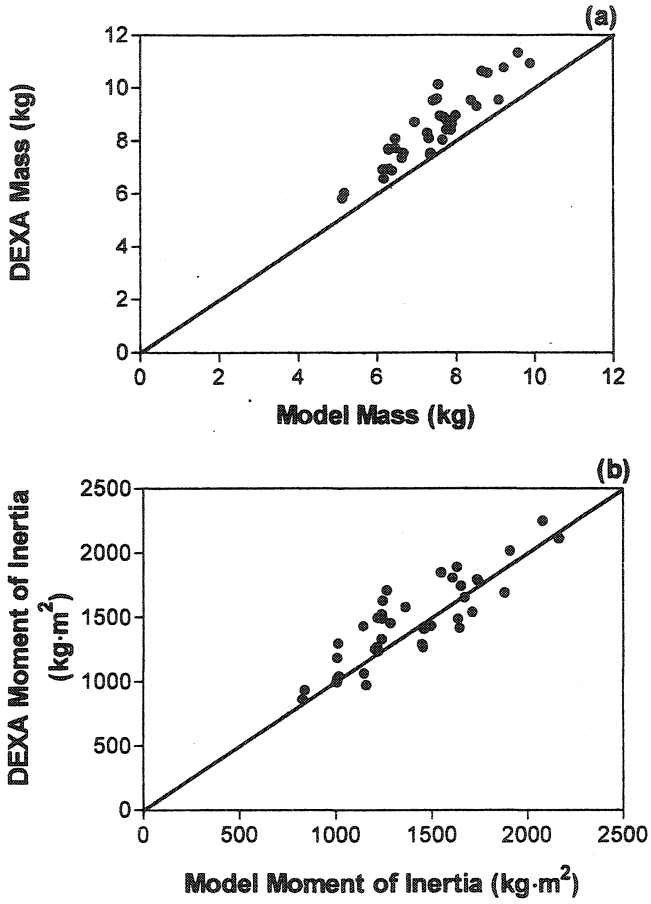

Figure 7. Scatterplots of model estimations vs. DEXA measurements of (a) mass and (b) I_{CM} for the Female (19-30 years) group. Solid line represents the unity line between the model predictions and DEXA measurements.

Table 9. Linear regression equations and coefficients of variation (r^2) resulting from correlating geometric model mass estimations with DEXA mass measurements.

Group	Regression Equation	r^2
Males (19-30 Years)	1.382x – 1.101	0.877
Females (19-30 Years)	1.219x + 0.332	0.893
Males (55+ Years)	2.302x – 6.998	0.927
Females (55+ Years)	1.279x – 0.716	0.784

x = Model mass (kg)

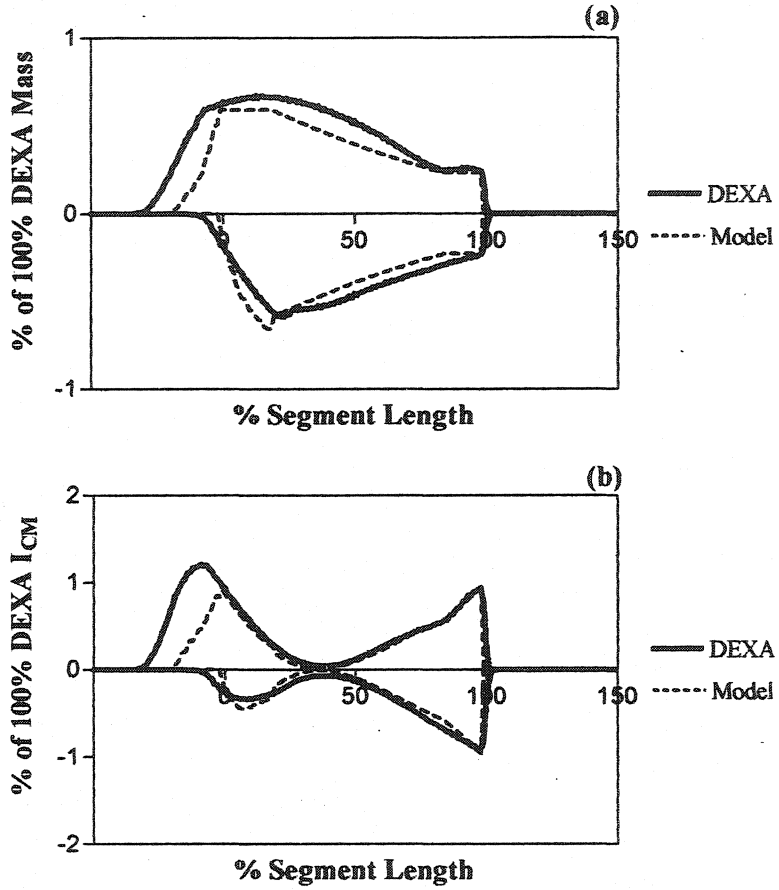

Figure 8. Ensemble averages of the (a) mass distribution properties and (b) I_{CM} distribution properties estimated by the developed model and measured by DEXA. Mean model estimates are displayed as a percent of DEXA mass to show where the model failed to estimate the desired parameter. The curves represent the mean ensemble averages from the male (19-30 years) group.

Table 10. Linear regression equations and coefficients of variation (r^2) resulting from correlating geometric model I_{CM} estimations with DEXA I_{CM} measurements.

Group	Regression Equation	r^2
Males (19-30 Years)	1.173x – 2.99	0.775
Females (19-30 Years)	0.954x + 139.09	0.810
Males (55+ Years)	1.945x + 780.43	0.618
Females (55+ Years)	1.196x + 52.68	0.625

x = Model I_{CM} ($kg \cdot m^2$)

I_{CM} measurements since mass from the proximal thigh would have been lost medially and then gained laterally at a distance further away from the CM. For these subjects, it is possible that the present model did not underestimate mass and I_{CM} quite as much at the proximal end as was indicated by the results.

An additional limitation of the segmentation patterns selected is that the methods differed slightly from those of Zatsiorsky et al. [15] and Dempster [6]. Zatsiorsky et al. [15] segmented the hip joint at an angle of 37° from the midline of the pelvis while this study sectioned the hip according to individual pelvic angles, which on average were approximately 20.5°. This difference should have resulted in an underestimation of mass and I_{CM} by the Zatsiorsky et al. [15] models when compared to DEXA measurements, however both these models overestimated thigh mass for all groups, the regression equations overestimated thigh I_{CM} for both male groups, and the geometric models overestimated I_{CM} for all groups except older males. It is therefore likely that errors from these models would have been larger if the segmentation methods were identical. Furthermore, Dempster [6] segmented his specimens in a flexed position, which was not possible with the DEXA method because subjects must be scanned in an extended position. Dempster [6] also made his cuts by slicing along the inguinal fold down to the bone, removing mass from the thigh in the gluteal region, a method which is not possible using DEXA where segmentation lines are limited to a plane perpendicular to that of the scan. The lack of tissue in the gluteal region should therefore have resulted in an

underestimation of thigh mass using the Dempster [6] equations when compared to the DEXA measurements, a trend that is positively displayed in the results.

The volunteers in this study were chosen to represent a wide variety of height and weight categories. As a result, some of the participants in the upper weight percentiles possessed large amounts of abdominal fat that lay over portions of the proximal thigh. Since this tissue could not be separated from the thigh in the digital image, some excess abdominal tissue may have been included in the digitization area and thus increased the mass and moment of inertia of the thigh segment at the proximal end. This problem was encountered for a few subjects in the older populations, possibly introducing error into the DEXA measurements.

The DEXA method requires that subjects be scanned while lying supine, a limitation that is common to many of the imaging techniques used to date including gamma-mass scanning, MRI and CT imaging. Since the subjects were lying down, some redistribution of tissues likely occurred which may have changed the inertial properties of the segments slightly. It has been assumed that this redistribution does not significantly change the body segment parameters measured and that although the anthropometric parameters were taken while the subjects were standing, these parameters would be similar if taken while lying supine. Since this limitation is inherent in the method, some amount of error in the results should be attributed to these differences.

The right and left thigh segments of each subject were treated as independent samples in the development and validation of the geometric model. Since these samples are not truly independent, the variability in the mass distribution characteristics of the

188 segments examined is less than would be if we examined one segment each from 188 subjects. However, individuals do display asymmetric characteristics and therefore, the variability is likely greater than would be obtained by including one segment from 94 subjects. It is believed that the variability in mass distribution characteristics included in this study is large enough to encompass the differences in morphology that exist in the general population for these age and gender groups.

DEXA is an imaging tool that is limited to providing mass distribution information in the frontal plane, therefore BSP measurements and model validations in this study were performed in one plane only. This is an issue that must be addressed in future research, however this study provides valuable insight into the benefits of using mass distribution properties to model human body segments for BSP estimation. The results have shown that humans are geometrically similar in the mass distribution properties of the thigh, indicating that one model can be applied to many adult populations. Furthermore, the results give an indication of the performance of other models in estimating thigh BSPs for different populations. Using DEXA to determine the mass distribution properties of segments provides advantages over other imaging techniques because it is significantly less onerous than MRI and CT imaging and requires less radiation than CT, allowing the development of large databases of subjects from which to develop models. The determination of mass distribution properties using DEXA in three dimensions will allow modification and validation of the present model in three dimensions and will enable the development of more accurate geometric models for the remaining segments of the human body.

Future research will involve the development and modification of geometric models in three dimensions in hopes of producing a whole body anthropometric model that accurately predicts human BSPs. However, the level of error that is acceptable for use in human motion analyses remains unknown. Pearsall and Costigan [27] evaluated the effect of BSP error on human gait analysis using a Monte Carlo method and found that errors of up to 40% significantly affected kinetic calculations, particularly during swing phase, although the effects were less than 1% body weight. Open chain movements or actions with high accelerations were presumed to be more sensitive to these errors, however. Furthermore, Cheng et al. [18] used MRI to directly measure BSPs from their subjects because the available models were thought to negatively affect lumbar moment calculations in lifting activities. The effect of BSP error on kinetic calculations likely depends on the movement being analyzed and should be considered in each movement problem. Furthermore, errors introduced by other parameters such as in marker digitization errors further obscures the true results. The reduction of BSP error therefore remains a valid and worthwhile endeavor. While BSP errors of the thigh segment may not have been significantly reduced in this study in comparison with some other models available, accurate knowledge of these errors is now available on a variety of human populations. Furthermore, a new method of developing geometric models is now available, possibly allowing further reduction of BSP error and validation of BSP estimates.

2.5 References

[1] Durkin, J. L., Dowling, J. J. and Andrews, D. M., 2002, "The Measurement of Body Segment Inertial Parameters Using Dual Energy X-Ray Absorptiometry", J Biomechanics, **35**(12), pp. 1575-1580.

[2] Pearsall, D. J. and Reid, J. G., 1994, "The Study of Human Body Segment Parameters in Biomechanics", Sports Med, **18**(2), pp. 126-140.

[3] Braune, W. and Fischer, O., 1889, "The Centre of Gravity of the Human Body as Related to the German Infantryman", ATI 138 452, National Technical Information Service, Leipzig.

[4] Chandler, R. F., Clauser, J. T., McConville, H. M., Reynolds, H. M. and Young, J. W., 1975, "Investigation of Inertial Properties of the Human Body", AMRL-TR-74-137, Aerospace Medical Research Laboratory, Wright-Patterson Air Force Base, Ohio.

[5] Clauser, C. E., McConville, J. T. and Young, J. W., 1969, "Weight, Volume, and Center of Mass of Segments of the Human Body", AMRL-TR-69-70, Aerospace Medical Research Laboratory, Wright Patterson Air Force Base, Ohio.

[6] Dempster, W. T., 1955, "Space requirements of the Seated Operator", WADC-TR-55-159, Wright Air Development Center, Wright Patterson Air Force Base, Ohio.

[7] Harless, E., 1860, "Die statischen Momente der menschlichen Gliedmassen", Abhandl Mathematische-Physikalischen Classe Konigl Bayerischen Akad Wissenschaft, **8**: pp. 69-96, 257- 294.

[8] Young, J. W., Chandler, R. F. and Snow, C. C., 1983, "Anthropometric and Mass Distribution Characteristics of the Adult Female", FAA-AM-83-16, FAA Civil Aeromedical Institute, Oklahoma.

[9] Drillis, R. and Contini, R., 1966, "Body Segment Parameters", TR-1166-03, New York University, School of Engineering Science, New York.

[10] Peyton, A. J., 1986, "Determination of the Moment of Inertia of Limb Segments by a Simple Method", J Biomechanics , **19**(5), pp. 405-410.

[11] Hanavan, E. P., 1964, "A Mathematical Model of the Human Body", AMRL-TR-64-102, Aerospace Medical Research Laboratory, Wright Patterson Air Force Base, Ohio.

[12] Jensen, R. K., 1978, "Estimation of the Biomechanical Properties of Three Body Types Using a Photogrammetric Method", J Biomechanics, **11**(8-9), pp 349-358.

[13] Hatze, H., 1980, "A Mathematical Model for the Computational Determination of Parameter Values of Anthropomorphic Segments", J Biomechanics, **13**(10), pp. 833-843.

[14] Zatsiorsky, V. and Seluyanov, V., 1983, "The Mass and Inertia Characteristics of the Main Segments of the Human Body", Biomechanics V-IIIB, H. Matsui. and K. Kobayashi "eds.", Human Kinetics Publishers Inc., Champaign, IL, pp. 1152-1159.

[15] Zatsiorsky, V., Seluyanov, V. and Chugunova, L. G., 1990, "Methods of Determining Mass-Inertial Characteristics of Human Body Segments", Contemporary Problems of Biomechanics, G.G. Chernyi and S.A. Regirer "eds.", CRC Press, Boston, pp. 272-291.

[16] Huang, H. K., 1983, "Evaluation of Cross-Sectional Geometry and Mass Density Distributions of Humans and Laboratory Animals Using Computerized Tomography", J Biomechanics, **16**(10), pp. 821-832.

[17] Pearsall, D. J., Reid, J. G. and Livingston, L. A., 1996, "Segmental Inertial Parameters of the Human Trunk as Determined from Computed Tomography", Ann Biomed Eng, **24**(2), pp. 198-210.

[18] Cheng, C.-K., Chen, H.-H., Chen, C.-S., Lee, C.-L. and Chen, C.-Y., 2000, "Segment Inertial Properties of Chinese Adults Determined from Magnetic Resonance Imaging", Clin Biomechanics, **15**(8), pp. 559-566.

[19] Martin, P. E., Mungiole, M., Marzke, M. W. and Longhill, J. M., 1989, "The Use of Magnetic Resonance Imaging for Measuring Segment Inertial Properties" J Biomechanics, **22**(4), pp. 367-376.

[20] Mungiole, M. and Martin, P. E., 1990, "Estimating Segment Inertial Properties: Comparison of Magnetic Resonance Imaging with Existing Methods", J Biomechanics, **23**(10), pp. 1039-1046.

[21] Durkin, J. L. and Dowling, J. J., 2003, "Analysis of Body Segment Parameter Differences Between Four Human Populations and the Estimation Errors of Four Popular Mathematical Models", J Biomech Eng. 125(4): 515-522.

[22] Ackland, T. R., Henson, P. W. and Bailey, D. A., 1988, "The Uniform Density Assumption: Its Effect Upon the Estimation of Body Segment Inertial Parameters", Int J Sport Biomech, **4**, pp. 146-155.

[23] Durkin, J.L., 1998, "The Prediction of Body Segment Parameters Using Geometric Modelling and Dual Photon Absorptiometry", Masters thesis, McMaster University, Hamilton.

[24] Wei, C. and Jensen, R. K., 1995, "The Application of Segment Axial Density Profiles to a Human Body Inertia Model", J Biomechanics, **28**(1), pp. 103-108.

[25] Demirjian, A., 1980, "Nutrition Canada Anthropometry Report: Height, Weight and Body Dimensions", Ottawa: Heath and Welfare Canada, pp. 28, 43.

[26] Winter, D. A., 1990, "Biomechanics and Motor Control of Human Movement", 2 Ed., John Wiley and Sons, Inc., New York, pp. 51-64.

[27] Pearsall, D.J. and Costigan, P.A., 1999, "The Effect of Segment Parameter Error on Gait Analysis Results", Gait and Posture, **9**(3), 173-183.

CHAPTER 3

GEOMETRIC SOLID MODELLING OF THE HUMAN FOREARM FOR BODY SEGMENT PARAMETER ESTIMATION

3.1 Introduction

Net joint forces and moments of force are calculated using inverse or forward dynamics methods to solve a number of kinetic problems. These may include identifying loading conditions of the lumbar spine in lifting activities, determining the efficacy of an exercise regimen in a rehabilitative protocol, or improving performance in a sport movement. Body segment inertial parameters (BSPs) are required to determine these net forces and moments of force and errors in their measurement may greatly affect kinetic estimates (Cheng et al., 2000). Early studies relied on cadavers for determining body segment masses, centre of mass locations and moments of inertia, carefully sectioning specimens and directly measuring these parameters on the segmented limbs (Braune and Fisher, 1889; Chandler et al., 1975; Clauser et al., 1969; Dempster, 1955). The limited availability of cadaveric specimens and the onerous task of sectioning and measuring the segments resulted in small sample sizes typically consisting of elderly Caucasian males. Furthermore, individual studies demonstrate different segmentation patterns, preventing the pooling of data.

Non-invasive measurement techniques have also been developed to directly measure BSPs from living subjects. Human body segments have been measured for volume using water immersion and the values converted to mass estimates using constant density values (Drillis and Contini, 1966; Plagenhoef, et al.,1983). These methods have

also been used to measure centre of mass location, however the assumption of constant density and the difficulties in measuring more proximal segments has resulted in limited use of this technique (Pearsall and Reid, 1994). Moments of inertia of distal body segments, such as the forearm and lower leg, have been measured using compound pendulum, quick release and oscillation techniques (Drillis and Contini, 1966; Peyton, 1986). These procedures assume that skeletal muscle involvement is negligible, however and therefore have not been considered reliable. Measuring BSPs directly on living humans has therefore proven difficult until recently with the development and increased availability of medical imaging technology.

Medical imaging tools such as gamma mass scanning, magnetic resonance imaging (MRI), computed tomography (CT) and dual energy x-ray absorptiometry (DEXA) have been used to determine BSPs accurately on living subjects. Zatsiorsky and Seluyanov (1983) used gamma-mass scanning to measure BSPs on young adult males and females. The results were considered reliable, however the machine is not available today, making the technique obsolete. Martin et al. (1989) used baboon cadaver segments to validate MRI as a BSP measurement tool. The method was accurate and safe but was very costly and laborious. This tediousness has precluded the analysis of many subjects and has discouraged its frequent use for direct BSP measurement. CT imaging has been used in a similar manner as MRI (Huang, 1983; Pearsall et al, 1996), yet the methods are bound by the same limitations, in addition to high radiation doses. Recently, DEXA has emerged as a method for determining BSPs from living subjects and offers the same level of accuracy as MRI and CT imaging. While the technology uses radiation to obtain mass

distribution information, the dosage is considered minimal and the method is rapid and simple. DEXA may not be readily available to most researchers, however, a limitation that diminishes its practicality.

Mathematical models such as regression equations and geometric models have been developed to provide a fast, accurate and convenient way of estimating BSPs for a group of subjects. Linear regression equations were developed using data from Dempster (1955) to predict segment masses from whole body mass and centre of mass locations and radii of gyration from segment length (Winter, 1990). These equations represent an expedient way of estimating BSPs, however they are based on elderly male cadaveric data that have not been validated on living subjects. Regression equations have also been developed from the cadaveric data of Chandler et al. (1975) and Clauser et al. (1969) and from the living subject experimental studies of Drillis and Contini (1966), Young et al. (1983) and Plagenhoef, et al. (1983). The integrity of these estimates are bound by the assumptions in the methods used to obtain the data and therefore remain less preferred sources in the literature. Zatsiorsky et al. (1990) later developed multiple regression equations using data from gamma-mass scanning, generating separate equations for young males and females. These models are considered reliable but are limited to a young Caucasian population. Furthermore, Durkin and Dowling (2003) developed linear regression equations for selected body segments on four human populations using DEXA and compared the accuracy of these estimates to other popular methods. The linear regression equations did not improve on estimates compared to other sources in the literature and it was found that no one BSP source performed best for a given segment,

BSP, or population group. Additionally, the regression equations adequately represented differences between the groups but did not account for individual variability within each population.

Geometric models of varying complexity have also been developed (Durkin, 1998; Hanavan, 1964; Hatze, 1980; Jensen, 1978; Zatsiorsky et al., 1990) to provide reasonable estimates of human BSPs. Hanavan (1964) used a series of ellipsoids, right circular cylinders and frusta to represent the body segments of young adult males. The models assumed constant density throughout the segments, however, and were validated for whole body mass and inertial properties only. Jensen (1978) used photogrammetry to develop elliptical models of human body segments in an effort to account for differences across age, gender, morphology, and race, although the models were validated for segment volume only and assumed constant density throughout. Hatze (1980) later developed a more detailed geometric model of the human body that has been considered reliable, but is largely avoided due to the required 242 anthropometric parameters needed. Models based on geometric considerations were developed by Zatsiorsky et al. (1990) for young male and female adults. The models were right circular cylinders scaled using mathematical constant to account for differences in shape and density between the model and the segment in question. Results were validated against gamma-mass scanning data and it was found that the geometric models performed better than the multiple regression equations developed in the same study. Recently, however, Durkin (1998) developed geometric models of selected body segments, each consisting of a composite of several geometric solids meant to accurately represent the changes in segment shape along the

length of the segment. The models were compared to DEXA measurements and were found to perform poorly, likely due to the assumption of constant density while modelling according to segment volume.

Durkin and Dowling (2003) found that linear regression equations developed in their study were superior to the geometric models of Hanavan (1964) and Zatsiorsky et al. (1990) in estimating BSPs, yet the regression equations still produced a significant amount of error. Two possible directions were suggested for improving the accuracy of predictive equations. The first was to develop multiple regression equations using a series of anthropometric parameters including limb circumferences and breadths. Individual sets of equations would be needed to represent differences according to age, race, gender and morphology, as population BSP variations have been clearly identified by Jensen (1989, 1994) and Durkin and Dowling (2003). The second option was to develop geometric models based on the mass distribution properties of segments rather than volume. This method would require a detailed analysis of the mass distribution properties of the human body on a segment by segment basis, followed by the development and validation of an appropriate geometric model. Geometric models constructed in this manner may have an advantage over multiple regression equations by encompassing the characteristics of a variety of populations as well as accounting for individual differences within groups. The purpose of this study is therefore to explore the mass distribution properties of one segment, the human forearm, for four human populations, to develop a geometric model accordingly, and to validate BSP estimates using DEXA. Model estimates from four other popular sources in the literature will also be evaluated by comparing against DEXA

measurements. It is hypothesized that there will be a high degree of geometric similarity in the mass distribution properties of the forearms between the four groups studied and that a geometric model based on these properties will estimate forearm BSPs with greater accuracy than the other models examined.

3.2 Methods

One hundred volunteers were recruited and matched to one of four groups separated by gender (male/female) and age (19-30 years old, 55+ years old). Average height and mass statistics for the 5^{th}, 25^{th}, 50^{th}, 75^{th} and 95^{th} percentiles of the Canadian population were obtained from Demirjian (1980) and 25 cells of unique height/mass combinations were constructed for each gender/age category. Subjects were recruited using posters on the McMaster University campus and within McMaster University Medical Centre. Participants included McMaster students and faculty as well as staff and visitors to the McMaster hospital. One volunteer from each group was selected to fill each cell, developing a subject database that represented a wide variety of height and mass combinations. Five participants from each group were randomly chosen to represent a model development group and the remaining 80 subjects were allotted to a model validation group (Tables 1 and 2). The mean heights and masses of both groups were normally distributed.

Each participant, clothed in a hospital gown and undergarments, was asked to lie supine on the DEXA scan table with forearms pronated, palms facing the table. A pronated forearm position was chosen due to width restrictions of the DEXA scan table.

Table 1. Descriptive statistics of model development group including mean ± standard deviation (SD) and range of participant ages, heights and masses.

			Age (Years)		Height (cm)		Mass (kg)	
Group	**N**	**n**	**Mean (SD)**	**Range**	**Mean (SD)**	**Range**	**Mean (SD)**	**Range**
Males (19-30 Years)	5	10	23.2 (2.7)	21.0-27.0	172.4 (6.3)	162.6-179.0	67.7 (10.7)	59.0-86.0
Females (19-30 Years)	5	10	21.2 (1.9)	19.0-24.0	165.1 (7.0)	155.0-173.0	56.6 (5.1)	50.0-63.6
Males (55+ Years)	5	10	67.8 (8.4)	58.0-76.0	176.2 (5.4)	170.0-183.0	83.2 (15.3)	70.0-106.0
Females (55+ Years)	5	10	62.4 (7.4)	55.0-73.0	161.5 (6.7)	153.0-170.0	57.8 (5.5)	51.0-65.5

N = number of participants, n = number of forearm segments examined

Table 2. Descriptive statistics of model validation group including mean ± standard deviation (SD) and range of participant ages, heights and masses.

			Age (Years)		Height (cm)		Mass (kg)	
Group	**N**	**n**	**Mean (SD)**	**Range**	**Mean (SD)**	**Range**	**Mean (SD)**	**Range**
Males (19-30 Years)	20	31	21.7 (1.7)	19.0-25.0	175.4 (7.4)	155.0-185.0	72.6 (11.2)	55.5-97.7
Females (19-30 Years)	20	38	21.7 (3.2)	19.0-30.0	163.3 (7.7)	152.0-180.0	56.5 (7.3)	47.0-70.5
Males (55+ Years)	20	30	68.3 (6.9)	55.0-78.0	174.5 (6.3)	162.6-188.0	80.4 (11.8)	59.0-107.7
Females (55+ Years)	20	26	68.0 (7.8)	56.0-83.0	158.9 (4.2)	150.0-170.2	61.2 (10.0)	50.9-86.4

N = number of participants, n = number of forearm segments examined

The subjects chosen for the study represented a large range of body sizes and the pronated position offered greater accommodation of hip width without touching the torso while still remaining within the scan field of view. One whole body DEXA scan was performed followed by a series of anthropometric measurements taken with a flexible tape measure accurate to ±0.05 cm (Table 3). All procedures were performed in compliance with approval from the McMaster University Research Ethics Board.

The DEXA scan files were processed as in Durkin et al. (2002). Digital images of the scan information were created including a density image (Fig. 1) to display the skeletal system and allow identification of bony landmarks, and a mass image (Fig. 2) to highlight the position of soft tissue. One whole body DEXA scan produces a data array of 146 x 112 mass elements, 1.32 cm x 0.53 cm in dimension. The spatial resolution of the mass data was increased by applying a cubic spline algorithm, interpolating the data to 40 times its original resolution. The spline was set to follow the data with as little smoothing as possible (Fig. 3) and resulted in a decrease in mass element size to 0.132 cm x 0.132 cm.

Table 3. Description of anthropometric measurements used in geometric models

Anthropometric Measurement	**Description**
Elbow Circumference	Circumference over olecranon process and over anterior crease of elbow with elbow in full extension and forearm supinated
Maximum Forearm Circumference	Largest circumference about forearm with elbow in full extension and forearm supinated
Forearm Length	Distance between lateral epicondyle and tip of distal radial styloid with elbow in full extension and forearm supinated

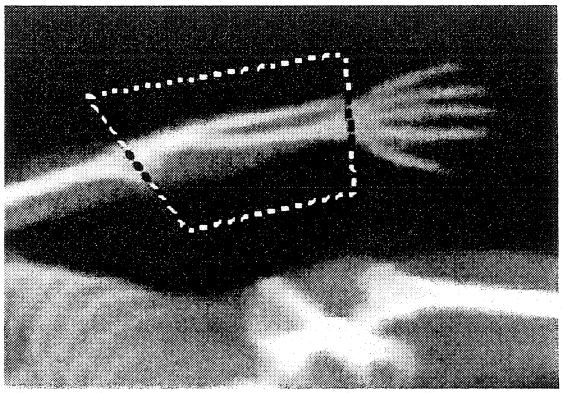

Figure 1. Partial display of density image created to make bony landmarks visible for forearm segmentation. Dashed line represents an example of forearm segmentation method.

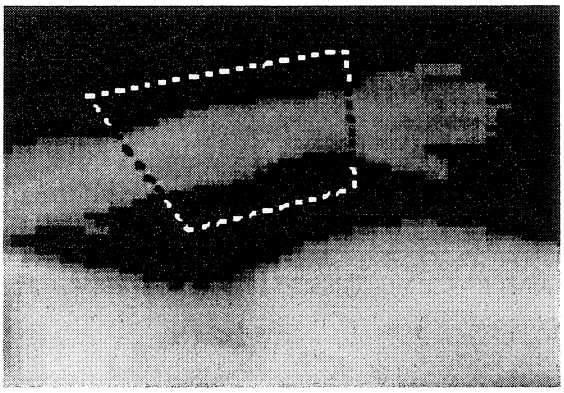

Figure 2. Partial display of mass image used to ensure all soft tissue is enclosed within segmentation area (dashed line).

The left and right forearms of each subject were segmented using custom software (DXA Digitization Software, Durkin, 1998) whereby the density image was used to section the segment following easily identifiable bony landmarks. The forearm was segmented at the elbow by a plane running in the anteroposterior direction, slicing through the lateral and medial epicondyles. The forearm was sectioned at the wrist by an anteroposterior plane slicing just distal to the distal radial and ulnar styloids. The proximal joint centre was selected as a point midway along the segmentation plane

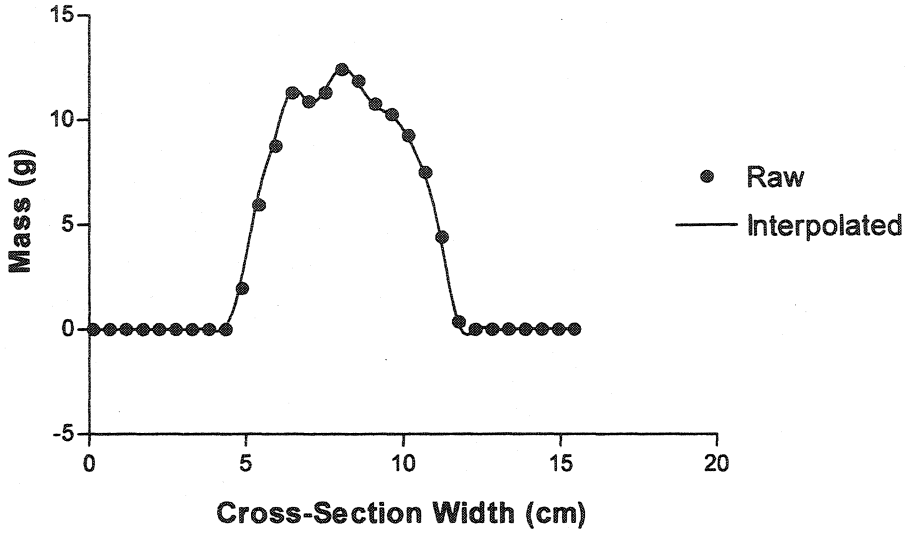

Figure 3. Example of interpolated data closely following raw data points with little smoothing effects. Cross-section is through right mid-forearm of a young female subject.

between the lateral and medial epicondyles and the distal joint centre was chosen as a point midway along the segmentation plane between the distal ulnar and radial styloids. Other segmentation points encircling the forearm were selected to ensure that all soft tissue was enclosed within the digitized area by toggling between the density and mass images.

BSP information was calculated from the segmented mass area as in Durkin et al. (2002) including forearm mass, centre of mass in the longitudinal direction (CM_x), centre of mass location in the mediolateral direction (CM_y) and moment of inertia about the centre of mass (I_{CMz}). The segmented mass array was then rotated to ensure that a line connecting the proximal and distal endpoints represented the horizontal axis.

Mass distribution information of the forearm was obtained by normalizing each data array to 100% segment length and 100% segment mass. Mass elements within each 1% segment length interval were summed and divided by the total forearm mass. Furthermore, separate distribution curves were created for mass lateral and medial to the proximal-to-distal segment line. The result was a mass distribution plot for the forearm segment normalized to 100% segment length with the area between the lateral and medial distribution curves equaling 100% segment mass. The mass distribution plots of the right forearms were then inverted to match the left segment plots and were treated as independent samples.

An ensemble average of the forearm mass distribution plots was created for each of the four populations from the model development group to yield the mean (±SD) mass distribution for each group (Fig. 4). The graphs were then examined visually for geometric similarity and were examined statistically by correlating the percent of 100% segment mass values between the groups (y-axis of Fig. 4) and calculating the Pearson Product Moment Correlation Coefficients. Correlations were performed separately for mass lateral and medial to the proximal-to-distal segment line. These mass distribution plots were then used for model development.

Model BSP estimation errors were determined by calculating the BSP estimations using the geometric equations developed and comparing to DEXA measurements by calculating the root mean squared error (RMSE) for each group and each BSP. Estimation errors from four other popular models in the literature were also determined using the methods in the corresponding papers. Forearm BSPs were determined using the

regression equations of Dempster (1955) (via Winter, 1990) (D), the geometric models of Hanavan (1964) (H) and both the multiple regression equations (ZR) and geometric models (ZG) of Zatsiorsky et al. (1990). These estimates were determined and compared to DEXA measurements by calculating the RMSE's. One way repeated measure Analyses of Variance (ANOVA) were performed for each group and each BSP to determine whether significant differences existed between model estimate errors. Squared error values used in the RMSE calculations were compared in the ANOVAs followed by Tukey HSD post hoc analyses to determine where these differences lay.

3.3 Results

3.3.1 Geometric Similarity

Visual inspection of the mass distribution plots indicated geometric similarity between groups. The high Pearson Product Moment correlations (Tables 4, 5) confirmed this observation, supporting the development of one geometric model to predict BSPs for all four groups. Within group variability in forearm mass distribution was examined by summing the standard deviation values along the segment length of the mean mass distribution plots. Standard deviations amounted to 38% of forearm mass for the younger male group, 39% for the younger female group, 34.8% for the older female group and 22.8% for the older male group. Individual variability in forearm mass distribution thus seemed to decrease with age and was higher in females than in males.

Figure 4. Ensemble average of mass distribution plots as determined from DEXA. Positive and negative y-axis values represent lateral and medial forearm mass distribution, respectively. The inner lines represent mean mass distribution and the outer lines represent positive standard deviations. The area between the mean curves represents 100% forearm mass.

Table 4. Linear regression equations and Pearson Product Moment Correlations comparing mean lateral forearm mass distribution information as obtained by DEXA for model development groups. OM = Males (55+ Years), OF = Females (55+ Years), YM = Males (19-30 Years), YF = Females (55+ Years).

Groups Correlated	Linear Regression Equation	Pearson r
OM vs. OF	OF = 0.0604 + 1.0170(OM)	0.895
OM vs. YM	YM = 0.0214 + 0.8528(OM)	0.906
OM vs. YF	YF = 0.0190 + 0.8750(OM)	0.927
OF vs. YM	YM = -0.0216 + 0.8228(OF)	0.992
OF vs. YF	YF = -0.0146 + 0.8219(OF)	0.989
YM vs. YF	YF = 0.0081 + 0.9959(YM)	0.993

Table 5. Linear regression equations and Pearson Product Moment Correlations comparing mean medial forearm mass distribution information as obtained by DEXA for model development groups. OM = Males (55+ Years), OF = Females (55+ Years), YM = Males (19-30 Years), YF = Females (55+ Years).

Groups Correlated	Linear Regression Equation	Pearson r
OM vs. OF	OF = 0.0203 + 0.6880(OM)	0.850
OM vs. YM	YM = 0.0485 + 0.9644(OM)	0.829
OM vs. YF	YF = 0.0301 + 1.0052(OM)	0.914
OF vs. YM	YM = 0.0144 + 1.4275(OF)	0.994
OF vs. YF	YF = 0.0298 + 1.3236(OF)	0.974
YM vs. YF	YF = 0.0216 + 0.9118(YM)	0.964

3.3.2 Model Development

Three geometric models were developed in an attempt to accurately estimate forearm segment inertial properties. Each model consisted of a composite of 4 geometric shapes. The proximal segment was represented by a right circular cylinder, the second and third segments were decreasing right circular frusta and the distal segment was an increasing right circular frustum (Fig. 5).

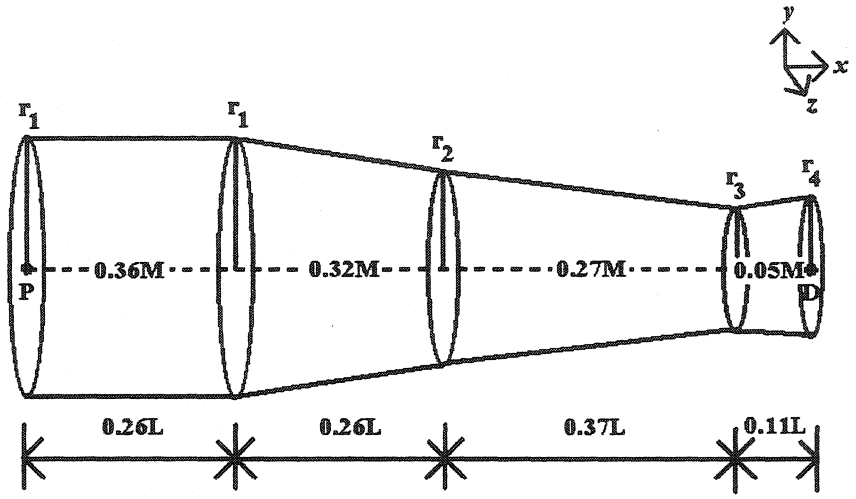

Figure 5. Schematic of 4-segment geometric model of the human forearm. The individual segments are scaled to percentages of forearm mass (M) and proportions of forearm length (L) running from proximal (P) to distal (D) ends.

Model 1 consisted of a 4-segment model requiring the input of three anthropometric parameters (Table 3). Radius r_1 was determined by calculating the mean of the elbow and maximum forearm radii. These radii were determined from their corresponding circumferences (radius = circumference / 2π). Length proportions for each model segment were determined by visually inspecting the mass distribution plots (Fig. 4) and selecting breakpoints that were common between all four groups. Mass proportions for each model segment were determined by summing the percent of 100% forearm mass values from the mass distribution plots (y-axis values, Fig. 4) within the length proportion boundaries for each group. An average of the group values was then

calculated for each model section to determine the appropriate segment mass proportions. The density (ρ) of the entire model was set at 0.0013 kg cm^{-3} (Winter, 1990).

Given the model section mass proportions, measured elbow and maximum forearm circumferences and segment lengths, the remaining radii were determined mathematically. First, the volume of the proximal segment (V_1) was determined using the formula for the volume of a cylinder:

$$V_1 = \pi r_1^2 h_1 \quad (1)$$

where h_1 = 0.26L. Since density is constant and the mass of the proximal segment (M_1) is equal to 0.36M, V_1 = 0.36V and the remaining radii can be calculated as follows:

$$V = \frac{V_1}{0.36} \quad (2)$$

$$V_2 = 0.32V = \frac{\pi h_2}{3}\left(r_1^2 + r_1 r_2 + r_2^2\right) \quad (3)$$

where h_2 = 0.26L. Balancing the equation to solve for r_2 results in a quadratic equation:

$$r_2 = \left(-b_2 + \sqrt{b_2^2 - 4a_2 c_2}\right)/2a_2 \quad (4)$$

where:

$$a_2 = \pi h_2 / 3 \quad (5)$$

$$b_2 = a_2 r_1 \quad (6)$$

$$c_2 = \left(a_2 r_1^2\right) - V_2 \quad (7)$$

V_3 and V_4 are calculated as:

$$V_3 = 0.27V = \frac{\pi h_3}{3}\left(r_2^2 + r_2 r_3 + r_3^2\right) \quad (8)$$

$$V_4 = 0.05V = \frac{\pi h_4}{3}\left(r_3^2 + r_3 r_4 + r_4^2\right) \quad (9)$$

where $h_3 = 0.37L$ and $h_4 = 0.11L$. r_3 and r_4 were calculated as was r_2:

$$r_3 = \left(-b_3 + \sqrt{b_3^{\,2} - 4a_3c_3}\right)/2a_3 \quad (10)$$

$$a_3 = (\pi h_3)/3 \quad (11)$$

$$b_3 = a_3 r_2 \quad (12)$$

$$c_3 = \left(a_3 r_2^2\right) - V_3 \quad (13)$$

$$r_4 = \left(-b_4 + \sqrt{b_4^{\,2} - 4a_4c_4}\right)/2a_4 \quad (14)$$

$$a_4 = (\pi h_4)/3 \quad (15)$$

$$b_4 = a_4 r_3 \quad (16)$$

$$c_4 = \left(a_4 r_3^2\right) - V_4 \quad (17)$$

Mass estimations for Model 1 were determined by multiplying the calculated volumes of the four segments by ρ and summing the four values:

$$M_1 = V_1 \rho \quad (18)$$

$$M_2 = V_2 \rho \quad (19)$$

$$M_3 = V_3 \rho \quad (20)$$

$$M_4 = V_4 \rho \quad (21)$$

$$M = M_1 + M_2 + M_3 + M_4 \quad (22)$$

The centre of mass locations for each model section were calculated according to the geometric properties of the segment shape. The centre of mass of the first segment (CM_1) was calculated as $0.5h_1$ which was equal to the centre of mass from the proximal

end (CM_{P1}). The centre of mass of the right circular frusta were calculated as in Hanavan (1964) and were converted to locations from the proximal end by:

$$CM_{P2}=CM_2+h_1 \tag{23}$$

$$CM_{P3}=CM_3+h_1+h_2 \tag{24}$$

$$CM_{P4}=CM_4+h_1+h_2+h_3 \tag{25}$$

The centre of mass of the entire composite from the proximal end (CM_P) was then calculated as:

$$CM_P=\left[\left(CM_{P1}M_1\right)+\left(CM_{P2}M_2\right)+\left(CM_{P3}M_3\right)+\left(CM_{P4}M_4\right)\right]/M \tag{26}$$

The moment of inertia of the first segment about its own centre of mass (I_{CM1}) was calculated as:

$$I_{CM1}=\frac{1}{12}M_1\left(h_1^2+3r_1^2\right) \tag{27}$$

and was converted to a moment of inertia about the proximal end (I_{P1})using parallel axis theorem:

$$I_{1P}=I_{CM1}+M_1CM_{P1}^2 \tag{28}$$

The moments of inertia of the remaining segments about their own centres of mass (I_{CM2}, I_{CM3}, and I_{CM4}) were calculated using equations for the I_{CM} of a right circular frusta as described in Hanavan (1964) and were converted to moments of inertia about the proximal end using parallel axis theorem as in Eq. 28. The moment of inertia of the entire

composite about the proximal end (I_P) was then calculated by summing the individual inertial calculations:

$$I_P = I_{P1} + I_{P2} + I_{P3} + I_{P4} \quad \textbf{(29)}$$

The moment of inertia of the entire composite about its centre of mass (I_{CM}) was calculated using parallel axis theorem:

$$I_{CM} = I_P - MCM_P^2 \quad \textbf{(30)}$$

BSP estimation errors for Model 1 were determined by applying the equations to the subjects in the model validation group and calculating the root mean squared errors (RMSE) between the model estimations and the benchmark DEXA measurements. Mass and I_{CM} estimation errors were reported as a %RMSE in units of %DEXA mass or I_{CM} whereas CM_x and CM_y estimation errors were reported as a RMSE in units of % segment length. CM errors were reported as RMSEs because calculating %RMSE with the mediolateral symmetry assumption of the models would result in 100% error when compared to the non-zero DEXA values. It was thought that reporting CM error terms in units of % segment length would more clearly highlight the magnitude of model errors.

Mass and I_{CM} distribution plots were created for the model estimations and ensemble averages were performed for each group. To identify where the model failed to estimate forearm mass and I_{CM}, the distribution plots were represented as a % of DEXA forearm mass or I_{CM} and overlaid with the DEXA distribution plots. The RMSE values showed rather high errors and the distribution plots revealed an overestimation of forearm

mass at the proximal end, indicating that the mean of the elbow and maximum forearm radii were poor predictors of proximal forearm mass.

Model 2 was constructed in a similar manner to Model 1 but used elbow radius alone as a measure of r_1. Model 2 was applied to the model validation group and the results were evaluated in a similar manner to Model 1. The results showed that elbow circumference was still a poor estimator of proximal forearm mass as an overestimation was obvious in Figure 6.

Model 3 was developed in a similar manner to Models 1 and 2 with r_1 represented as a scaled version of elbow radius (r_s). A slice 1% segment length in width was extracted from the mass distribution plots of each individual within the model development group. The 20th segment length slice was chosen from the proximal forearm, the volume of which was set to represent a circular cylinder and a value for r_s was determined by:

$$r_s = \sqrt{\frac{V_{20}}{\pi L 0.01}} \tag{31}$$

where V_{20} = volume of a cylinder within the 20th percent segment length column of the mass distribution plot and L = measured segment length.

$$V_{20} = \left(\frac{\%of100\%mass}{100}\right)\left(\frac{totalDEXAmass}{\rho}\right) \tag{32}$$

The measured elbow radii (r_1) were then correlated with the scaled radii (r_s) for the 20 model development subjects using linear regression analysis with a y-intercept forced to zero (Fig. 7).

Model 3 was then applied to the model validation group as was Models 1 and 2 with r_1 = 0.938 x elbow radius. BSP estimation errors were calculated for Model 3 by determining the RMSE's for each group and the mean model mass and I_{CM} distribution plots were overlaid with the DEXA data to determine where the model failed (Fig. 6).

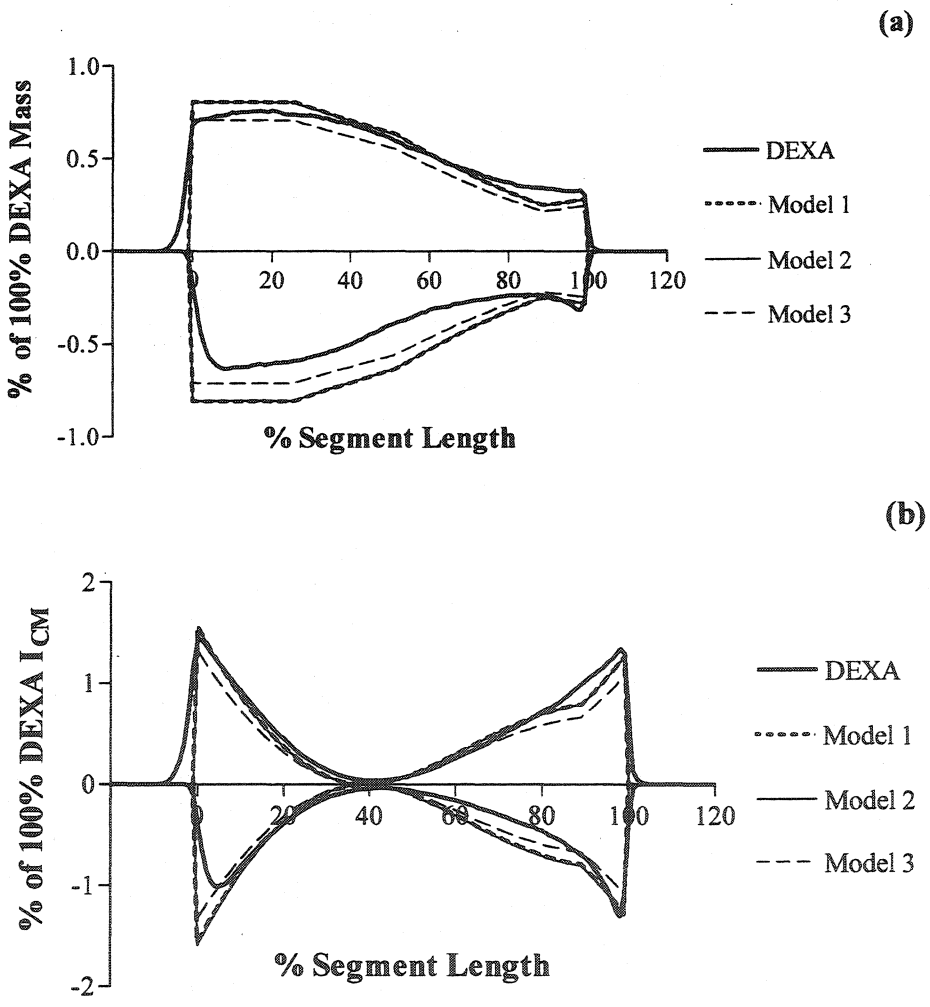

Figure 6. Mean distribution plots of Model 1, Model 2 and Model 3 and DEXA forearm mass for Females (55+ Years). Distribution plots of Model 1, Model 2 and Model 3 are normalized to 100% DEXA forearm mass. Models 1 and 2 are nearly identical in shape and therefore overlie each other on the plot.

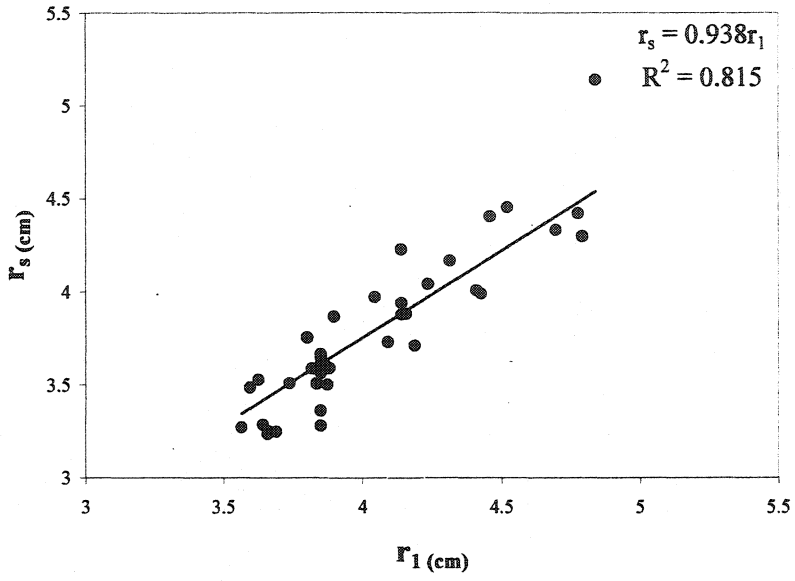

Figure 7. Linear correlation of measured elbow radius (r_l) vs. scaled elbow radius (r_s) for all subjects in model development group.

3.3.3 Model Accuracy

The mass distribution plots showed an overestimation of mass at the proximal end with all models. Models 1 and 2 were almost identical in their tracings and obviously overestimated mass at the proximal end. Model 3 improved on these estimates for all groups but still resulted in an overestimation of mass at the elbow. Models 1 and 2 underestimated mass at the distal end for all groups but less so for the older groups. Model 3 resulted in a greater underestimation of mass at the distal end than Models 1 and 2 for all groups.

Examining the I_{CM} distribution plots showed an overestimation at the proximal end by Models 1 and 2 with a smaller overestimation by Model 3. At the distal end, Models 1 and 2 resulted in slightly underestimated inertia with further underestimation

using Model 3 for the older groups. The younger groups showed a slight overestimation of inertia at the distal end for models 1 and 2 whereas Model 3 closely approached DEXA measurements in this region.

Linear correlations comparing M1, M2 and M3 estimations with DEXA measurements for mass and I_{CM} show that Models 1 and 2 overestimated forearm mass for all groups and that Model 3 improved on these estimates (Fig. 8, Table 6). Models 1 and 2 resulted in both over and underestimations in I_{CM}, however, and the application of Model 3 resulted in overall underestimations of I_{CM} (Fig. 9, Table 7). A greater difference in I_{CM} error was seen from M1 and M2 to M3 in the male subjects, whereas the female groups showed a lesser decrease in accuracy.

Model 1 (M1) and Model 2 (M2) provided poor estimations of forearm mass in comparison with the other models (Table 8). On average, mass estimations for all models were more accurate for the male groups than the female groups. Comparisons of average model estimates with DEXA measurements revealed that D, ZR and ZG overestimated mass compared to DEXA measurements for the female groups and underestimated massfor the male groups. H overestimated mass for all populations and all seven models resulted in greater mass estimation error for the female groups than the male groups. Repeated measures ANOVAs showed that significant differences existed between the error terms for the models in all groups. Model 3 (M3), D, ZR and ZG appeared to provide the most accurate estimations and the Tukey HSD post hoc analyses showed that Model 3 was not significantly better or worse than D, ZR or ZG for all groups. H was

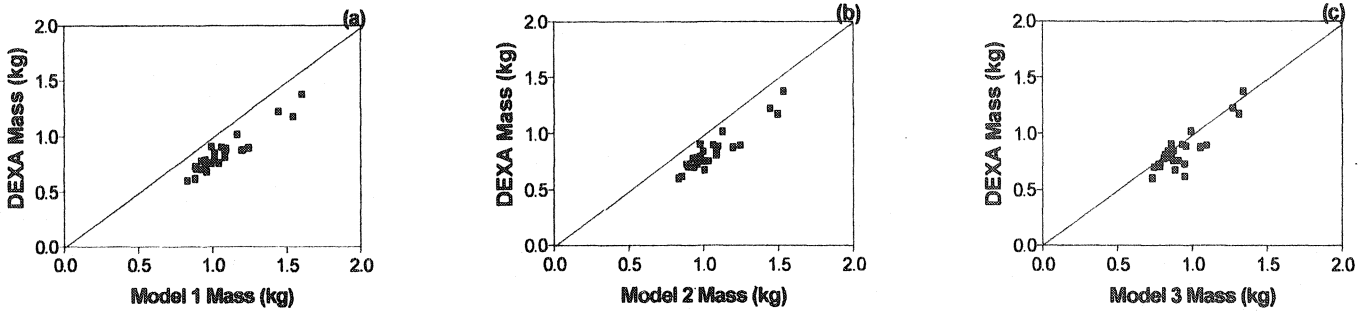

Figure 8. Scatterplots of model forearm mass estimations compared with DEXA forearm mass estimations for Females (55+ Years). (a) Model 1 (b) Model 2, (c), Model 3. Solid lines represent unity line where Model mass = DEXA mass

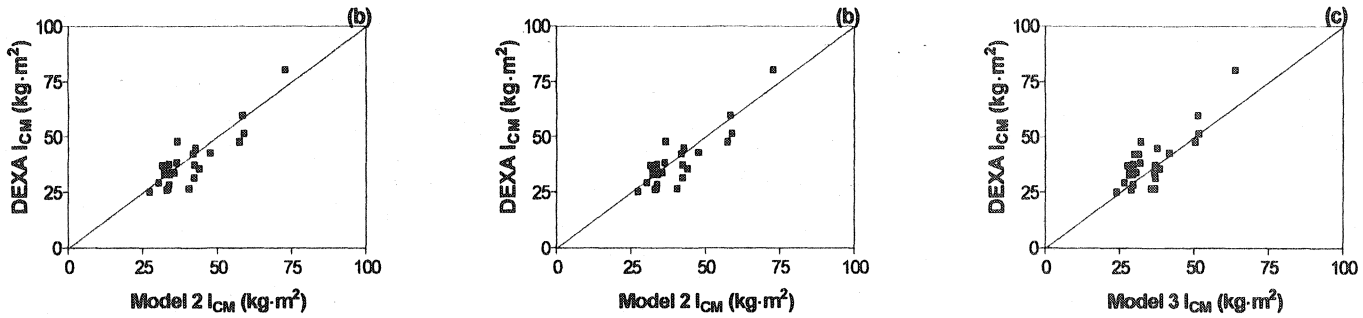

Figure 9. Scatterplots of model forearm I_{CM} estimations compared with DEXA forearm I_{CM} estimations for Females (55+ Years). (a) Model 1 (b) Model 2, (c), Model 3. Solid lines represent unity line where Model mass = DEXA mass

Table 6. Linear regression equations and coefficients of variation of comparisons between model estimates and DEXA forearm mass measurements.

	Model 1		Model 2		Model 3	
Group	**Linear Regression Equation**	**r^2**	**Linear Regression Equation**	**r^2**	**Linear Regression Equation**	**r^2**
Males (19-30 Years)	y=0.841x+0.051	0.80	y=0.766x+0.197	0.69	y=0.871x+0.198	0.68
Females (19-30 Years)	y=0.961x-0.112	0.64	y=0.990x-0.124	0.68	y=1.125x-0.124	0.68
Males (55+ Years)	y=0.879x-0.035	0.75	y=0.887x-0.045	0.70	y=1.009x-0.437	0.70
Females (55+ Years)	y=0.852x-0.058	0.89	y=0.888x-0.089	0.86	y=0.948x-0.032	0.76

y = DEXA mass (kg), x = model mass (kg)

Table 7. Linear regression equations and coefficients of variation of comparisons between model estimates and DEXA forearm I_{CM} measurements.

	Model 1		Model 2		Model 3	
Group	**Linear Regression Equation**	**r^2**	**Linear Regression Equation**	**r^2**	**Linear Regression Equation**	**r^2**
Males (19-30 Years)	y=0.849x+13.220	0.77	y=0.813x+17.620	0.72	y=0.940x+16.760	0.71
Females (19-30 Years)	y=0.985x-1.369	0.67	y=1.016x+0.852	0.70	y=1.158x+0.847	0.70
Males (55+ Years)	y=0.938x+0.568	0.77	y=0.979x-0.730	0.76	y=1.046x+1.806	0.66
Females (55+ Years)	y=1.028x+2.171	0.71	y=1.032x+1.643	0.74	y=1.175x+2.060	0.71

y = DEXA I_{CM} (kg m^2), x = model I_{CM} (kg m^2)

Table 8. % RMSE values and ANOVA results of model mass estimates compared with DEXA mass measurements. RMSE values are in units of % DEXA forearm mass.

Group	M1	M2	M3	D	H	ZR	ZG	F	p
Males (19-30 Years)	16.7	14.8	9.2	11.3	8.7	10.0	5.4	8.8	< 0.001
Female (19-30 Years)	27.6	25.5	15.8	23.0	34.0	21.1	17.3	14.0	< 0.001
Males (55+ Years)	19.7	19.9	9.1	9.3	15.3	9.2	7.1	19.8	< 0.001
Female (55+ Years)	27.7	27.2	16.4	21.8	35.9	15.6	14.8	17.6	< 0.001

M1 = Model 1, M2 = Model 2, M3 = Model 3, D = Dempster (1955) via Winter (1990), H = Hanavan (1964), ZR = Multiple regression equations from Zatsiorsky et al. (1990), ZG = Geometric equations from Zatsiorsky et al. (1990).

Table 9. RMSE values and ANOVA results of model CM_x estimates compared with DEXA CM_x measurements. RMSE values are in units of % forearm segment length.

Group	M1	M2	M3	D	H	ZR	ZG	F	p
Males (19-30 Years)	1.6	1.6	1.6	2.0	1.3	4.9	8.8	235.3	< 0.001
Female (19-30 Years)	2.6	2.6	2.6	1.5	1.6	1.9	7.9	209.4	< 0.001
Males (55+Years)	1.6	1.6	1.6	1.8	1.5	5.6	8.6	160.4	< 0.001
Female (55+Years)	1.9	1.9	1.9	2.1	2.0	2.0	8.7	187.6	< 0.001

M1 = Model 1, M2 = Model 2, M3 = Model 3, D = Dempster (1955) via Winter (1990), H = Hanavan (1964), ZR = Multiple regression equations from Zatsiorsky et al. (1990), ZG = Geometric equations from Zatsiorsky et al. (1990).

Table 10. RMSE values and ANOVA results of model CM_y estimates compared with DEXA CM_y measurements. RMSE values are in units of % forearm length.

Group	M1	M2	M3	D	H	ZR	ZG
Males (19-30 Years)	1.4	1.4	1.4	1.4	1.4	1.4	1.4
Female (19-30 Years)	2.9	2.9	2.9	2.9	2.9	2.9	2.9
Males (55+ Years)	2.2	2.2	2.2	2.2	2.2	2.2	2.2
Female (55+ Years)	2.6	2.6	2.6	2.6	2.6	2.6	2.6

M1 = Model 1, M2 = Model 2, M3 = Model 3, D = Dempster (1955) via Winter (1990), H = Hanavan (1964), ZR = Multiple regression equations from Zatsiorsky et al. (1990), ZG = Geometric equations from Zatsiorsky et al. (1990).

Table 11. % RMSE values and ANOVA results of model I_{CM} estimates compared with DEXA I_{CM} measurements. RMSE values are in units of % DEXA forearm I_{CM}.

Group	M1	M2	M3	D	H	ZR	ZG	F	p
Males (19-30 Years)	10.8	13.4	20.7	10.6	11.2	18.8	14.1	12.5	< 0.001
Female (19-30 Years)	14.7	14.0	18.6	32.4	31.1	17.3	15.2	15.6	< 0.001
Males (55+ Years)	12.5	12.8	19.2	14.5	15.7	18.7	16.9	2.9	< 0.01
Female (55+ Years)	17.9	17.5	18.7	43.3	43.6	23.8	20.7	7.6	< 0.001

M1 = Model 1, M2 = Model 2, M3 = Model 3, D = Dempster (1955) via Winter (1990), H = Hanavan (1964), ZR = Multiple regression equations from Zatsiorsky et al. (1990), ZG = Geometric equations from Zatsiorsky et al. (1990).

significantly worse than all other models for all groups except younger males and D had significantly less error than M1 and M2 for both male groups.

Longitudinal centre of mass calculations showed that D, H, ZR and ZG all overestimated CM_x compared with DEXA measurements for all groups (Table 9). Conversely, M1, M2 and M3 predicted CM_x location at 40% segment length, resulting in a slight underestimation compared with DEXA measurements. Repeated measures ANOVAs revealed significant differences between model error terms for all groups. CM_x estimates by M1, M2 and M3 were identical and therefore were not significantly different from each other. Tukey post hoc analyses showed that only ZG had significantly more error than the other models for the female groups whereas ZR and ZG had significantly more error than the other models for the male groups. In the latter case, ZR also had significantly less error than ZG.

Each of the seven models examined assumed mediolateral symmetry, therefore all CM_y estimations were identical (Table 10). This symmetry resulted an underestimation of the slightly lateral CM_y location determined through the DEXA measurements. ANOVAs were not performed to identify differences between the groups for this BSP.

I_{CM} calculations showed that D overestimated I_{CM} for the female groups and underestimated I_{CM} for the male groups (Table 11). Furthermore, ZR and ZG were found to underestimate I_{CM} for all groups while H overestimated I_{CM} for all groups. Repeated measures ANOVAs revealed statistically significant differences between models for all groups. On average, I_{CM} estimation errors from M3 were greater than those from M1 and M2, however the results were statistically significant for the male groups only. D and H

produced the greatest errors for the female groups and the only significant difference found in the older male group was between M1 and M3. The younger males were predicted equally well by M1, M2, D, H and ZG whereas M3 and ZR provided poor I_{CM} estimations for this group.

3.4 Discussion

Three geometric models were developed to represent the mass distribution properties of the forearm for four human populations as determined from DEXA and each model was an adaptation of the previous one in an attempt to reduce errors in BSP estimation. The models were validated by applying geometric formulas to 80 subjects from four populations and comparing the results to benchmark DEXA measurements. Four other popular models currently available in the literature were also examined by applying the respective equations to the model validation groups and comparing estimations with DEXA measurements. On average, M1, M2, M3, ZR and ZG provided the lowest errors in BSP estimation, the results of which, depending on the group and BSP, were not significantly different from each other. Furthermore, the adjustments made for Model 3 significantly improved mass estimations at the expense of I_{CM} accuracy due to greater underestimations at the distal end.

The participants in this study were selected to represent a wide range of height and mass combinations, therefore each group demonstrated large variations in body morphology. Furthermore, racial origin was not controlled, resulting in a collection of individuals with diverse backgrounds including Caucasian, African-, Asian-, Indo- and

Native-Canadians. These large morphological and racial differences may partially account for the variability in forearm mass distributions seen within the groups. Furthermore, standard deviations were found to decrease with age, possibly due to specific age-related characteristics. The participants selected for this study were not controlled by activity level, therefore some subjects may have demonstrated significantly more muscle mass than less active subjects. These differences may have been greater in the younger groups, partially contributing to the larger standard deviations in the younger samples. The mass distribution standard deviations were also found to be lowest in the older male group. A possible reason for this could be the greater similarity in height and mass profiles of individuals within this group compared to the other samples. Fitting volunteers into the lower height/mass cells for the older male group proved to be difficult, therefore slightly more homogeneous height and mass characteristics are represented in this sample. This resulted in distributions that were skewed slightly towards the higher end and may have correspondingly decreased the mass distribution variability for this group.

The right and left forearms of each subject in this study were treated as independent samples. These limbs are not truly independent, however, resulting in mass distribution variability that is less than what would be found with a research protocol using one limb from twice as many subjects. Due bilateral asymmetry, it is likely that the variability represented in this study is greater than what would be found by incorporating only one limb from each participant in the analysis. It is believed that the amount of mass

distribution variability provided by the samples is sufficient to represent the characteristics of the representative populations at large.

Models 1, 2 and 3 estimated BSPs with errors similar to those of the other models examined in this study. While these models may not have dramatically improved BSP estimates, the results show that geometrically representing mass distribution improves BSP estimations over models that mimic segment volume. Furthermore, the results show that one model has the potential to account for differences both within and between groups. One reason the models in this study did not improve on current estimates could be due to the transverse symmetry of the chosen shapes. Limb circumferences were used to determine joint radii and segment mass distribution properties were estimated using circular geometric solids. Greater accuracy may be obtained with the use of limb breadths and the development of elliptical models to more accurately account for differences between the frontal and sagittal planes. Such transverse differences may explain why the female subjects displayed greater error in mass and I_{CM} estimations than the male subjects, possibly a result of differences in adipose content.

Development of an elliptical forearm model may improve BSP estimates, however validation of geometric models in other planes using DEXA is an issue that must be addressed in the future. DEXA is a two-dimensional imaging technique that currently limits the validation of models to the frontal plane. Since the forearm is a distal segment, it is possible to perform two scans, one in the frontal plane and another in the sagittal plane. Arrangement of the forearm to ensure a perfectly orthogonal view while maintaining wrist and elbow transverse positions (pronation-supination) would be

extremely difficult since this situation would require the subject to lie in a non-supine manner which may be difficult to standardize and maintain. The two-dimensional nature of this study is a limitation that must be overcome in the future, however the results of this study remain beneficial by demonstrating geometric similarity between different populations. The results further demonstrate the potential of geometric models for providing accurate BSP estimations by representing segmental mass distribution properties.

The results of the models developed in this study closely approximated those of Zatsiorsky et al. (1990). While Zatsiorsky et al. (1990) used rather simple cylindrical models, a constant was applied to the models to account for differences between model shape and density compared to those of the forearm. These models performed as well as M3 for mass and as well as M1 and M2 for I_{CM}. ZR and ZG produced the largest errors in CM_x position, however, particularly ZG, which resulted in differences of approximately 8% of segment length. For a forearm length of 26 cm, this would result in an overestimation of CM_x by 2 cm.

The results from Dempster (1955) showed rather large errors for mass and I_{CM} for the female subjects when compared to DEXA measurements. These errors may be partially attributed to a slight disparity in segmentation methods. Dempster (1955) sectioned limbs while frozen in a flexed position of 70° that appeared to be in neutral rotation about the longitudinal axis. Conversely, this study required that the subjects lie supine with forearms pronated, palms facing the table. This position resulted in a partially flexed elbow angle that varied slightly from subject to subject but was less than 70°.

Elbow flexion differences may have altered mass and I_{CM} properties at the proximal end and the pronated position of our study may have resulted in I_{CM} differences at the distal end. BSP estimates between M1, M2, M3 and Dempster (1955) were not significantly different for the male subjects, however, suggesting that the effects of these segmentation differences were minimal, particularly given the similarity in estimation errors for the older male group. Further, the smaller errors for the male groups may be attributed to the comparable gender characteristics of the samples.

The assumption of constant density in estimating human BSPs has been a necessary but concerning component of human BSP modelling. Wei and Jensen (1995) developed segment density profiles from axial CT images to account for said changes along the length of segments but were unable to confirm whether improved estimates of inertia would result. The models developed in this study demonstrate the improved predictive abilities of geometric solids representing the mass distribution properties of the segments over those approximating segment volume. These models account for the changes in density along the length of the segment without having to apply density profiles, thus alleviating concern for the constant density assumption.

There is a current concern and need for improved BSP measurement or estimation methods in the biomechanics community (Martin et al., 1989, Cheng et al. 2000). Pearsall and Costigan (1999) investigated the influence of BSP estimation errors on gait analysis results, however, and found that variations in error of up to 40% had merely a 1% body weight influence during stance phase. The implications were deemed to be higher during swing phase, however, and during open chain movements or movements involving high

accelerations. Since the forearm is often studied under the two latter conditions (i.e. throwing), the reduction of these errors seems imperative. A question therefore remains as to what influence BSP errors have on kinetic results. Andrews and Mish (1996) identify two characteristics that make identifying the impact of BSP propagation error on motion analysis difficult. The first problem is that there is no identification of the amount of error in estimating a given BSP for an individual subject. This study provides specific error values on the human forearm for a range of human populations and therefore partially addresses this issue. The second problem is the dependence of the error on joint resultants during the activity of interest. This issue is one that is unique to each movement problem and therefore needs to be considered on an individual basis.

This study demonstrates an attempt to accurately model the mass distribution properties of the forearm on four human populations using a combination of geometric solids. The results reveal geometric similarity between the four groups studied and provide precise validation of model errors by comparing estimations to DEXA-derived measurements. Furthermore, four other popular models in the literature were evaluated, enabling the analysis of these equations on individuals of varying race, gender, morphology and age. The models developed in this study did not significantly improve on estimates from other models, but the method provides a base from which to direct future improvements. Development of an elliptical model using limb breadths and circumferences may significantly improve BSP estimates, as may accounting for the slight lateral position of the centre of mass. These adaptations, coupled with a validation

in three dimensions could significantly reduce the effects of BSP propagation error in human movement studies.

3.5 References

Andrews, J.G. and Mish, S.P. (1996). Methods for investigating the sensitivity of joint resultants to body segment parameter variations. *Journal of Biomechanics*, 29(5), 651-654.

Braune, W. and Fischer, O. (1889). *The centre of gravity of the human body as related to the German infantryman*. ATI 138 452. Leipzig: National Technical Information Service.

Chandler,R.F., Clauser,J.T., McConville,H.M., Reynolds,H.M. and Young,J.W. (1975). *Investigation of inertial properties of the human body*. AMRL-TR-74-137. Ohio: Aerospace Medical Research Laboratory. Wright-Patterson Air Force Base.

Cheng,C-K., Chen,H-H., Chen,C-S., Lee,C-L. and Chen,C-Y. (2000). Segment inertial properties of Chinese adults determined from magnetic resonance imaging. *Clinical Biomechanics*, 15(8), 559-566.

Clauser,C.E., McConville,J.T. and Young,J.W. (1969). *Weight, volume, and center of mass of segments of the human body*. AMRL-TR-69-70. Ohio: Aerospace Medical Research Laboratory, Wright Patterson Air Force Base.

Demirjian, A. (1980). *Nutrition Canada anthropometry report: height, weight and body dimensions*. Ottawa: Health and Welfare Canada.

Dempster, W.T. (1955). *Space requirements of the seated operator*. WADC-TR-55-159. Ohio: Wright Air Development Center, Wright Patterson Air Force Base.

Drillis, R. and Contini, R. (1966). *Body segment parameters*. TR-1166-03. New York: New York University School of Engineering Science.

Durkin, J.L. (1998). *The prediction of body segment parameters using geometric modelling and dual photon absorptiometry*. Masters Thesis. Hamilton, ON: McMaster University.

Durkin, J.L., Dowling, J.J. and Andrews, D.A. (2002). The measurement of body segment inertial parameters using dual energy x-ray absorptiometry. *Journal of Biomechanics*, 35(12), 1575-1580

Durkin, J.L. and Dowling, J.J. (2003). Analysis of body segment parameter differences between four human populations and the estimation errors of four popular mathematical models. *Journal of Biomechanical Engineering*. 125(4), 515-522.

Hanavan, E.P. (1964). *A mathematical model of the human body*. AMRL-TR-64-102. Ohio: Aerospace Medical Research Laboratories, Wright-Patterson Air Force Base.

Hatze, H. (1980). A mathematical model for the computational determination of parameter values of anthropomorphic segments. *Journal of Biomechanics*, 13(10), 833-843.

Huang, H.K. (1983). Evaluation of cross-sectional geometry and mass density distributions of humans and laboratory animals using computerized tomography. *Journal of Biomechanics*, 16(10), 821:832.

Jensen, R.K. (1978). Estimation of the biomechanical properties of three body types using a photogrammetric method. *Journal of Biomechanics*, 11(8-9), 349-358.

Jensen, R.K. (1989). Changes in segment inertia proportions between 4 and 20 years. *Journal of Biomechanics*, 22(6-7), 529-536.

Jensen, R.K. and Fletcher, P. (1994). Distribution of mass to the segments of elderly males and females. *Journal of Biomechanics*, 27(1): 89-96.

Martin,P.E., Mungiole,M., Marzke,M.W. and Longhill,J.M. (1989). The use of magnetic resonance imaging for measuring segment inertial properties. *Journal of Biomechanics*, 22(4), 367-376.

Pearsall, D.J. and Costigan, P.A. (1999). The effect of segment parameter error on gait analysis results. *Gait and Posture*, 9(3), 173:183.

Pearsall, D.J. and Reid, J.G. (1994). The study of human body segment parameters in biomechanics. *Sports Medicine*, 18(2), 126:140.

Pearsall, D.J., Reid, J.G. and Livingston, L.A. (1996). Segmental inertial parameters of the human trunk as determined from computed tomography. *Annals of Biomedical Engineering*, 24(2), 198-210.

Peyton, A.J. (1986). Determination of the moment of inertia of limb segments by a simple method. *Journal of Biomechanics*, 19(5), 405-410.

Plagenhoef, S., Evans, F.G. and Abdelnour, T. (1983). Anatomical data for analyzing human motion. *Research Quarterly for Exercise and Sport*, 52(4), 169-178.

Wei, C. and Jensen, R.K. (1995). The application of segment axial density profiles to a human body inertia model. *Journal of Biomechanics*, 28(1), 103-108.

Winter, D.A. (1990). *Biomechanics and motor control of human movement.* (2nd Ed.) New York: John Wiley and Sons, Inc, pp. 51-64.

Young, J.W., Chandler, R.F. and Snow, C.C. (1983). *Anthropometric and mass distribution characteristics of the adult female.* FAA-AM-83-16. Oklahoma: FAA Civil Aeromedical Institute.

Zatsiorsky, V. and Seluyanov, V. (1983). The mass and inertia characteristics of the main segments of the human body. IN Matsui,H.; Kobayashi,K. (Eds.). *Biomechanics V-IIIB.* Champaign, IL: Human Kinetics Publishers Inc., pp. 1152: 1159.

Zatsiorsky, V., Seluyanov, V. and Chugunova, L.G. (1990). Methods of determining mass-inertial characteristics of human body segments. IN Chernyi,G.G.; Regirer,S.A. (Eds.). *Contemporary Problems of Biomechanics*, (Ch. 11). Boston, MA: CRC Press, pp. 272-291.

CHAPTER 4

BODY SEGMENT PARAMETER ESTIMATION OF THE HUMAN LEG USING AN ELLIPTICAL MODEL

4.1 Introduction

Determining kinetic measures of motion requires accurate knowledge of kinematic movement profiles and body segment inertial parameter (BSP) information. Attempts to obtain reliable human BSP information have been made as early as the late 19th century, yet due to methodological limitations, these efforts continue today. Early studies used cadaveric specimens whereby limb segments were sectioned and a variety of parameters were determined including volume and mass measurements (Braune and Fischer, 1889; Clarys and Marfell-Jones, 1986; Harless, 1860) as well as centre of mass locations and moments of inertia (Chandler et al., 1975; Clauser, et al., 1969; Dempster, 1955). Regression equations were developed from this cadaveric data to enable BSP estimation for living humans, however, the sample sizes were often small and results from various studies cannot be pooled due to differences in segmentation methods (Pearsall and Reid, 1994). Furthermore, the sample populations were typically elderly Caucasian males and thus may not be representative of the segmental inertial properties of other human populations.

Measurement methods using living human subjects have enabled the collection of data on large numbers of individuals. Segment volume and mass estimates have been made using water immersion, centre of mass locations have been determined using water immersion and reaction change methods and moments of inertia have been approximated

using quick release and oscillation techniques (Drillis and Contini, 1966; Plagenhoef, et al., 1983; Young et al. 1983). These methods have involved questionable assumptions, however, which have resulted in their limited use, including the respective regression equations that were developed from the various studies.

The use of medical imaging techniques to measure BSPs directly on living subjects has emerged in the last few decades and has become more popular with improvements in technology and increases in accessibility. Zatsiorsky and Seluyanov (1983) first used gamma-mass scanning to measure BSPs on 100 young adult males with accurate results. Later, Martin et al. (1989) determined BSPs on baboon cadaver segments with MRI, Huang (1983) used CT imaging to measure BSPs on a porcine specimen and on a young female child cadaver, and Pearsall et al. (1996) investigated the inertial properties of the human trunk using CT imaging. MRI and CT imaging have both provided reliable BSP measurements, however the popularity of these techniques has been limited due to the onerous methods involved, high costs, and in the case of CT imaging, high radiation doses. Furthermore, gamma-mass scanners have limited availability today, although a similar technology has recently been employed by Durkin et al. (2002) to measure BSPs directly on humans. Dual energy x-ray absorptiometry (DEXA) is a tool used clinically to measure bone density and body composition and is currently widely available in hospitals. The method is safe and easy to use, and Durkin et al. (2002) found errors of less than 3.2% in BSP measurements. Access to the technology may not be possible for all researchers and scanning individual subjects may not be a

practical option, however. These limitations support the need for alternate reliable methods of estimating human BSPs.

Predictive equations have been developed to alleviate the need for direct BSP measurement on individual subjects. Regression equations have been generated from cadaver data (Dempster,1955 (via Winter, 1990); Chandler et al., 1975; Clauser et al., 1969) and from living subject data (Drillis and Contini, 1966; Plagenhoef, 1983; Young et al., 1983) including studies using medical imaging techniques (Durkin and Dowling, 2003a; Zatsiorsky et al., 1990). Regression equations allow the rapid estimation of human BSPs using specific parameters such as whole body weight and height, and may include a number of anthropometric parameters such as limb circumferences and breadths. These regression equations are limited by the methods from which they were derived, however, and are also limited to the population from which they were developed. Furthermore, Durkin and Dowling (2003a) found that while simple linear and multiple regression equations could account for differences between human populations, they could not adequately explain individual differences within groups.

Mathematical models have been developed as an alternative to regression equations in an attempt to accurately estimate human BSPs. Hanavan (1964) created a geometric model of the human body based on a series of ellipsoids, right circular cylinders and frusta. The model was developed to represent the segmental inertial properties of the young adult male, but was validated for whole body inertial properties only. Hatze (1980) later produced a detailed geometric model of the human body, however the method has been largely avoided due to the required 242 anthropometric

parameters. Jensen (1978) designed an elliptical modelling method using photogrammetry to account for differences in morphology, gender, age, race and activity level. The method also enables the estimation of BSPs for children and for women during pregnancy, yet, the model assumes constant density throughout, was validated for segment volume only, and the software is not currently available for use. Models based on geometric considerations were developed by Zatsiorsky et al. (1990) and were validated against gamma-mass scanning data. The models were constructed as right circular cylinders and a constant was applied to account for differences in shape and density between the segment and the model. Similar to their regression equations, however, the models have been validated on young Caucasian males and females only. Durkin (1998) later created geometric models for selected body segments and validated results for four human populations against DEXA data. Each model consisted of a series of geometric solids combined to form a composite that would more accurately represent the changes in segment shape along the length of the segment. The results yielded high errors, however, and it was concluded that assuming constant density while modelling according to segment volume resulted in large over-estimations in segment mass and moments of inertia.

There is currently a need for an accurate method of estimating human BSPs that accounts for differences in morphology, age, gender and race. Cheng et al. (2000) recently used MRI to directly measure the BSPs of Chinese males, since the use of other resources were thought to cause large errors in lumbar spine moment estimates. Medical imaging techniques provide accurate results, however the methods can be onerous and

costly, or access to the technology may simply not be practical. Regression equations provide an expedient way of estimating BSPs, yet they may not accurately account for differences between individuals within a group where there is a wide range of morphology types. Furthermore, current geometric models are either too laborious (i.e. Hatze, 1980) or are too simple in shape to account for changes in density along the segment length (Durkin, 1998; Hanavan, 1964). Durkin and Dowling (2003a) suggested that geometric models may accurately estimate BSP differences between individuals if constructed to represent changes in segment mass distribution rather than volume. By constructing a geometric model that mimics the mass distribution of a segment, it is possible that assuming constant density will not compromise the integrity of the model. Furthermore, it is possible that if individuals in different population groups show geometric similarity, one model may be sufficient to estimate BSPs accurately for individuals across gender, age, race and morphology. Segment mass distribution information may be easily obtained using DEXA, enabling the development and validation of such geometric models on a variety of human populations. The purposes of this study are therefore to i) examine the mass distribution properties of one human body segment, the leg, between four human populations, ii) determine if geometric similarity exists between these groups, iii) develop a geometric model based on these mass distribution properties, iv) calculate BSPs using the geometric properties of the model, v) validate the model by comparing to DEXA measurements, and vi) compare the accuracy of this model with four other popular models in the literature. It is hypothesized that one geometric model will be sufficient to accurately estimate the BSPs of the lower leg for all

four groups. Furthermore, it is hypothesized that this geometric model will provide more accurate estimates than the other models examined in this study.

4.2 Methods

Forty volunteers were recruited and categorized into one of four groups according to age (19-30 Years Old/55+ Years Old) and gender (male/female). Each of the four populations was then randomly divided into two subgroups: a model development group and a model validation group (Tables 1 and 2). The mean age, height and mass values were compared between the model development and model validation groups within each population using t-tests to determine if significant differences existed. Participants were recruited from the McMaster University campus and McMaster University Medical Centre using posters. Volunteers included university students and faculty/staff as well as staff and visitors to the hospital.

Each participant underwent two DEXA scans followed by a series of anthropometric measurements (Table 3). Participants were asked to change into shorts and one leg was randomly chosen for analysis. The first DEXA scan was performed with the subject lying supine and the second scan was performed with the lateral side of the leg positioned downward on the table. During both scans, the participant was positioned with knees extended and feet slightly dorsiflexed to simulate a standing position. For the sagittal plane scan, the leg was positioned perpendicular to that of the frontal plane scan. The anthropometric measurements were obtained while the participant was standing erect with feet pointed anteriorly. Circumference measurements were determined with a

Table 1. Descriptive statistics of model development group including mean ± standard deviation (SD) and range of group ages, whole body masses and whole body heights.

		Age (Years)		Mass (kg)		Height (cm)	
Group	N	Mean (±SD)	Range	Mean (±SD)	Range	Mean (±SD)	Range
Females (19-30 Years)	5	22.6(2.9)	20.0-27.0	58.0(5.1)	51.0-64.3	167.2(10.1)	152.0-176.5
Males (19-30 Years)	5	24.2(3.1)	19.0-27.0	76.2(15.8)	52.0-89.5	185.1(10.5)	167.0-194.3
Females (55+ Years)	5	68.4(11.0)	55.0-82.0	65.0(10.7)	55.0-77.3	158.2(5.3)	149.0-162.0
Males (55+ Years)	5	69.2(9.9)	59.0-80.0	98.2(33.9)	67.5-149.0	172.5(6.3)	167.6-182.9

Table 2. Descriptive statistics of model validation group including mean ± standard deviation (SD) and range of group ages, whole body masses and whole body heights.

		Age (Years)		Mass (kg)		Height (cm)	
Group	N	Mean (±SD)	Range	Mean (±SD)	Range	Mean (±SD)	Range
Females (19-30 Years)	5	22.4(1.1)	21.0-24.0	61.6(8.1)	50.5-71.5	167.6(7.4)	160.0-180.0
Males (19-30 Years)	5	25.0(3.3)	21.0-30.0	77.7(13.0)	62.0-92.2	179.2(7.4)	173.0-191.0
Females (55+ Years)	5	69.0(4.8)	64.0-74.0	67.4(8.8)	52.0-73.0	160.1(6.1)	152.5-167.0
Males (55+ Years)	5	65.8(9.0)	55.0-76.0	80.3(11.4)	64.0-91.0	171.7(8.0)	165.0-185.0

Table 3. Description of anthropometric measurements.

Anthropometric Parameter	**Description**
Lateral leg length (LL)	Distance between lateral proximal end of tibial plateau to distal end of lateral malleolus
Medial leg length (ML)	Distance between medial proximal end of tibial plateau to distal end of medial malleolus
Knee circumference (KC)	Circumference about knee along joint line at tibial plateau
Knee breadth (KB)	Breadth of knee at level of knee circumference
Maximum leg circumference (XC)	Largest circumference about leg
Maximum leg breadth (XB)	Breadth taken at level of maximum leg circumference
Ankle circumference (AC)	Smallest circumference about distal end of leg, just proximal to lateral and medial malleoli
Ankle breadth (AB)	Breadth of ankle at level of ankle circumference
Malleolar circumference (MC)	Largest circumference about leg at level of lateral and medial malleoli
Malleolar breadth (MB)	Breadth of malleoli at level of malleolar circumference

flexible tape measure accurate to ±0.05 cm and breadths were taken with an F-shaped adjustable anthropometer accurate to ±0.05 cm. All procedures were performed in compliance with guidelines approved by the McMaster University Research Ethics Board.

All frontal and sagittal plane DEXA scan files were processed as in Durkin et al. (2002). Two images were developed from each scan to enable sectioning of the leg segment. A density image (Fig. 1) was created to display the skeletal system and allow segmentation of the leg using easily identifiable bony landmarks. A mass image (Fig. 2) was created to enable visualization of the soft tissue surrounding the segment. Following development of the scan images, a cubic spline was applied to the raw mass data to increase the areal resolution by 40 times. The original spatial resolution of mass data

within a whole body DEXA scan is 1.32 cm X 0.53 cm per scanned element, however, Durkin (1998) found that increasing the areal resolution of the raw data reduced errors in length and centre of mass estimation by as much as 15%. The interpolation procedure was set to apply as little smoothing as possible (Fig. 3) and resulted in a mass resolution of 0.132 cm X 0.132 cm per scanned element.

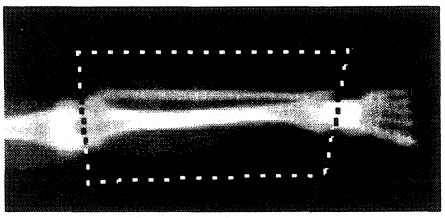

Figure 1. Partial density image of a whole body DEXA scan displaying the skeletal structures of the lower limb of a Female (19-30 Years Old) subject in the frontal plane. Dashed line represents an example of lower leg segmentation method.

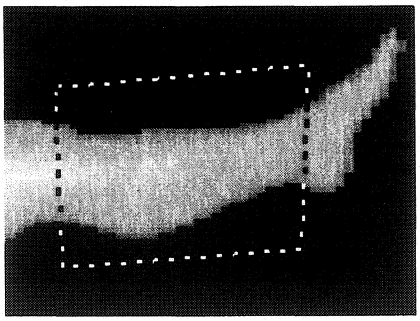

Figure 2. Partial mass image of a whole body DEXA scan displaying the soft tissue of the lower limb of a Female (19-30 Years Old) subject in the sagittal plane. Dashed line represents an example of lower leg segmentation method. Data resolution is presented in raw format.

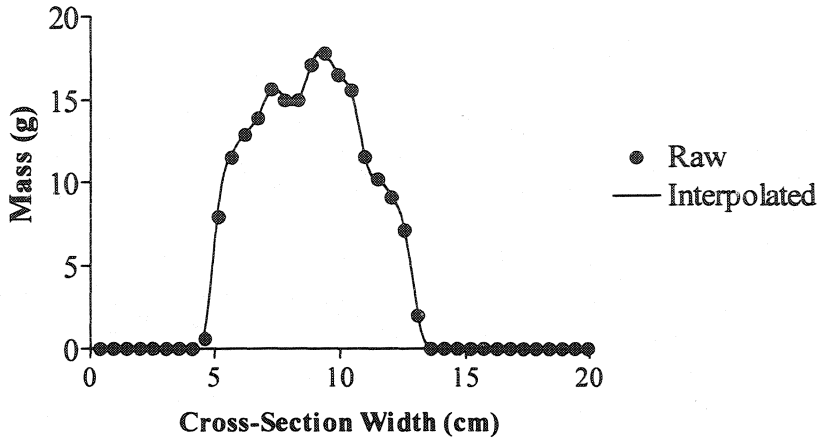

Figure 3. Example of interpolated data following raw data with little smoothing. Data represents an axial view of the quantity of mass within one slice of a frontal plane scan from a male subject (19-30 Years Old) in the mid-leg region.

The frontal and sagittal plane DEXA scan files of all 40 subjects were digitized using custom software (DXA Digitization Software, Durkin, 1998) following specific segmentation guidelines. The density image (Fig. 1) was used to visualize the skeletal system, allowing segmentation of the leg according to clearly identifiable bony landmarks. The leg scans were sectioned at the proximal end by a plane slicing between the tibial plateau and the base of the femoral condyles. The leg was sectioned at the distal end by a plane running just distal to the base of the lateral and medial malleoli. The proximal segment endpoint was selected as a location midway along the tibial plateau at the segmentation plane. The distal segment endpoint was selected as a location midway along the segmentation plane at the ankle. Other segmentation points were selected about the leg by toggling between the density and mass (Fig. 2) images to ensure all soft tissue was enclosed within the digitized area.

Leg BSPs were calculated from mass within the digitized scan area as in Durkin et al. (2002). Leg mass, length, and centre of mass in the longitudinal direction (CM_x) were calculated from both the frontal and sagittal plane scans. The mean of the frontal and sagittal plane measurements were then used to represent DEXA leg mass, length and CM_x values. T-tests were performed between the pairs of measurements to determine if significant differences existed. Centre of mass in the mediolateral direction (CM_y) and moment of inertia about the centre of mass in the anteroposterior direction (I_{CMz}) were calculated from the frontal plane scans and centre of mass in the anteroposterior direction (CM_z) and moment of inertia about the centre of mass in the mediolateral direction (I_{CMy}) were calculated from the sagittal plane scans.

Mass distribution properties of the leg segments were determined by normalizing the segmented DEXA leg mass data to 100% segment length and 100% segment mass and plotting the results. Mass elements within columns of 1% segment length in width were summed and each mass column was then divided by the total measured DEXA leg mass. The mass sums were performed separately for mass medial and lateral to the proximal-to-distal segment line for the frontal plane scans and were calculated separately for mass anterior and posterior to the proximal-to-distal segment line for the sagittal plane scans. The mass distribution properties of digitized right limbs were inverted to match those of the left limbs so that lateral leg mass was represented in the positive y-axis and medial leg mass was displayed in the negative y-axis for the frontal plane scans. Similarly, mass anterior to the proximal-to-distal segment line was represented in the

positive y-axis and posterior leg mass was displayed in the negative y-axis for the sagittal plane scans (see Fig. 4).

Twenty participants from the subject pool were selected to represent a model development group while the remaining volunteers were placed in a model validation group. Each of these two groups contained representatives from four human populations separated by age and gender, therefore each of the four subgroups was comprised of 5 subjects each. Ensemble averages of the individual mass distribution plots were created for each population within the model development group, where separate ensemble averages were created for frontal and sagittal plane scans (Figs. 4 and 5). These ensemble averages were then used to determine geometric similarity in leg mass distribution properties between the four groups and to develop a geometric model of the lower leg. Noise displayed in the frontal plane mass distribution plots was simply a sawtooth effect resulting from rotation of the mass array following segmentation.

Geometric similarity between the four populations was determined visually by examining the mass distribution plots and statistically by performing linear correlations of the % of 100% leg mass values (y-axis values, Figs 4 and 5) between the individual populations in the model development group. Linear correlations were performed and Pearson Product Moment Correlations were calculated for both frontal and sagittal plane scans and were determined separately for mass lateral and medial to, or anterior and posterior to, the proximal-to-distal segment line.

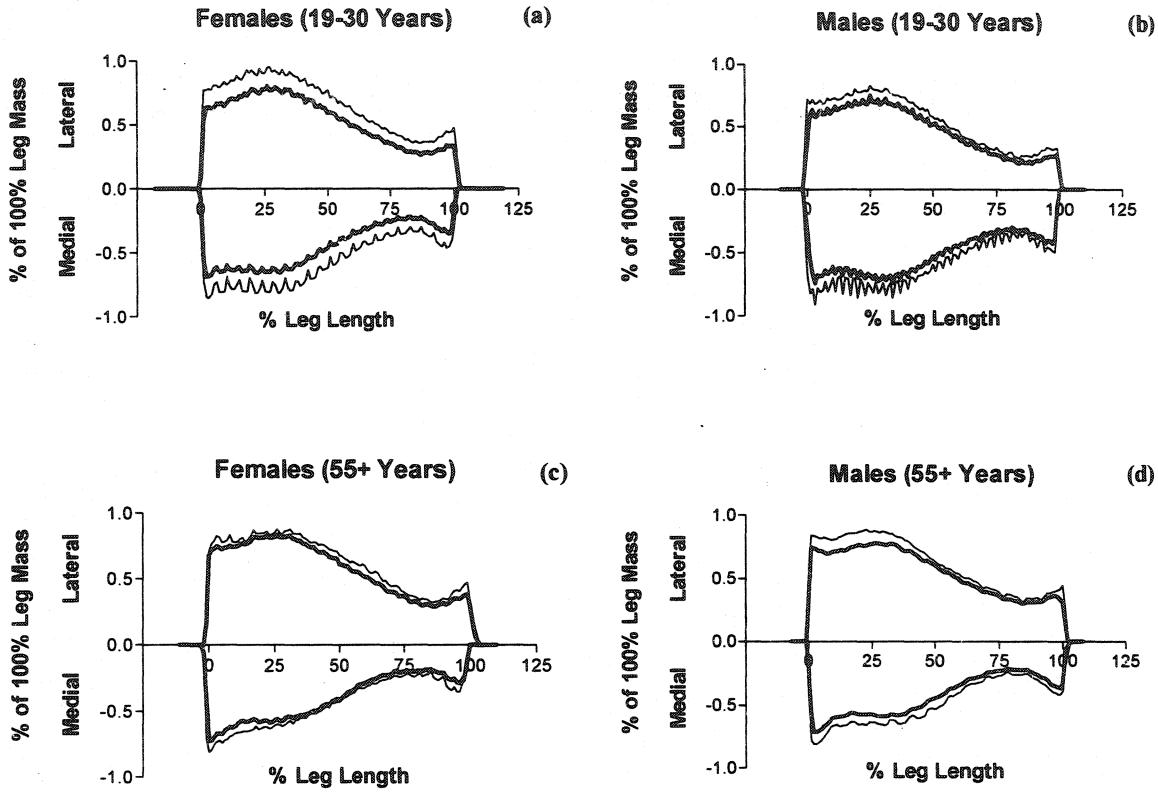

Figure 4. Ensemble averages of frontal plane leg mass distribution plots for four populations as determined using DEXA. (a) Females (19-30 Years Old), (b) Males (19-30 Years Old), (c) Females (55+ Years Old), (d) Males (55+ Years Old). Inner lines represent mean mass distribution, outer lines represent positive standard deviation.

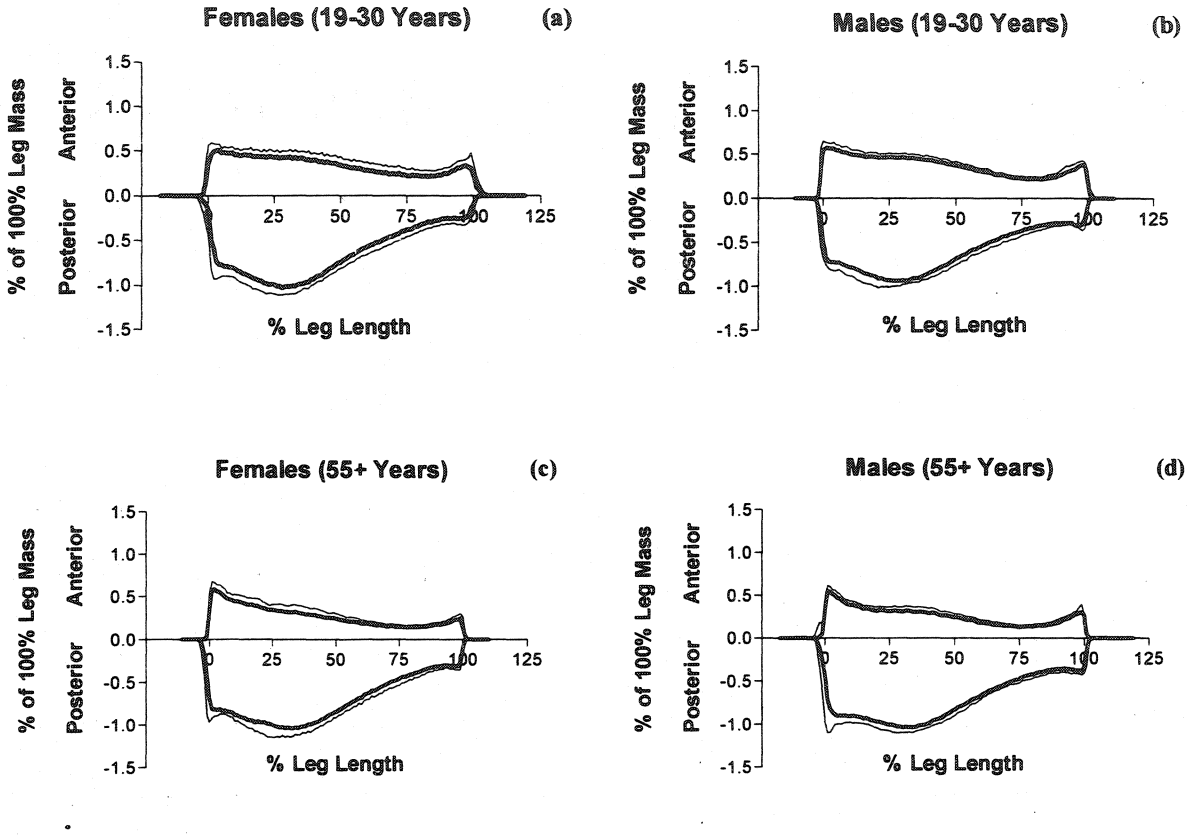

Figure 5. Ensemble averages of sagittal plane leg mass distribution plots for four populations as determined using DEXA. (a) Females (19-30 Years Old), (b) Males (19-30 Years Old), (c) Females (55+ Years Old), (d) Males (55+ Years Old). Inner lines represent mean mass distribution, outer lines represent positive standard deviation.

4.3 Results

T-tests were performed to compare the differences between frontal and sagittal plane DEXA measurements for all 40 subjects. No significant differences were found between mass ($t = -0.82$, $p=0.42$), length ($t=1.17$, $p=0.25$) and CM_x ($t=-1.00$, $p=0.32$). Furthermore, t-tests showed no significant differences in population age, mass and height values between the model development and model validation groups (Table 4).

Table 4. t-test results comparing age, mass and height characteristics between model development groups and model validation groups.

	Age (years)		Mass (kg)		Height (cm)	
	t-Value	p	t-Value	p	t-Value	p
Females (19-30 Years)	0.14	0.89	-0.07	0.95	-0.85	0.42
Males (19-30 Years)	-3.93	0.70	1.02	0.34	-0.16	0.88
Females (55+ Years)	-0.11	0.91	-0.54	0.60	-0.40	0.70
Males (55+ Years)	0.57	0.59	0.17	0.87	1.12	0.30

4.3.1 Geometric Similarity

Ensemble averages of the mass distribution plots were created to determine if geometric similarity existed between the four population groups. Visual inspection of the mass distribution plots from the model development group indicated geometric similarity between populations for both frontal and sagittal plane views. The linear correlations supported this similarity, revealing high Pearson Product Moment correlations between all populations for both frontal and sagittal comparisons (Tables 5 and 6). The results therefore suggest that one geometric model may accurately represent the mass distribution properties of the lower leg for all four groups.

4.3 2 Model Development

Three geometric solids of varying complexity were constructed in an attempt to accurately depict the mass distribution properties of the lower leg. Model 1 consisted of three elliptical solids joined end to end (Fig. 6). The proximal segment was that of an

Table 5. Linear regression equations and Pearson Product Moment correlations comparing lateral and medial mass distribution properties between model development groups as determined from frontal plane DEXA scans.

	Lateral Leg Mass Distribution		Medial Leg Mass Distribution	
Group	Linear Regression Equation	r	Linear Regression Equation	r
YF vs. YM	YM = -0.117 + 0.908(YF)	0.996	YM = -0.031 + 1.054(YF)	0.980
YF vs. OF	OF = 0.010 + 1.057(YF)	0.997	OF = 0.006 + 0.918(YF)	0.980
YF vs. OM	OM = 0.010 + 1.005(YF)	0.992	OM = -0.009 + 0.935(YF)	0.992
YM vs. OF	OF = 0.026 + 1.156(YM)	0.993	OF = 0.014 + 0.824(YM)	0.944
YM vs. OM	OM = 0.026 + 1.098(YM)	0.989	OM = 0.005 + 0.852(YM)	0.972
OF vs. OM	OM = 0.001 + 0.950(OF)	0.996	OM = -0.023 + 0.991(OF)	0.985

YF = Females (19-30 Years Old), YM = Males (19-30 Years Old), OF = Females (55+ Years Old), OM = Males (19-30 Years Old).

Table 6. Linear regression equations and Pearson Product Moment correlations comparing anterior and posterior mass distribution properties between model development groups as determined from sagittal plane DEXA scans.

	Anterior Leg Mass Distribution		Posterior Leg Mass Distribution	
Group	Linear Regression Equation	r	Linear Regression Equation	r
YF vs. YM	YM = -0.006 + 1.106(YF)	0.992	YM = -0.020 + 0.914(YF)	0.997
YF vs. OF	OF = -0.027 + 0.894(YF)	0.958	OF = -0.042 + 1.026(YF)	0.991
YF vs. OM	OM = -0.013 + 0.810(YF)	0.948	OM = -0.054 + 1.015(YF)	0.990
YM vs. OF	OF = 0.216 + 0.805(YM)	0.962	OF = -0.019 + 1.124(YM)	0.995
YM vs. OM	OM = -0.127 + 0.748(YM)	0.975	OM = -0.031 + 1.114(YM)	0.995
OF vs. OM	OM = 0.017 + 0.881(OF)	0.992	OM = -0.132 + 0.988(OF)	0.998

YF = Females (19-30 Years Old), YM = Males (19-30 Years Old), OF = Females (55+ Years Old), OM = Males (19-30 Years Old).

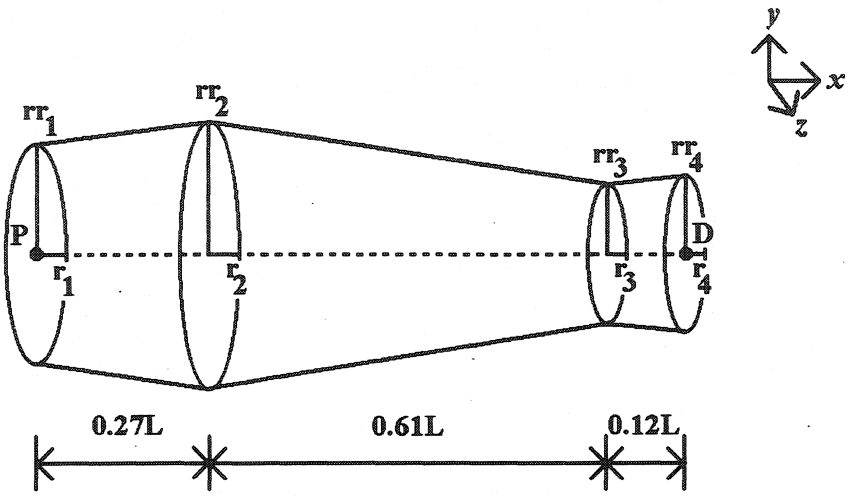

Figure 6. Diagram of 3-segment geometric model of the leg segment. Dimensions represent the frontal plane characteristics of Models 1, 2 and 3. rr values represent radii along mediolateral axis, r values represent radii along anteroposterior axis, and L represents total segment length. In Model 3, $r_1 = r_2$, $rr_1 = rr_2$. P and D represent proximal and distal segment endpoints, respectively. Model 1 is symmetrical in the sagittal plane along the anteroposterior axis.

elliptical frustum and was defined by the knee and maximum leg measurements. This frustum was either increasing or decreasing depending on the difference between these two parameters. The middle segment was a decreasing elliptical frustum and was defined by the maximum leg and ankle measurements. The distal segment was an increasing elliptical frustum and was defined by the ankle and malleolar measurements. The length of the entire leg model was defined by the mean of the lateral and medial leg length measurements and the transverse dimensions of the model were defined by the circumference and breadth measurements. The model was assumed to have a constant density of 0.00109 kg cm^3 (Winter, 1990).

Model segment length was calculated as the mean between the lateral and medial anthropometric leg length measurements:

$$L=\frac{(LL+ML)}{2} \quad (1)$$

The radius of the ellipse in the mediolateral direction (rr) was determined by the acquired anthropometric breadth measurements divided by 2. The circumference measurements were then combined with the breadth measurements to determine the sagittal radii of the ellipse (r) by:

$$rr_1=\frac{KB}{2} \quad (2) \qquad r_1=\sqrt{2\left(\frac{KC}{2\pi}\right)^2-rr_1^2} \quad (3)$$

$$rr_2=\frac{XB}{2} \quad (4) \qquad r_2=\sqrt{2\left(\frac{XC}{2\pi}\right)^2-rr_2^2} \quad (5)$$

$$rr_3=\frac{AB}{2} \quad (6) \qquad r_3=\sqrt{2\left(\frac{AC}{2\pi}\right)^2-rr_3^2} \quad (7)$$

$$rr_4=\frac{MB}{2} \quad (8) \qquad r_4=\sqrt{2\left(\frac{MC}{2\pi}\right)^2-rr_4^2} \quad (9)$$

The volume of Model 1 was determined by integrating the volume of elliptical plates along the length of the segment:

$$V_1=\int_1^{100} A\cdot dx=\int_1^{100}\pi\ r\ rr\,dx \quad (10)$$

where dx = 0.01L. The magnitudes of r and rr were dependent on the location of the elliptical plate along the segment length (x). Within the proximal model segment, r and rr were determined by:

$$r = m_{r1}\,x + r_1,\ 1 \le x \le 27 \quad \textbf{(11)} \qquad m_{r1} = \frac{(r_2 - r_1)}{27} \quad \textbf{(12)}$$

$$rr = m_{rr1}\,x + rr_1,\ 1 \le x \le 27 \quad \textbf{(13)} \qquad m_{rr1} = \frac{(r_2 - r_1)}{27} \quad \textbf{(14)}$$

Within the middle segment, r and rr were determined by:

$$r = m_{r2}\,x + r_2,\ 28 \le x \le 88 \quad \textbf{(15)} \qquad m_{r2} = \frac{(r_3 - r_2)}{61} \quad \textbf{(16)}$$

$$rr = m_{rr2}\,x + rr_2,\ 28 \le x \le 88 \quad \textbf{(17)} \qquad m_{rr2} = \frac{(r_3 - r_2)}{61} \quad \textbf{(18)}$$

Within the distal segment, r and rr were determined by:

$$r = m_{r3}\,x + r_3,\ 89 \le x \le 100 \quad \textbf{(19)} \qquad m_{r3} = \frac{(r_4 - r_3)}{12} \quad \textbf{(20)}$$

$$rr = m_{rr3}\,x + rr_3,\ 89 \le x \le 100 \quad \textbf{(21)} \qquad m_{rr3} = \frac{(r_4 - r_3)}{12} \quad \textbf{(22)}$$

The mass of Model 1 was determined by integrating the masses of the individual elliptical plates (m_x) which were defined by the product of the volumes of the corresponding slices and a constant density value (ρ):

$$M = \int_{1}^{100} m_x = \int_{1}^{100} A \rho \, dx \tag{23}$$

The centre of mass calculations for Model 1 were then determined as:

$$CM_x = \frac{\sum_{x=1}^{100} (m_x x)}{M} \tag{24}$$

$$CM_y = 0 \tag{25}$$

$$CM_z = 0 \tag{26}$$

The moments of inertia of Model 1 about the anteroposterior (I_{CMz}) and mediolateral (I_{CMy}) centres of mass were determined by first calculating the moments of inertia of the individual elliptical planes about their own centres of mass (I_{CMzi}, I_{CMyi}):

$$I_{CMzi} = \frac{1}{4} m_x r r^2, \quad 1 \le x \le 100, \quad 1 \le i \le 100 \tag{27}$$

$$I_{CMyi} = \frac{1}{4} m_x r^2, \quad 1 \le x \le 100, \quad 1 \le i \le 100 \tag{28}$$

The I_{CMi} values of the individual elliptical plates were then converted to moments of inertia about the proximal segment endpoint (I_{Pzi}, I_{Pyi}) using parallel axis theorem:

$$I_{Pxi} = I_{CMxi} + m_x x^2, \quad 1 \le x \le 100, \quad 1 \le i \le 100 \tag{29}$$

$$I_{Pyi} = I_{CMyi} + m_x x^2, \quad 1 \le x \le 100, \quad 1 \le i \le 100 \tag{30}$$

The I_{Pi} values were then summed to yield the total model moments of inertia about the proximal endpoint (I_{Pz}, I_{Py}) and then converted to moments of inertia about the centre of mass (I_{CMx}, I_{CMy}) using parallel axis theorem:

$$I_{Pz} = \sum_{1}^{100} I_{Pzi} \quad \textbf{(31)}$$

$$I_{Py} = \sum_{1}^{100} I_{Pyi} \quad \textbf{(32)}$$

Model BSPs were determined using the appropriate equations for the 20 participants in the model validation group and were validated by comparing model estimates to DEXA measurements by calculating the root mean squared error (RMSE).

$$I_{CMz} = I_{Pz} - MCM_x^2 \quad \textbf{(33)}$$

$$I_{CMy} = I_{Py} = MCM_x^2 \quad \textbf{(34)}$$

Errors for mass, I_{CMz} and I_{CMy} were reported as a % RMSE in units of % DEXA values whereas CM_z, CM_y, and CM_z were reported as RMSE values in units of % segment length. To visualize where Model 1 failed to accurately estimate leg BSPs, mass and I_{CM} distribution plots were developed from the model data and were normalized to 100% DEXA values. Ensemble averages of the model mass and I_{CM} distribution plots were created for each population and were overlaid with the previously developed DEXA distribution plots. The RMSE values showed rather high errors in BSP estimation, particularly in the I_{CM} estimates (Tables 7-12). Furthermore, the mass distribution plots

revealed a posterior shift in CM_z location not accounted for by Model 1, indicating a possible source of error in I_{CM} estimation (Figs. 8 and 9). Model 2 was therefore developed to more accurately represent this characteristic.

Model 2 was constructed as an adapted form of Model 1 such that the entire model was translated posteriorly 1% segment length. This translation value was determined by calculating the mean shift in % of 100% segment mass values for the entire segment length and representing this value as a % of the mean segment length from all four ensemble averaged groups. Further, the proximal segment was skewed posteriorly at an angle of 9° (α) (Figs 6 and 7). This value was determined by calculating the slope between the median mass values for the first and 27th segment length intervals. The middle and distal segments were constructed to reverse the skew (θ) while still maintaining the 1% posterior translation. Leg mass, CM_x, and CM_y were therefore calculated as in Model 1, however, CM_z was calculated as:

$$CM_z = \frac{\sum_{1}^{100}\left[m_x\left(x\tan\alpha - 0.01L\right)\right]}{M}, \quad 1 \le x \le 27 \tag{35}$$

$$CM_z = \frac{\sum\left[m_x\left(x\tan\theta - 0.01L\right)\right]}{M}, \quad 28 \le x \le 100 \tag{36}$$

$$\theta = \tan^{-1}\left(\frac{27\tan\alpha}{73}\right) \tag{37}$$

Moments of inertia for the individual elliptical plates were calculated as in Model 1 for I_{CMzi}, I_{Pzi}, and I_{CMyi}, however, I_{Pyi} was calculated as:

$$I_{Pyi} = I_{CMyi} + m_x\left(x^2 = (x\tan\alpha - 0.01L)^2\right), \quad 1 \le x \le 27 \tag{38}$$

$$I_{Pyi} = I_{CMyi} + m_x\left(x^2 + (x\tan\theta - 0.01L)^2\right), \quad 28 \le x \le 100 \tag{39}$$

Model BSPs were computed and compared to DEXA values by calculating the respective group RMSE's. Model mass and I_{CM} distribution plots were also created and overlaid with the DEXA plots. The error values and distribution plots revealed little improvement over Model 1, and a slight increase in I_{CM} errors was apparent (Tables 7-12). Furthermore, the mass distribution plots indicated that the posterior skew of 9° may have been too large, possibly contributing to the increase in I_{CM} errors (Figs. 8 and 9). Due to these results, an alternative modelling approach was taken with Model 3.

Model 3 also consisted of 3 geometric solids connected end to end where the proximal segment was designed as an elliptical cylinder, the middle segment was constructed as a decreasing elliptical frustum, and the distal segment was developed as an increasing elliptical frustum. The model segment length proportions were identical to Models 1 and 2, as was the calculation of total model length, however only the mean of the knee and maximum leg measurements were used to determine all radii of the model. The volume of the proximal segment was determined by integrating the volumes of elliptical plates as follows:

$$V_1 = \int_1^{27} A \cdot dx \quad = \int_1^{27} \pi r_1 \, rr_1 \, dx \tag{40}$$

where dx = 0.01L and

$$r_1 = r_2 = \frac{KB+XB}{2} \tag{41}$$

$$rr_1 = rr_2 = \sqrt{2\left(\frac{C_1}{2\cdot\pi}\right)^2 - r_1^2} \tag{42}$$

$$C_1 = \frac{(KC+XC)}{2} \tag{43}$$

where KC = knee circumference and XC = maximum leg circumference.

Each model segment was assigned a fixed proportion of total model mass that was determined by summing the % of 100% segment mass values within each segment length proportion boundary from the ensemble averages of the DEXA mass distribution plots. The mean mass proportion was calculated from the four population values within the model development group for each model segment, resulting in mean segment proportions of 42%, 51%, and 7% total model mass for the proximal, middle and distal segments, respectively.

To calculate the remaining radii, the total model volume was first determined from the cylinder volume and its set proportions of total model volume:

$$V_1 = 0.42V = \pi r_1 rr_1 h_1 \tag{44}$$

$$V = \frac{\pi r_1 rr_1 h_1}{0.42} \tag{45}$$

where h_1 = 0.27L. The middle segment was then modelled as an elliptical frustum, the volume of which was determined from the volume of a right circular frustum ($V_{CircFrust}$) and the area of an elliptical plate ($A_{ElliptPlate}$):

$$V_{CircFrust}=\frac{h}{3}\pi(r_1^2+r_1r_3+r_3^2) \quad (46)$$

$$A_{ElliptPlate}=\pi\, r\, rr \quad (47)$$

where rr represents the mediolateral axis and r represents the anteroposterior axis. The volume of an elliptical frustum was therefore calculated as:

$$V_{ElliptFrust}=\frac{h}{3}\pi\left(r_1rr_1+\sqrt{r_1rr_1r_3rr_3}+r_3rr_3\right) \quad (48)$$

V_2 was set at 0.51V and rr_3 was determined by setting r_3 as a function of rr_3. An r:rr ratio was quantified by dividing the frontal plane ankle and malleolar radii by the respective sagittal plane radii for each individual within the model development group and calculating the mean ratio. The resulting proportion was $r_3 = 0.75rr_3$, allowing the determination of r_3:

$$0.51V=0.51\left(\frac{\pi r_1rr_1h_1}{0.42}\right)=\left(\frac{h_2}{3}\pi\right)\left(r_1rr_1+\sqrt{r_1rr_10.75rr_3^2}+0.75rr_3^2\right) \quad (49)$$

where h_2 = 0.61L. Balancing Eq. 48 resulted in a quadratic solution:

$$rr_3=\frac{\left(-b_3+\sqrt{b_3^2-4a_3c_3}\right)}{2a_3} \quad (50)$$

where:

$$a_3 = \frac{0.75h_2}{3}\pi \quad (51)$$

$$b_3 = \left(\frac{h_2}{3}\pi\right)\sqrt{0.75r_1 rr_1} \quad (52)$$

$$c_3 = \left(\frac{h_2}{3}\pi\right)(r_1 rr_1) - 0.51V \quad (53)$$

Similarly, r_4 and rr_4 were determined by:

$$0.07V = 0.07\left(\frac{\pi r_1 rr_1 h_1}{0.42}\right) = \left(\frac{h_3}{3}\pi\right)\left(r_3 rr_3 + \sqrt{r_3 rr_3 0.75 rr_4^2} + 0.75 rr_4^2\right) \quad (54)$$

where $h_3 = 0.12L$, $r_4 = 0.75rr_4$ and:

$$rr_4 = \frac{\left(-b_4 + \sqrt{b_4^2 - 4a_4 c_4}\right)}{2a_4} \quad (55)$$

where:

$$a_4 = \frac{0.75h_3}{3}\pi \quad (56)$$

$$b_4 = \left(\frac{h_3}{3}\pi\right)\sqrt{0.75r_3 rr_3} \quad (57)$$

$$c_4 = \left(\frac{h_3}{3}\pi\right)(r_3 rr_3) - 0.07V \quad (58)$$

Once r_3, rr_3, r_4 and rr_4 were determined, the volumes of the corresponding segments were calculated (Eqs. 10-22) and the individual slice volumes were summed and multiplied by constant density to determine the segment mass (Eq. 23).

CM_x and CM_y of the solid were determined by integrating elliptical plates as was done for Models 1 and 2 (Eqs. 24 and 25). Similar to Model 2, however, CM_z was skewed posteriorly with a translation of 1% segment length, although a posterior skew of 3° (α) was used to reduce errors in I_{CM}. The resulting CM_z and I_{Pyi} calculations were calculated as in Eqs. 35-39. I_{CMxi}, I_{CMyi}, I_{Pxi}, I_{Pz}, I_{Py}, I_{CMz}, and I_{CMy} were calculated as in Model 1 (Eqs. 27, 29, 31-34).

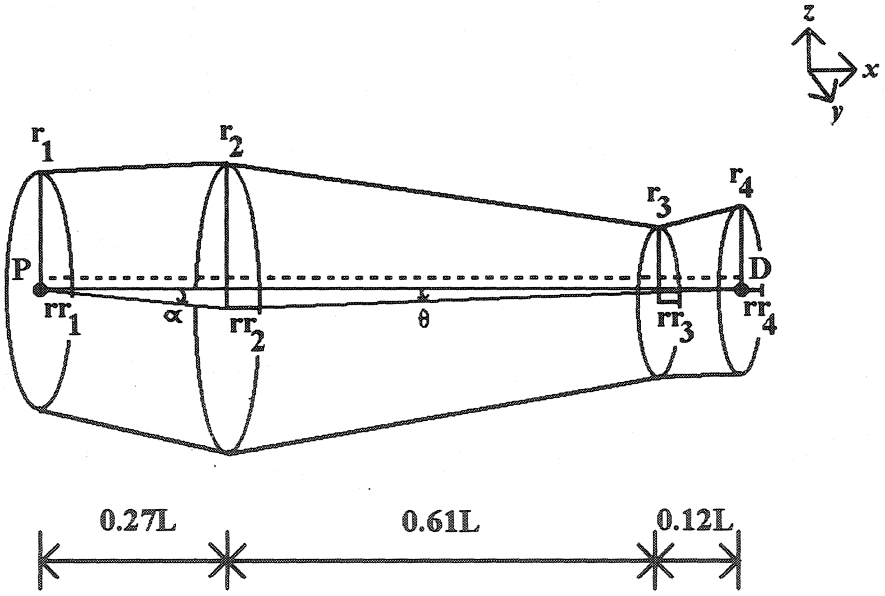

Figure 7. Diagram of 3-segment geometric model of the lower leg segment. Model dimensions represent the sagittal plane characteristics of Models 2 and 3. rr values represent radii along mediolateral axis, r values represent radii along anteroposterior axis, and L represents total segment length. In Model 3, $r_1 = r_2$, $rr_1 = rr_2$. P and D represent proximal and distal segment endpoints, respectively. Model is translated posteriorly 1% segment length and is skewed by α degrees. Model 2: $\alpha = 9^\circ$. Model 3: $\alpha = 3^\circ$.

BSP estimates from Model 3 were then calculated for the participants in the model validation group and RMSEs were computed by comparing Model estimates to benchmark DEXA data (Tables 7-12). Furthermore, model mass and I_{CM} distribution plots were created and overlaid with DEXA distribution plots as was done for Models 1 and 2 (Figs. 8 and 9).

BSP estimates from four literature sources were also assessed by applying the individual equations to the model validation group and comparing against DEXA measurements. The sources chosen included the regression equations of Dempster (1955) (via Winter, 1990) (D), the geometric models of Hanavan (1964) (H), the multiple regression equations of Zatsiorsky et al. (1990) (ZR) and the geometric models of Zatsiorsky et al. (1990) (ZG). These models were chosen for analysis because they were thought to represent popular sources in the literature and because they characterized different modelling techniques based on various populations and validation protocols. BSPs were calculated for each individual within the model validation group following the guidelines for the individual sources and the RMSEs were calculated between BSP estimates and DEXA measurements to determine the accuracy of each model (Tables 7-12). Furthermore, repeated measures analyses of variance (ANOVAs) were performed for each BSP and each population group to determine if significant differences existed between the error terms of the seven different models evaluated. Tukey HSD post hoc analyses were subsequently applied to determine where these differences lay.

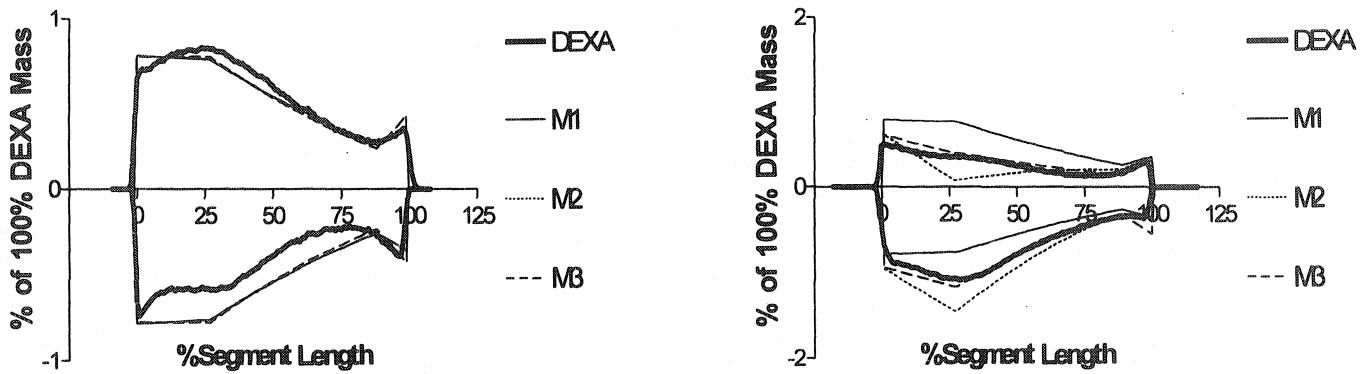

Figure 8. Ensemble averages of model mass distribution plots compared to DEXA mass distribution plots for Males (19-30 Years Old). Model mass plots are normalized to 100% DEXA mass. M1 = Model 1, M2 = Model 2, M3 = Model 3. The mass distribution plots from M1 and M2 in the frontal plane were nearly identical and are therefore superpositioned.

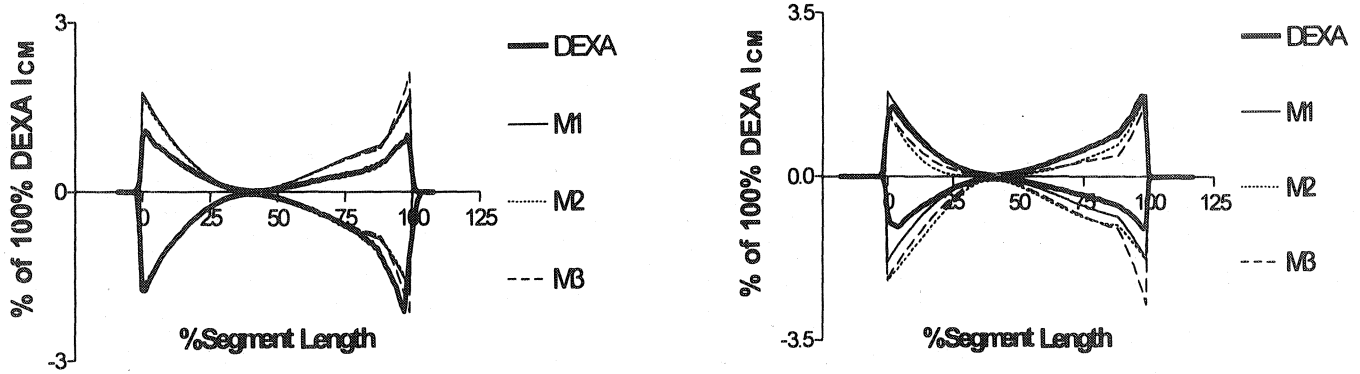

Figure 9. Ensemble averages of model I_{CM} distribution plots compared to DEXA I_{CM} distribution plots for Males (19-30 Years Old). Model mass plots are normalized to 100% DEXA I_{CM}. M1 = Model 1, M2 = Model 2, M3 = Model 3. The I_{CM} distribution plots of M1 and M2 in the frontal plane are identical and are therefore superpositioned.

Table 7. % RMSE values of model mass estimates compared with DEXA mass measurements. Values are reported in units of % DEXA mass.

Group	M1	M2	M3	D	H	ZR	ZG	F	p
Females (19-30 Years)	9.99	10.06	11.50	8.85	17.86	9.32	34.51	7.58	<0.001
Males (19-30 Years)	9.96	9.96	11.00	7.31	10.16	6.58	26.69	1.51	>0.05
Females (55+ Years)	12.63	12.63	14.08	19.70	15.29	18.99	35.43	4.64	<0.01
Males (55+ Years)	9.48	11.23	9.62	11.90	8.34	9.29	9.72	0.19	>0.05

M1 = Model 1, M2 = Model 2, M3 = Model 3, D = Dempster (1955) (via Winter, 1990),
H = Hanavan (1964), ZR = Regression equations from Zatsiorsky et al. (1990),
ZG = geometric models from Zatsiorsky et al. (1990).

Table 8. RMSE values of model CM_x estimates compared with DEXA CM_x measurements. Values are reported in units of % segment length.

Group	M1	M2	M3	D	H	ZR	ZG	F	p
Females (19-30 Years)	0.51	0.52	1.29	3.08	3.14	1.06	9.59	35.06	<0.001
Males (19-30 Years)	0.56	0.56	1.20	2.61	0.90	4.91	9.12	34.04	<0.001
Females (55+ Years)	0.61	0.61	0.74	2.87	1.14	1.83	9.51	153.33	<0.001
Males (55+ Years)	0.71	0.71	0.85	3.01	1.09	3.65	9.63	42.54	<0.001

M1 = Model 1, M2 = Model 2, M3 = Model 3, D = Dempster (1955) (via Winter, 1990),
H = Hanavan (1964), ZR = Regression equations from Zatsiorsky et al. (1990),
ZG = geometric models from Zatsiorsky et al. (1990).

Table 9. RMSE values of model CM_y estimates compared with DEXA CM_y measurements. Values are reported in units of % segment length.

Group	M1	M2	M3	D	H	ZR	ZG
Females (19-30 Years)	0.45	0.45	0.45	0.45	0.45	0.45	0.45
Males (19-30 Years)	2.63	2.63	2.63	2.63	2.63	2.63	2.63
Females (55+ Years)	1.17	1.17	1.17	1.17	1.17	1.17	1.17
Males (55+ Years)	2.38	2.38	2.38	2.38	2.38	2.38	2.38

M1 = Model 1, M2 = Model 2, M3 = Model 3, D = Dempster (1955) (via Winter, 1990), H = Hanavan (1964), ZR = Regression equations from Zatsiorsky et al. (1990), ZG = geometric models from Zatsiorsky et al. (1990).

Table 10. RMSE values of model CM_z estimates compared with DEXA CM_z measurements. Values are reported in units of % segment length.

Group	M1	M2	M3	D	H	ZR	ZG	F	p
Females (19-30 Years)	4.17	1.89	2.53	4.17	4.17	4.17	4.17	18.86	<0.001
Males (19-30 Years)	5.80	3.92	4.43	5.80	5.80	5.80	5.80	0.09	>0.05
Females (55+ Years)	4.15	1.92	2.52	4.15	4.15	4.15	4.15	17.71	<0.001
Males (55+ Years)	4.95	4.38	4.41	4.95	4.95	4.95	4.95	0.29	>0.05

M1 = Model 1, M2 = Model 2, M3 = Model 3, D = Dempster (1955) (via Winter, 1990), H = Hanavan (1964), ZR = Regression equations from Zatsiorsky et al. (1990), ZG = geometric models from Zatsiorsky et al. (1990).

Table 11. %RMSE values of model I_{CMz} estimates compared with DEXA I_{CMz} measurements. Values are reported in units of % DEXA I_{CMz}.

Group	M1	M2	M3	D	H	ZR	ZG	F	p
Females (19-30 Years)	18.24	18.35	20.40	40.96	12.40	17.13	63.44	18.29	<0.001
Males (19-30 Years)	19.48	19.64	23.07	41.33	17.81	14.32	31.11	2.90	<0.01
Females (55+ Years)	29.53	29.75	31.09	57.79	30.50	28.98	75.96	5.13	<0.01
Males (55+ Years)	21.86	28.93	23.58	48.69	24.43	17.48	35.56	5.19	<0.01

M1 = Model 1, M2 = Model 2, M3 = Model 3, D = Dempster (1955) (via Winter, 1990),
H = Hanavan (1964), ZR = Regression equations from Zatsiorsky et al. (1990),
ZG = geometric models from Zatsiorsky et al. (1990).

Table 12. %RMSE values of model I_{CMy} estimates compared with DEXA I_{CMy} measurements. Values are reported in units of % DEXA I_{CMy}.

Group	M1	M2	M3	D	H	ZR	ZG	F	p
Females (19-30 Years)	29.70	31.58	33.16	25.36	23.61	20.00	80.53	8.35	<0.001
Males (19-30 Years)	24.97	25.26	28.91	47.38	22.92	13.36	37.02	4.98	<0.01
Females (55+ Years)	29.08	29.49	28.85	56.34	28.68	31.43	76.64	7.24	<0.001
Males (55+ Years)	18.28	24.51	20.09	45.48	21.50	20.44	37.00	6.06	<0.001

M1 = Model 1, M2 = Model 2, M3 = Model 3, D = Dempster (1955) (via Winter, 1990),
H = Hanavan (1964), ZR = Regression equations from Zatsiorsky et al. (1990),
ZG = geometric models from Zatsiorsky et al. (1990).

4.3.3 Model Accuracy

The results showed that M1, M2 and M3 overestimated mass for all groups (Figs. 10-12, Tables 13-15) and that errors were greatest in mass estimation for the older female group. On average, the knee and maximum leg measurements caused an overestimation of mass at the proximal end of the leg, particularly for the older male and female subjects (Fig. 8). Furthermore, overestimations in leg mass within the ankle and malleolar regions of Models 1 and 2 were evident, while using knee and maximum leg measurements to estimate the remaining radii for Model 3 resulted in lesser overestimations at the ankle.

Comparison of mass estimates from all models through repeated measures ANOVAs revealed that significant differences existed for the female groups where Tukey HSD post hoc analyses showed that ZG had significantly greater error than the other models. No significant differences were found between mass estimates for all models for the male groups.

Examination of CM_x estimates revealed rather low errors for all three developed models, however errors were increased with M3. Repeated measures ANOVAs showed significant differences and Tukey HSD post hoc analyses revealed that ZG had significantly more error than the other models for all groups. Furthermore, ZR had significantly more error in CM_x estimation than M1 and M2 for the younger male group. ANOVAs were not performed to compare CM_y estimates since all models assumed mediolateral symmetry and therefore produced the same amount of error. This error was generated due to a slightly lateral position of CM_y as measured by DEXA.

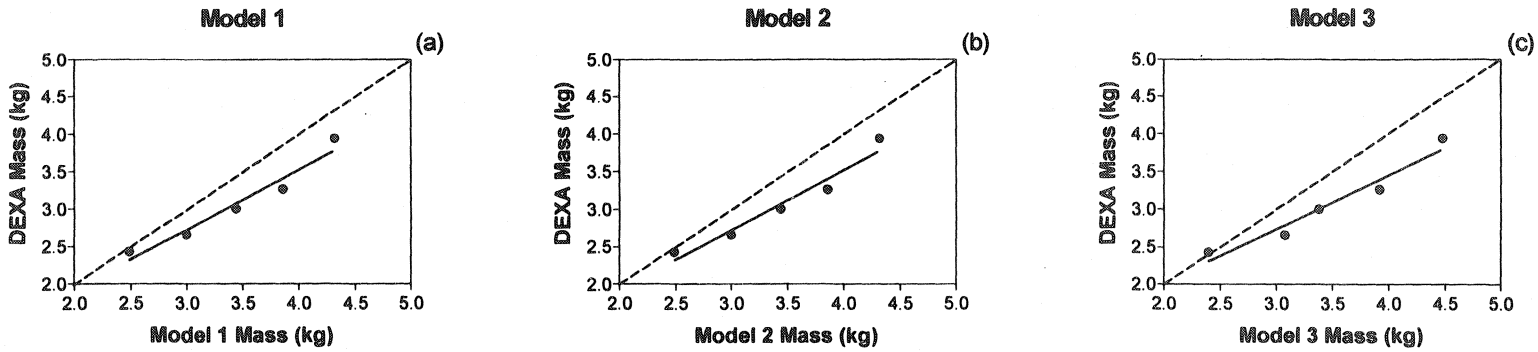

Figure 10. Scatterplots comparing model leg mass estimates with DEXA leg mass measurements for Females (55+ Years Old). Solid line represents linear regression line predicting DEXA mass from model mass, dashed line represents unity line where DEXA mass equals model mass.

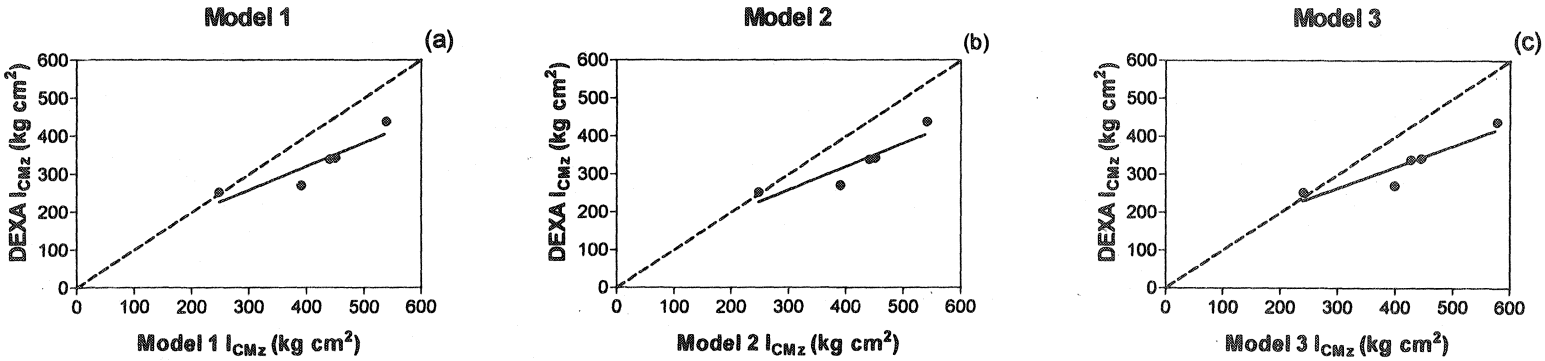

Figure 11. Scatterplots comparing model leg I_{CMz} estimates with DEXA leg I_{CMz} measurements for Females (55+ Years Old). Solid line represents linear regression line predicting DEXA I_{CMz} from model I_{CMz}, dashed line represents unity line where DEXA I_{CMz} equals model I_{CMz}.

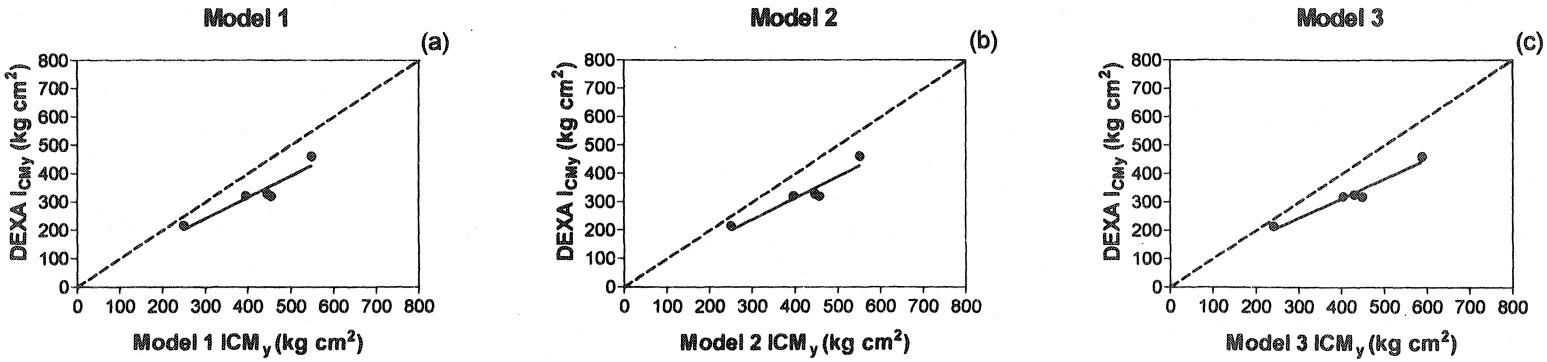

Figure 12. Scatterplots comparing model leg I_{CMy} estimates with DEXA leg I_{CMy} measurements for Females (55+ Years Old). Solid line represents linear regression line predicting DEXA I_{CMy} from model I_{CMy}, dashed line represents unity line where DEXA I_{CMy} equals model I_{CMy}.

Table 13. Linear regression equations and coefficients of variation comparing model leg mass estimates and DEXA leg mass estimates (kg).

	Model 1		Model 2		Model 3	
Group	Regression Equation	r^2	Regression Equation	r^2	Regression Equation	r^2
Females (19-30 Years)	D = 0.67M + 0.75	0.87	D = 2.67M + 0.74	0.87	D = 0.45M + 1.43	0.75
Males (19-30 Years)	D = 0.70M + 0.82	0.91	D = 0.70M + 0.82	0.91	D = 0.61M + 1.20	0.87
Females (55+ Years)	D = 0.89M + 0.12	0.93	D = 0.84M + 0.26	0.85	D = 0.91M + 0.05	0.87
Males (55+ Years)	D = 0.80M + 0.34	0.95	D = 0.80M + 0.34	0.13	D = 0.72M + 0.59	0.95

Table 14. Linear regression equations and coefficients of variation comparing model leg I_{CMz} estimates and DEXA leg I_{CMz} estimates (kg cm^2).

	Model 1		Model 2		Model 3	
Group	Regression Equation	r^2	Regression Equation	r^2	Regression Equation	r^2
Females (19-30 Years)	D = 0.68M + 64.81	0.94	D = 0.68M + 64.90	0.94	D = 0.58M + 100.50	0.92
Males (19-30 Years)	D = 0.61M + 137.80	0.78	D = 0.61M + 140.90	0.78	D = 0.50M + 200.20	0.64
Females (55+ Years)	D = 0.62M + 73.39	0.82	D = 0.61M + 74.66	0.83	D = 0.55M + 97.61	0.85
Males (55+ Years)	D = 0.75M + 43.73	0.84	D = 0.59M + 118.20	0.62	D = 0.74M + 50.21	0.78

Table 15. Linear regression equations and coefficients of variation comparing model leg I_{CMy} estimates and DEXA leg I_{CMy} estimates (kg cm^2).

	Model 1		Model 2		Model 3	
Group	Regression Equation	r^2	Regression Equation	r^2	Regression Equation	r^2
Females (19-30 Years)	D = 0.66M + 44.98	0.90	D = 0.67M + 38.10	0.88	D = 0.53M + 91.31	0.79
Males (19-30 Years)	D = 0.65M + 104.60	0.69	D = 0.64M + 107.60	0.68	D = 0.51M + 179.50	0.52
Females (55+ Years)	D = 0.76M + 12.52	0.89	D = 0.75M + 14.24	0.89	D = 0.69M + 37.18	0.89
Males (55+ Years)	D = 0.87M – 6.86	0.94	D = 0.71M + 63.31	0.77	D = 0.85M - 1.83	0.89

CM_z measurements revealed a slightly posterior location of centre of mass that amounted to an average of 3.76% segment length. Models 1, 2 and 3 all underestimated this position by 3.76%, 1.19% and 1.97%, respectively. Repeated measures ANOVAs showed significant differences for the female groups but not for the male groups. Tukey HSD post hoc analyses revealed that M2 and M3 produced significantly less error than all other models. Models 2 and 3 were not significantly different from each other, however.

I_{CMz} calculations resulted in over-estimations by M1, M2 and M3. Little difference was found between estimates from M1 and M2, however increases in error were found with M3. Repeated measures ANOVAs showed significant differences between models in all groups. Tukey HSD post hoc analyses showed ZG to have significantly more error than other models for the female groups, however H had significantly less error than D for the younger female group and ZG was not significantly different from D for the older female group. The ANOVA from the younger male group showed ZR to have significantly less error than D whereas the older male group showed significantly more error from D over all other models except ZG.

I_{CMy} calculations revealed over-estimations by M1, M2 and M3 with an increase in error from M3. Repeated measures ANOVAs showed significant differences between models for all groups and Tukey HSD post hoc analyses revealed significantly greater errors by ZG than all other models except D for the female groups. The male groups showed significantly greater errors from D compared with all other models except ZG.

4.4 Discussion

The purpose of this study was to use DEXA as a means of designing and validating a geometric model of the human leg for the estimation of segment inertial properties. The geometric models were constructed based on frontal and sagittal plane leg mass distribution properties determined for four human populations. The results showed a high degree of geometric similarity between the groups, supporting the use of one model to estimate BSPs for all four populations. Three geometric models of varying complexity were developed and validated using a split-half reliability method, in addition to the analysis of four other popular sources in the literature. Comparison of all seven estimators by means of repeated measures Analyses of Variance showed few significant differences between the models developed in this study and the other sources examined from the literature.

The results show that knee and maximum leg circumferences and breadths caused overestimations in leg mass and I_{CM} and therefore indicate that these measurements are poor estimators of proximal leg mass. However, this is in direct opposition to the results of Durkin and Dowling (2003b), who showed in study modelling the mass distribution properties of the human thigh, that knee circumference was a good estimator of thigh mass at the distal end. Durkin and Dowling (2003b) used knee circumference as a distal measurement and used a circular model to estimate BSPs, indicating that a circular model may be more appropriate for estimating leg BSPs. Two additional reasons for the disparity between proximal leg mass distribution and knee measurements could include physical differences between the participants in the two studies and the small sample

sizes used. The former is an unlikely explanation since both experiments examined four populations from identical gender and age groups and included a variety of racial backgrounds and morphological characteristics. The latter explanation is a possibility since only five subjects in each group were included for model validation. Durkin and Dowling (2003b) used 100 volunteers to develop and validate their thigh models and while only 20 subjects were used to generate the model, the equations were validated on 80 participants, possibly reducing the variability in BSP estimations. Future model development and validation should therefore involve increasing sample sizes to improve the validity of BSP estimation errors and may include scaling the knee and maximum leg measurements to more accurately represent the quantity of mass at the proximal end.

Few significant differences between the seven models examined were found using the repeated measures ANOVAs and these trends persisted across population groups for all BSPs despite obvious differences in RMSE values between models. For instance, ZR and H produced errors two and six times greater, respectively, than M1 and M2 for CM_x estimates of females aged 19 to 30 years, yet the only significant difference found was between ZG and the other models. Similarly, D produced errors that were almost twice those of M1, M2 and M3 for both female groups in I_{CMz} estimation, yet only ZG was found to be significantly greater in error than all other models. The limited differences found in the ANOVAs may be due to the small sample sizes used, since only four groups of five subjects each were included in the BSP means for comparison. It is possible that there was insufficient statistical power with the number of subjects included in the model

validation groups, thus decreasing the ability to detect true differences between the models.

The geometric models developed in this study were constructed to represent the mass distribution properties of the leg as determined by frontal and sagittal plane DEXA scans. A current limitation of DEXA, however, is that mass information is provided in one plane only, yielding four BSP parameters per scan (i.e. mass, CM_x, CM_y, I_{CMz} for a frontal plane scan). Due to the distal position of the lower leg, dual scanning was possible, providing six of seven possible BSP parameters in a three-dimensional set. This repeat scanning procedure likely caused differences in tissue redistribution between the two scans, however. A disparity in information between frontal and sagittal plane scans may have occurred due to changes in soft tissue displacement from one scan to the other as well as from differences in knee and ankle joint positions between the two scans. Furthermore, inexact positioning of the leg in perpendicular scan planes may have introduced errors into DEXA BSP measurements, however it was assumed that the effects of these three error sources were minimal. It is likely that the most influential source of error between the frontal and sagittal plane scans was that of soft tissue displacement, however comparisons of BSP measurements common between the two scans (i.e. mass, length and CM_x) using t-tests showed that these differences were not statistically significant.

Repeated measures ANOVAs showed that ZG produced significantly more error than the other models for all BSPs and almost all of the groups examined. Some possible explanations for this greater error could be the simple geometric shape chosen, however

gender-specific constants were applied to the model to account for differences between segment and model shape and density. Durkin (1998) found that modelling segments according to volume resulted in large errors in BSP estimation. This finding would suggest that Hanavan's (1964) frusta model would similarly cause large errors, however the results did not support this assumption. The greater errors in ZG estimates could be attributed to morphological differences between the subjects in this study and those of ZG. Zatsiorsky et al. (1990) recruited athletic young Caucasian participants for their models whereas this study included individuals of varying morphology as well as age and race. The ZR equations were generated from the same sample pool as ZG, however, and since the ZR errors were similar to and sometimes lower than M1, M2 and M3 for mass and inertia estimates, morphological and age-related differences are an unlikely explanation for the high ZG errors. Failure of ZG to adequately estimate leg BSPs may therefore be primarily due to the simple geometric shape chosen and the inability of the constant to account for changes in shape and density along the length of the segment.

Repeated measures ANOVAs often found D not to be significantly different from the other models examined in this study. BSP differences between D and DEXA measurements may be partially explained by a dissimilarity in segmentation methods as Dempster (1955) sectioned his specimens while frozen in a flexed position while participants in this study were sectioned in a mainly extended position. Furthermore, segmentation of DEXA scan images were limited to one plane only. Examination of RMSE values comparing D estimates to DEXA measurements showed higher errors for the elderly populations than for the younger ones, yet the specimens used by Dempster

(1955) were elderly male war veterans. The D equations may have more accurately represented the leg mass distribution properties of the younger groups due to a greater similarity in morphology compared with the older groups, as the specimens used by Dempster (1955) had lower average body masses than the elderly groups examined here (59.8 kg).

There is currently a need for a complete anthropometric model of the human body to accurately estimate the BSPs of human segments for individuals of varying morphology, age, gender and race. The geometric models generated for the leg did not greatly improve on estimates over the other models evaluated, however this study improves on past methods by identifying a reliable approach to modelling the human leg for BSP estimation. This modelling technique could potentially provide more accurate BSP estimates with increases in the number of subjects involved and with adaptations to the models developed such as scaling of anthropometric measurements. Such improvements in model generation and validation will help reduce BSP error, however how much error is acceptable in kinetic calculations remains unknown. Pearsall and Costigan (1999) used a Monte Carlo method to determine the effect of BSP error on gait analysis results and found that BSP variations of 40% caused errors in kinetic measurements of only 1% body mass. The effects on kinetic calculations were thought to be greater in open chain movements or in movements involving high accelerations, however. Furthermore, Andrews and Mish (1996) investigated the sensitivity of joint resultants to BSP error and found that small percentages of BSP error can quite substantially affect joint kinetic calculations. For instance, knee moment calculations

showed a 12% propagation error when 5% BSP error was considered. The study concluded that the effects of BSP propagation error were both subject and motion specific, indicating that an acceptable level of error is unique to each problem investigated. Due to the increased sensitivity of open chain and high acceleration movements, continued efforts on building a robust anthropometric model that is accurate and easy to apply remains a worthwhile endeavour. Further development of geometric models based on the mass distribution properties of body segments will provide a reliable source of BSP information and will ultimately lead us to a greater understanding of human movement.

4.5 References

Andrews, J.G. and Mish, S.P. (1996). Methods for investigating the sensitivity of joint resultants to body segment parameter variations. *Journal of Biomechanics*, 29(5), 651-654.

Braune, W. and Fischer, O. (1889). *The centre of gravity of the human body as related to the German infantryman*. ATI 138 452. Leipzig: National Technical Information Service.

Chandler, R.F., Clauser, J.T., McConville, H.M., Reynolds, H.M. and Young, J.W. (1975). *Investigation of inertial properties of the human body*. AMRL-TR-74-137. Ohio: Aerospace Medical Research Laboratory. Wright-Patterson Air Force Base.

Cheng,C-K., Chen,H-H., Chen,C-S., Lee,C-L. and Chen,C-Y. (2000). Segment inertial properties of Chinese adults determined from magnetic resonance imaging. *Clinical Biomechanics*, 15(8), 559-566.

Clarys, J.P. and Marfell-Jones, M.J. (1986). Anatomical segmentation of humans and the prediction of segmental masses from intra-segmental anthropometry. Human Biology, 58(5), 771-782.

Clauser, C.E., McConville, J.T. and Young, J.W. (1969). *Weight, volume, and center of mass of segments of the human body*. AMRL-TR-69-70. Ohio: Aerospace Medical Research Laboratory. Wright Patterson Air Force Base.

Dempster, W.T. (1955). *Space requirements of the seated operator*. WADC-TR-55-159. Ohio: Wright Air Development Center, Wright Patterson Air Force Base.

Drillis, R. and Contini, R. (1966). *Body segment parameters*. TR-1166-03. New York, NY: New York University School of Engineering Science.

Durkin, J.L. (1998). *The prediction of body segment parameters using geometric modelling and dual photon absorptiometry*. Masters Thesis. Hamilton, ON: McMaster University.

Durkin, J.L., Dowling, J.J. and Andrews, D.A. (2002). The measurement of body segment inertial parameters using dual energy x-ray absorptiometry. *Journal of Biomechanics*, 35(12), 1575:1580

Durkin, J.L. and Dowling, J.J. (2003a). Analysis of body segment parameter differences between four human populations and the estimation errors of four popular mathematical models. *Journal of Biomechanical Engineering*, 125(4), 515-522.

Durkin, J.L. and Dowling, J.J. (2003b). Using Mass Distribution Information to Model the Human Thigh for Body Segment Parameter Estimation. *Journal of Biomechanical Engineering*. In Review.

Hanavan, E.P. (1964). *A mathematical model of the human body*. AMRL-TR-64-102. Ohio: Aerospace Medical Research Laboratories, Wright-Patterson Air Force Base.

Harless, H. (1860). Die statischen Momente der menschlichen Gliedmassen. *Abhandl Mathematische-Physikalischen Classe Konigl Bayerischen Akad Wissenschaft*, 8, 69-96, 257- 294.

Hatze, H. (1980). A mathematical model for the computational determination of parameter values of anthropomorphic segments. *Journal of Biomechanics*, 13(10), 833-843.

Huang, H.K. (1983). Evaluation of cross-sectional geometry and mass density distributions of humans and laboratory animals using computerized tomography. *Journal of Biomechanics*, 16(10), 821:832.

Jensen, R.K. (1978). Estimation of the biomechanical properties of three body types using a photogrammetric method. *Journal of Biomechanics*, 11(8-9), 349-358.

Martin,P.E., Mungiole,M., Marzke,M.W. and Longhill,J.M. (1989). The use of magnetic resonance imaging for measuring segment inertial properties. *Journal of Biomechanics*, 22(4), 367-376.

Pearsall, D.J. and Costigan, P.A. (1999). The effect of segment parameter error on gait analysis results. *Gait and Posture*, 9(3), 173:183.

Pearsall, D.J. and Reid, J.G. (1994). The study of human body segment parameters in biomechanics. *Sports Medicine*, 18(2), 126:140.

Pearsall, D.J., Reid, J.G. and Livingston, L.A. (1996). Segmental inertial parameters of the human trunk as determined from computed tomography. *Annals of Biomedical Engineering*, 24(2), 198-210.

Plagenhoef, S., Evans, F.G. and Abdelnour, T. (1983). Anatomical data for analyzing human motion. *Research Quarterly for Exercise and Sport*, 52(4), 169-178.

Winter, D.A. (1990). *Biomechanics and motor control of human movement*. (2nd Ed.) New York: John Wiley and Sons, Inc., pp. 51-64.

Young, J.W., Chandler, R.F. and Snow, C.C. (1983). *Anthropometric and mass distribution characteristics of the adult female.* FAA-AM-83-16. Oklahoma: FAA Civil Aeromedical Institute.

Zatsiorsky, V. and Seluyanov, V. (1983). The mass and inertia characteristics of the main segments of the human body. IN Matsui,H.; Kobayashi,K. (Eds.). *Biomechanics V-IIIB.* Champaign, IL: Human Kinetics Publishers Inc., pp. 1152: 1159.

Zatsiorsky, V., Seluyanov, V. and Chugunova, L.G. (1990). Methods of determining mass-inertial characteristics of human body segments. IN Chernyi,G.G.; Regirer,S.A. (Eds.). *Contemporary Problems of Biomechanics*, (Ch. 11). Boston, MA: CRC Press, pp. 272-291.

CHAPTER 5

CONCLUSIONS AND RECOMMENDATIONS FOR FUTURE RESEARCH

5.1 Conclusions

The purpose of this study was to examine a geometric modelling approach for estimating the body segment parameters (BSPs) of human limbs. This approach was based on representing the mass distribution properties of segments with series of geometric solids to more accurately account for changes in density along the length of the segment as well as to encompass the morphological differences between individuals. Three body segments were chosen for analysis including the thigh, forearm and leg. Their mass distribution properties were examined for four human populations separated by age (19-30 Years Old/55+ Years Old) and gender (Male/Female) using dual energy x-ray absorptiometry (DEXA). DEXA was used to determine the mass distribution properties of the body segments in the frontal plane and to measure the mass, centre of mass in the longitudinal (CM_x) and mediolateral (CM_y) directions, and the moment of inertia about the centre of mass along an anteroposterior axis (I_{CMz}). Analysis of the leg was extended to the sagittal plane and included measurements of centre of mass in the anteroposterior direction (CM_z) and moment of inertia about the centre of mass along a mediolateral axis (I_{CMy}). Geometric models of varying complexity were designed for each segment based on the mass distribution properties of a random sample from the four population groups (model development group). The thigh and forearm models consisted of 3 and 4 geometric solids, respectively, connected end to end. Each segment was circular in nature in the transverse plane. The leg models were constructed with three geometric segments joined end to end and were elliptical in the transverse plane. Segment

BSPs were estimated for the remaining subjects (model validation group) using the models and the results were compared to DEXA measurements to determine the model errors. Four other popular models available in the literature were also examined by estimating the BSPs for the model validation group and comparing to DEXA measurements. These four sources included the linear regression equations of Dempster (1955) (via Winter, 1990), the geometric models of Hanavan (1964), and both the multiple regression equations and geometric models of Zatsiorsky et al. (1990). The following conclusions can be drawn from the results:

1. **Thigh mass and I_{CMz} estimates from the geometric model tested did not significantly improve on the other methods examined, however CM_x and CM_y estimates were significantly better than the other models.** The results showed an overall underestimation of mass by the geometric model and regional underestimations of mass and I_{CMz} at the proximal end of the thigh. Furthermore, the multiple regression equations of Zatsiorsky et al. (1990) provided the most accurate estimates of mass and I_{CMz}, however repeated measures analyses of variance (ANOVAs) showed that the regression equation estimates were not significantly different than those from the developed geometric model.

2. **On average, little improvement in forearm BSP estimations was made with the developed geometric models.** Forearm mass and I_{CMz} estimates were overestimated by all three geometric models, particularly at the proximal end. Furthermore, Model 3 improved on mass estimates over Models 1 and 2, but at the expense of I_{CMz}

estimates. The geometric models of Zatsiorsky et al. (1990) were found to produce significantly more error in mass estimations and on occasion, the regression equations produced equally high errors. Greater errors were also found in the female groups compared with the males.

3. **Little improvement in leg BSP estimation was achieved with the developed models, however insufficient statistical power may have underestimated the presence of statistical differences.** Leg mass and I_{CM} estimates were overestimated by all three developed models, particularly at the proximal end of the segment. Generally, errors from Model 3 were greater than those from Models 1 and 2 for I_{CM} estimations. Models 2 and 3 improved estimates of CM over other models. The geometric models of Zatsiorsky et al. (1990) provided the greatest errors in mass, CM, and I_{CM} estimates and were significantly worse than all other models examined.

4. **Using mass distribution properties as a guide for geometric model development provides promise for more accurate BSP estimations.** The research conducted in this study represents a novel method for generating geometric models for the estimation of human BSPs. Representing the mass distribution properties of body segments allows more accurate representation of segmental inertial properties in comparison with methods using volume distribution. Furthermore, the results of this study indicate geometric similarity among individuals of varying morphology, allowing the representation of segmental inertial properties with a single model. This characteristic of the thigh, forearm and leg segments, and potentially other segments

of the body, alleviates the need for individual sets of predictive equations according to gender, race, age or morphology. While the models developed in this study did not substantially improve over estimates from the other equations examined, the results show that they were among the most accurate for each segment, population and BSP. With greater sample sizes and validation of models in three dimensions, improvements can be made to enable more accurate estimates of human BSPs.

5.2 Suggestions for Future Research

The main hypothesis of this study was that developing geometric models based on the mass distribution properties of segments would significantly improve BSP estimates over other models examined. The results of this study supported this hypothesis where CM_x and CM_z estimates were concerned, however mass and I_{CM} estimates were not significantly improved over the other models examined in this study. One possible reason for this finding is the limitation of DEXA to providing mass distribution information in one plane only. Studies 1 and 2 were limited to the frontal plane, therefore circular models were generated and were validated in this plane only. The possibility that this transverse symmetry was limiting the performance of the segment models was considered for the third study, where the lower leg was scanned twice to obtain information in two planes. This allowed the development and validation of an elliptical model in the frontal and sagittal planes. Still, however, error levels were not markedly reduced, although the two dimensional nature of DEXA may have resulted in tissue redistribution as well as segmentation differences due to dual scanning, introducing error into the geometric model and its BSP estimates. A recommendation for future research is therefore to use other forms of medical imaging

technology, possibly in addition to DEXA, to enable the assessment of the mass distribution properties of limbs in three dimensions.

Another possible reason for the limited performance of the models, particularly in Study 3, could be the small sample sizes used to validate the models. It is possible that insufficient statistical power resulted in greater error variability of BSP estimations of the models developed and therefore reduced the possibility of detecting statistical differences between all models examined. Future research should therefore include a power analysis to determine adequate sample sizes for model generation and validation.

This study presented a novel approach for designing geometric models for BSP estimation. Only three body segments were examined, however, and three-dimensional validation was not achieved. To improve kinetic estimates, a complete model of the human body that accurately estimates human BSPs for all body segments in three dimensions is needed. Future research should therefore focus on developing models of the remaining segments of the human body as well as improving those generated in this study. The quest for more accurate anthropometric information is ongoing and requires careful analysis of the methods currently available. Consideration of the level of precision needed in BSP estimates should be used with the generation of new models until satisfactory performance is achieved for a given research question.

5.3 References

Dempster, W.T. (1955). *Space requirements of the seated operator*. WADC-TR-55-159. Ohio: Wright Air Development Center, Wright Patterson Air Force Base.

Hanavan, E.P. (1964). *A mathematical model of the human body*. AMRL-TR-64-102. Ohio: Aerospace Medical Research Laboratories, Wright-Patterson Air Force Base.

Winter, D.A. (1990). *Biomechanics and motor control of human movement*. (2nd Ed.) New York: John Wiley and Sons, Inc., pp. 51-64.

Zatsiorsky, V., Seluyanov, V. and Chugunova, L.G. (1990). Methods of determining mass-inertial characteristics of human body segments. IN Chernyi,G.G.; Regirer,S.A. (Eds.). *Contemporary Problems of Biomechanics*, (Ch. 11). Boston, MA: CRC Press, pp. 272-291.

CHAPTER 6

APPENDIX

6.1 Scatterplots

6.1.1 Scatterplots of thigh model mass estimates vs. DEXA mass measurements.

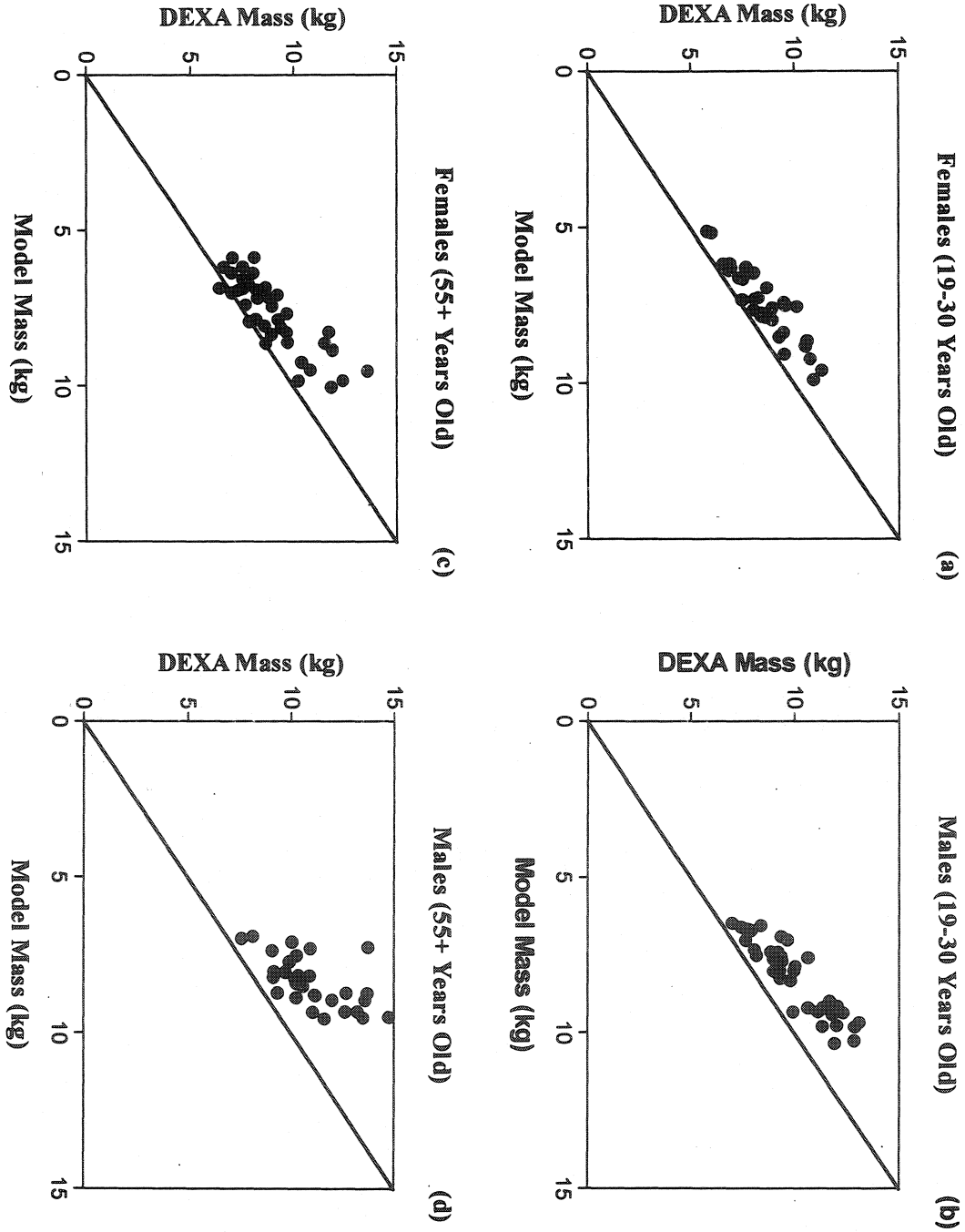

6.1.2 Scatterplots of thigh model I_{CM} estimates vs. DEXA I_{CM} measurements.

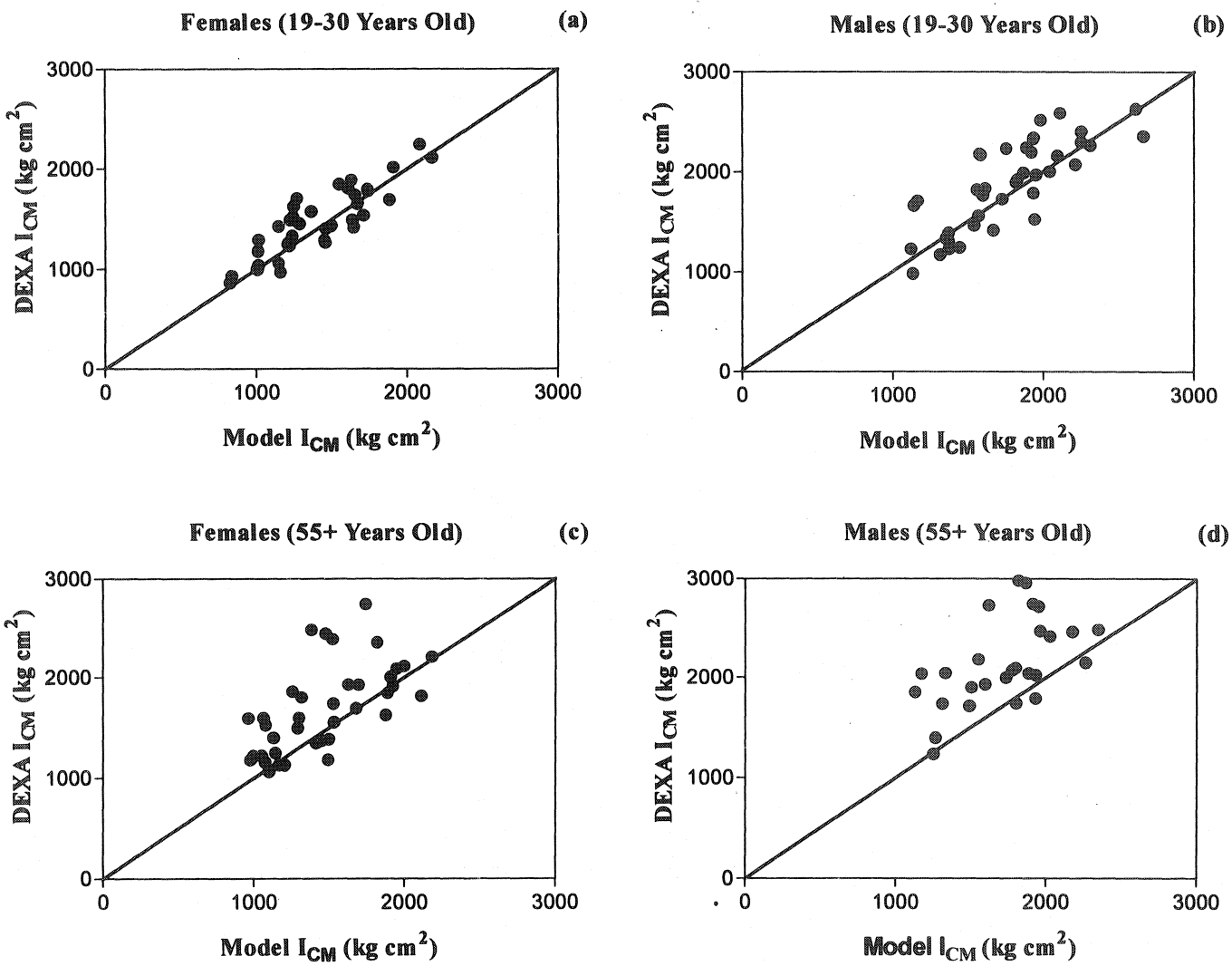

6.1.3 Scatterplots of forearm Model 1 mass estimates vs. DEXA mass estimates.

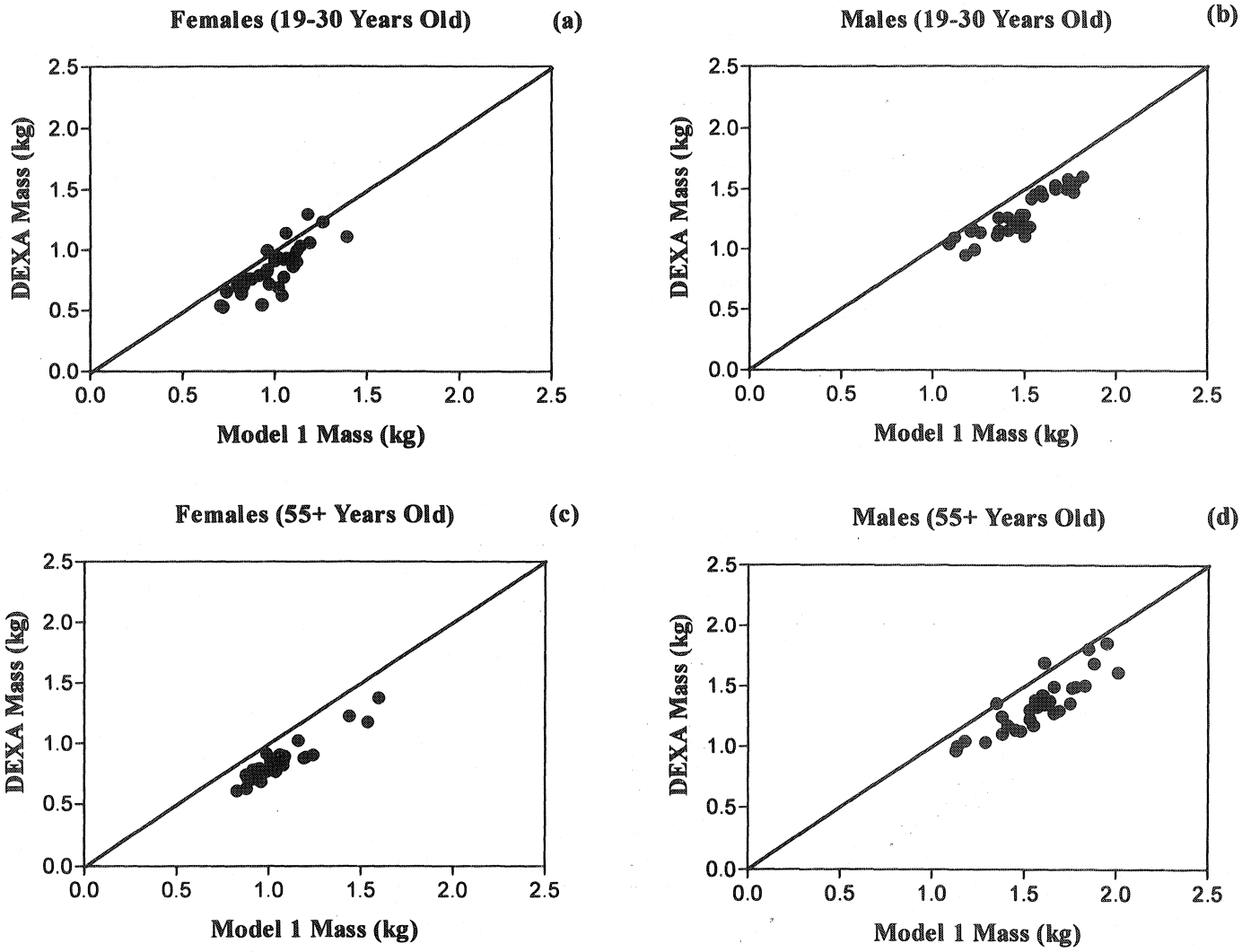

6.1.4 Scatterplots of forearm Model 2 mass estimates vs. DEXA mass estimates.

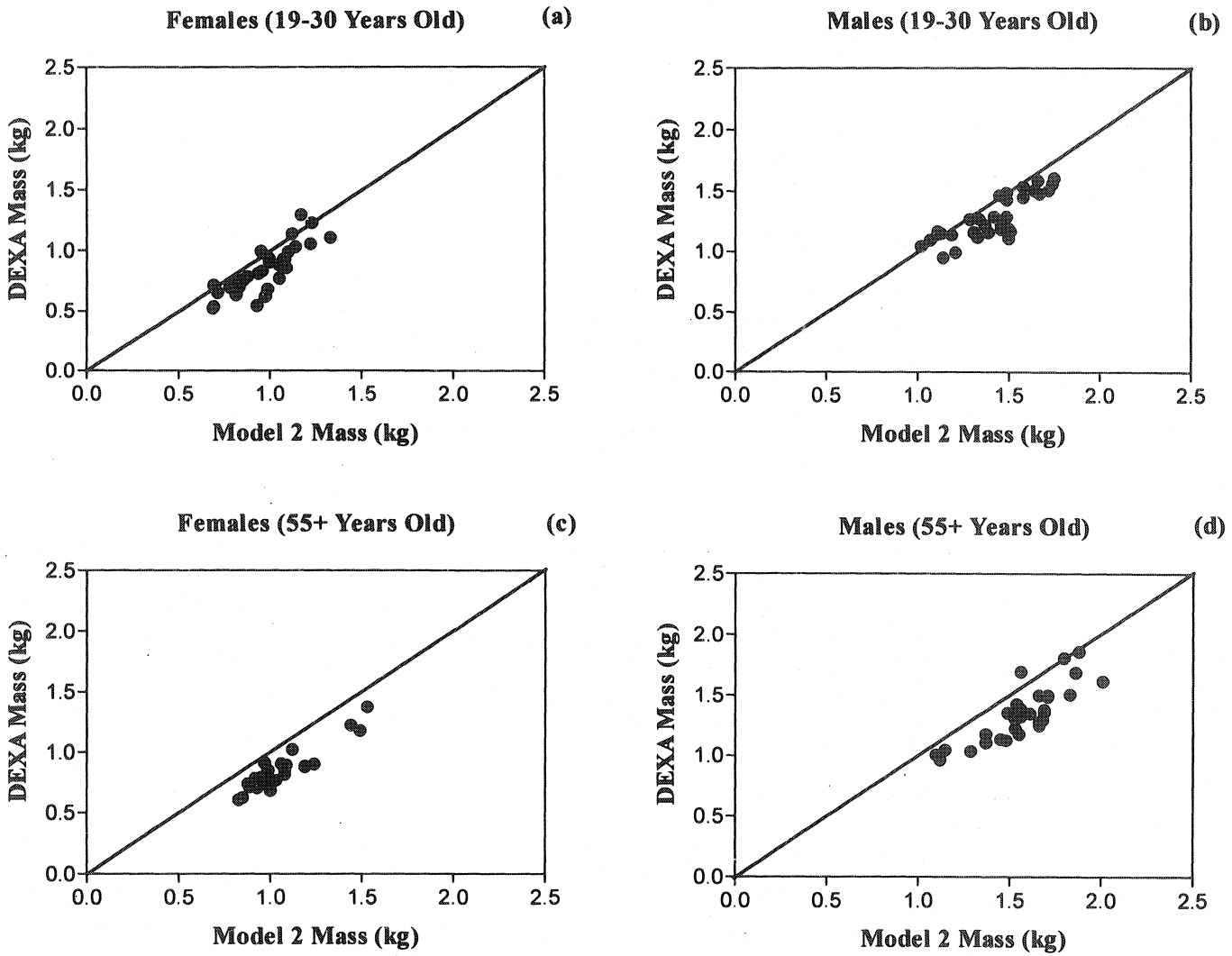

6.1.5 Scatterplots of forearm Model 3 mass estimates vs. DEXA mass estimates.

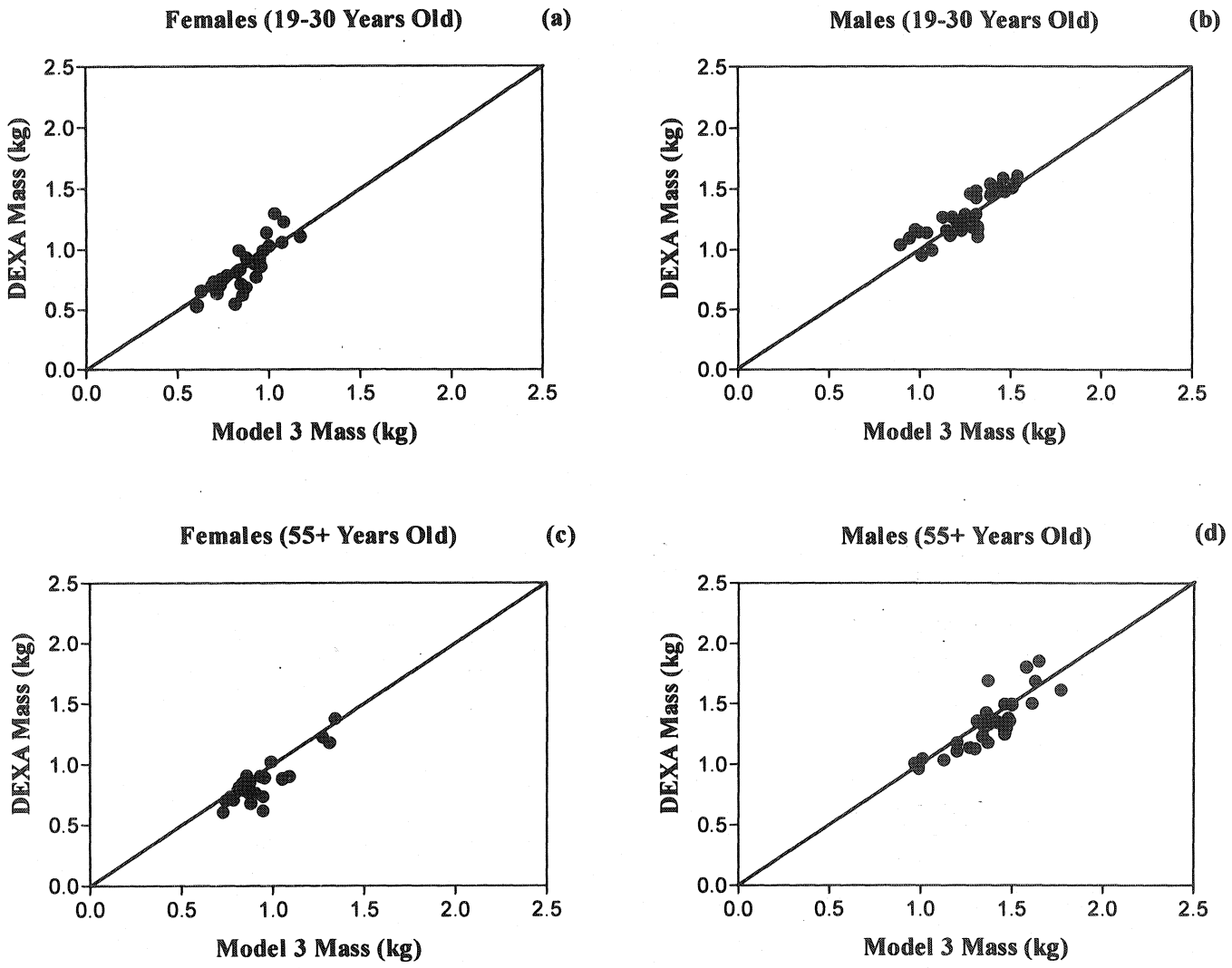

6.1.6 Scatterplots of forearm Model 1 I_{CM} estimates vs. DEXA I_{CM} estimates.

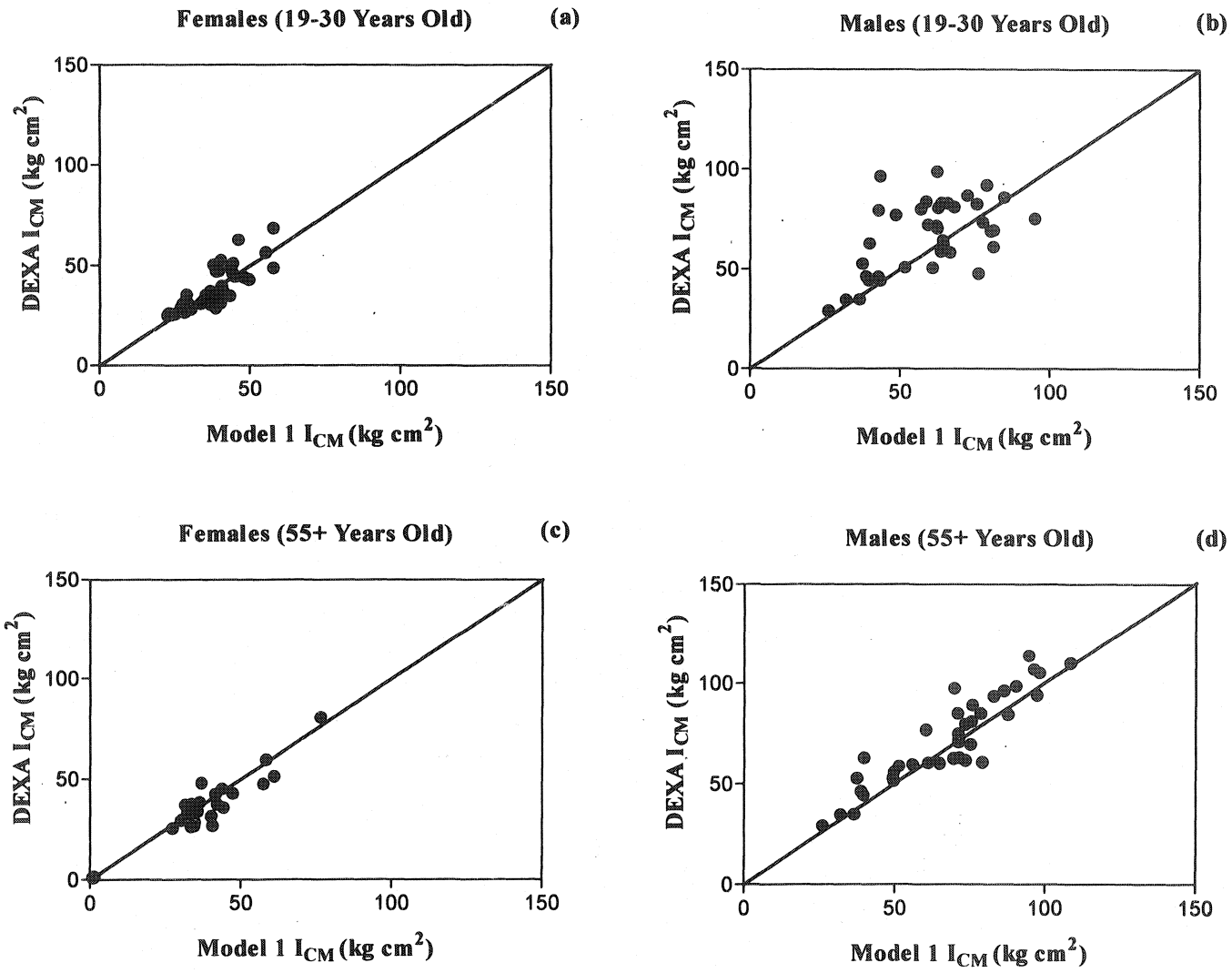

6.1.7 Scatterplots of forearm Model 2 I_{CM} estimates vs. DEXA I_{CM} estimates.

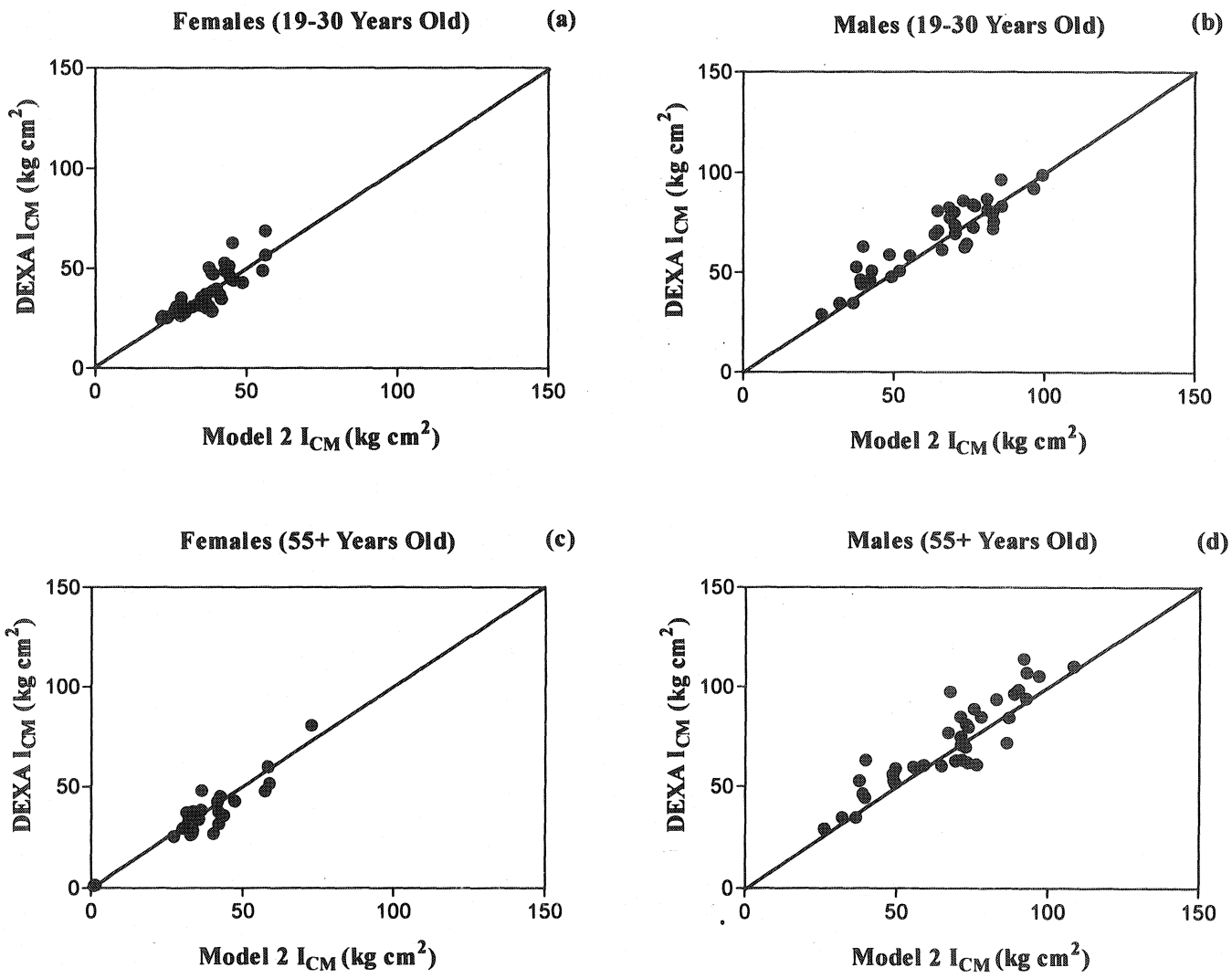

6.1.8 Scatterplots of forearm Model 3 I_{CM} estimates vs. DEXA I_{CM} estimates.

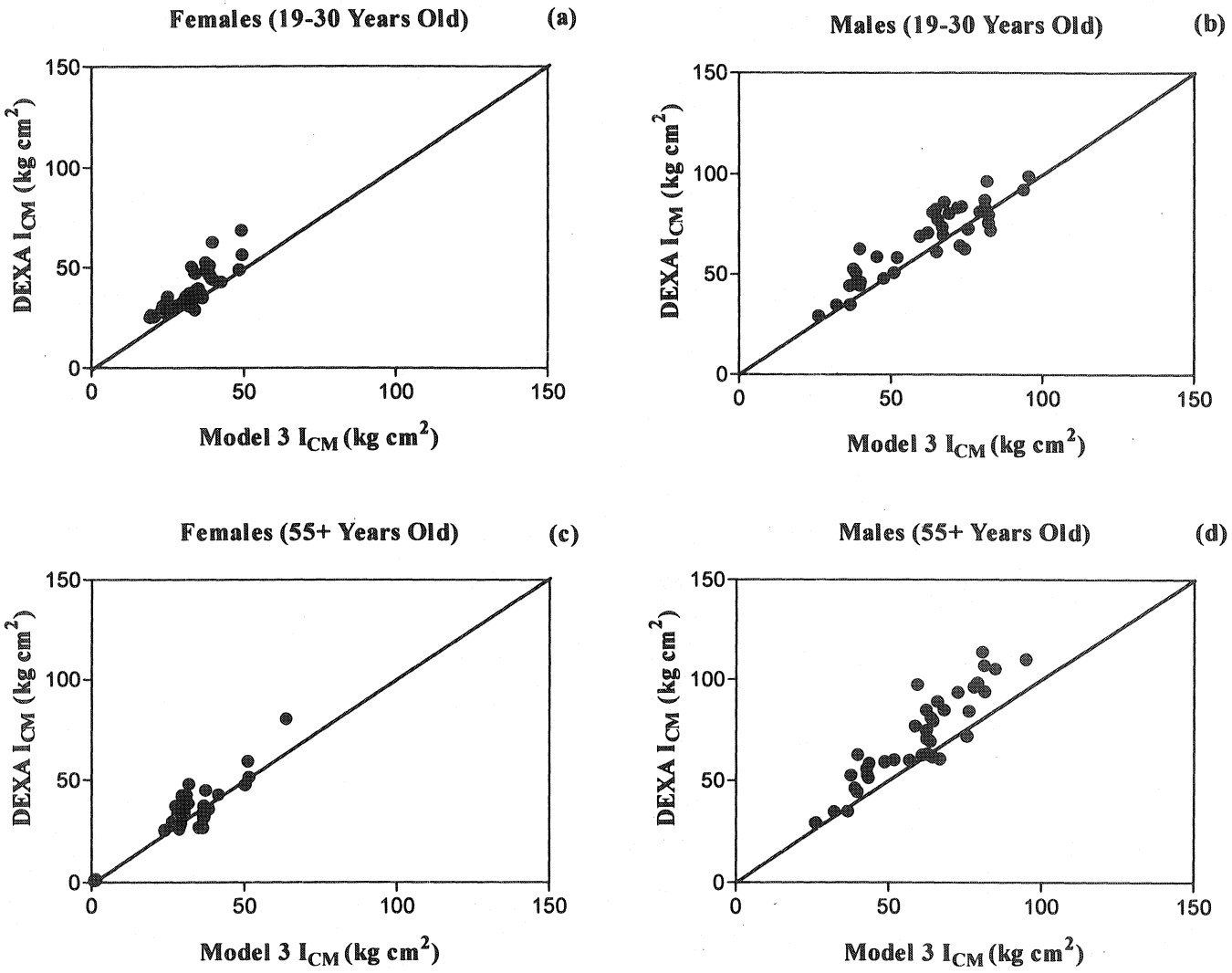

6.1.9 Scatterplots of leg Model 1 mass estimates vs. DEXA mass estimates.

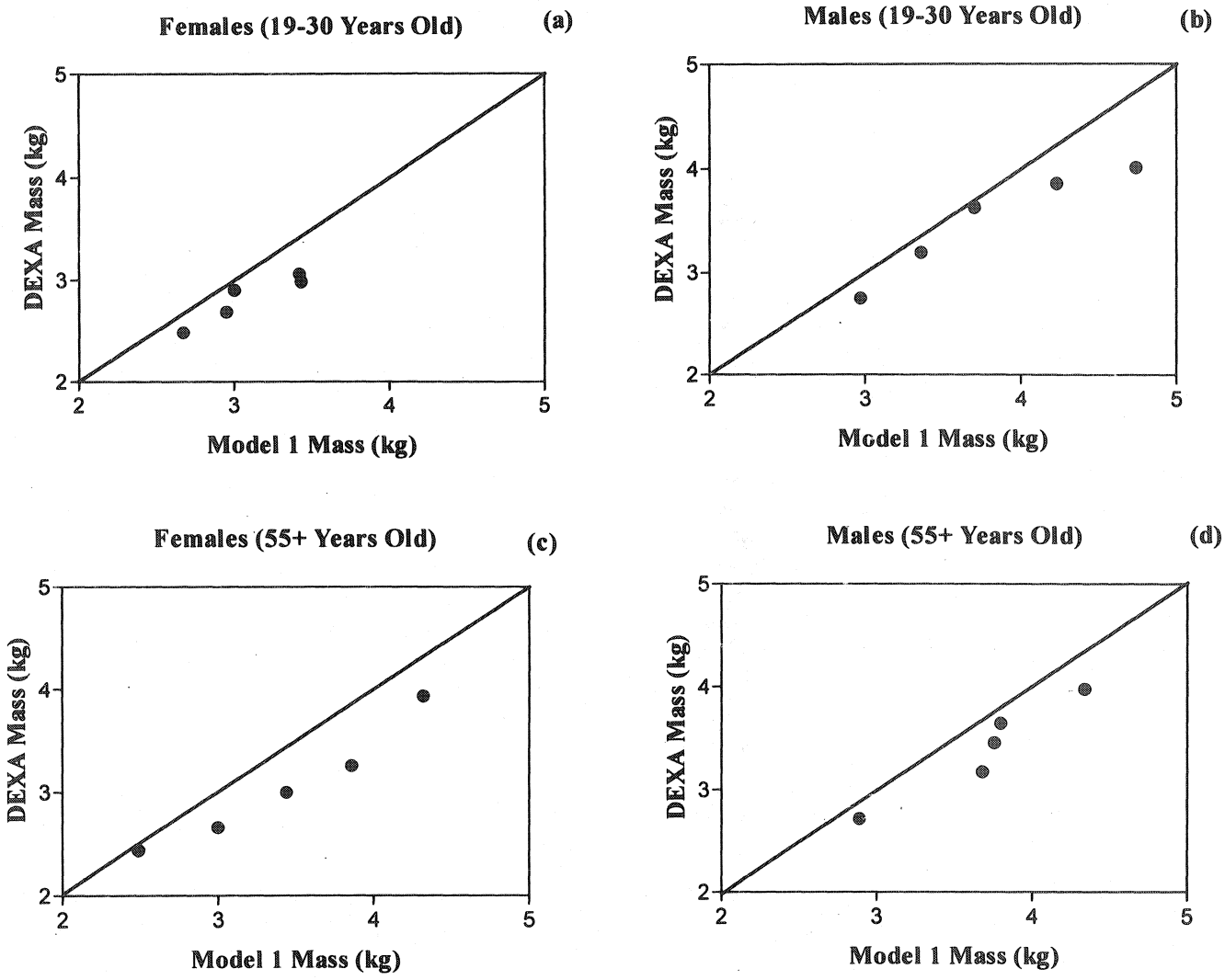

6.1.10 Scatterplots of leg Model 2 mass estimates vs. DEXA mass estimates.

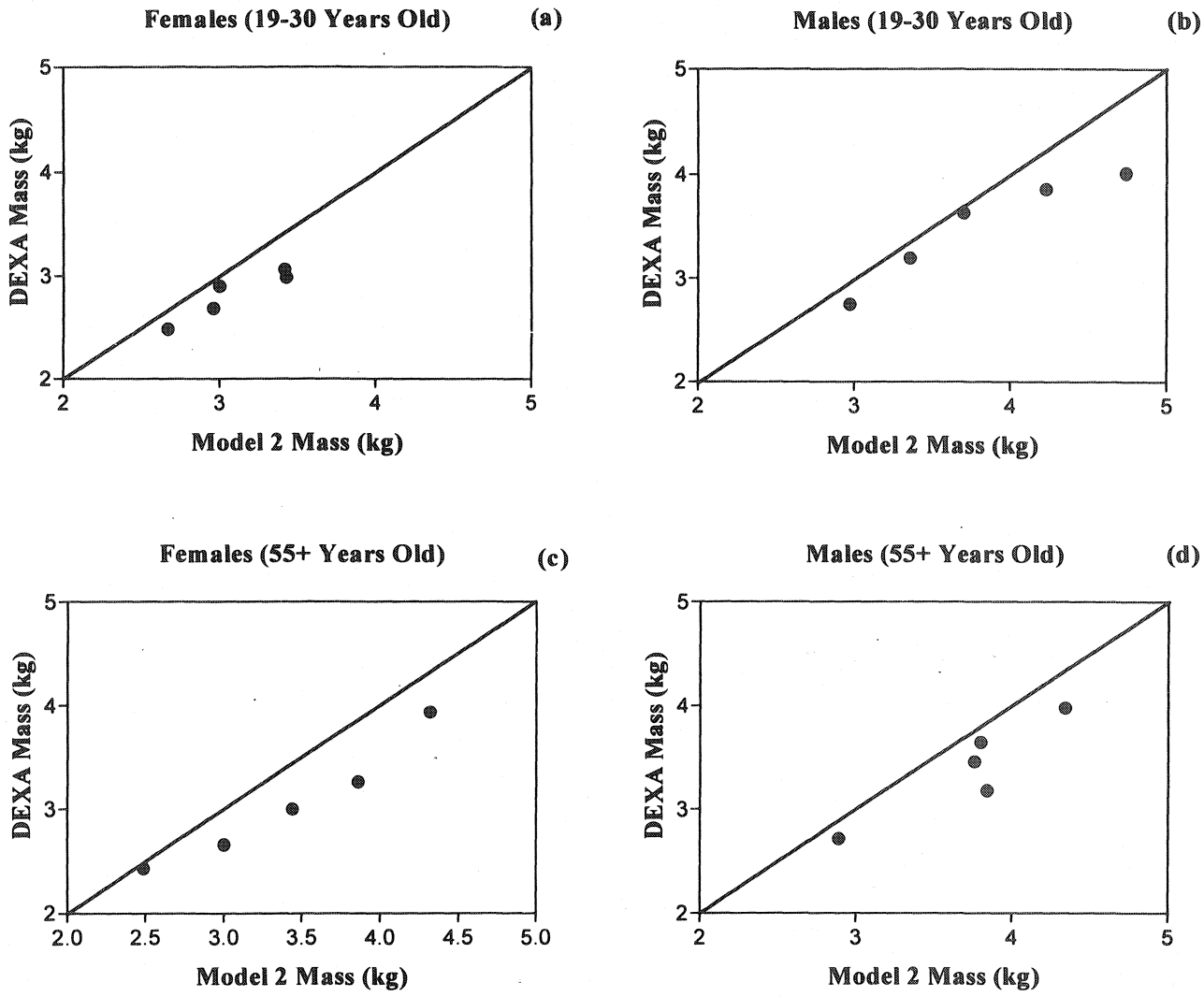

6.1.11 Scatterplots of leg Model 3 mass estimates vs. DEXA mass estimates.

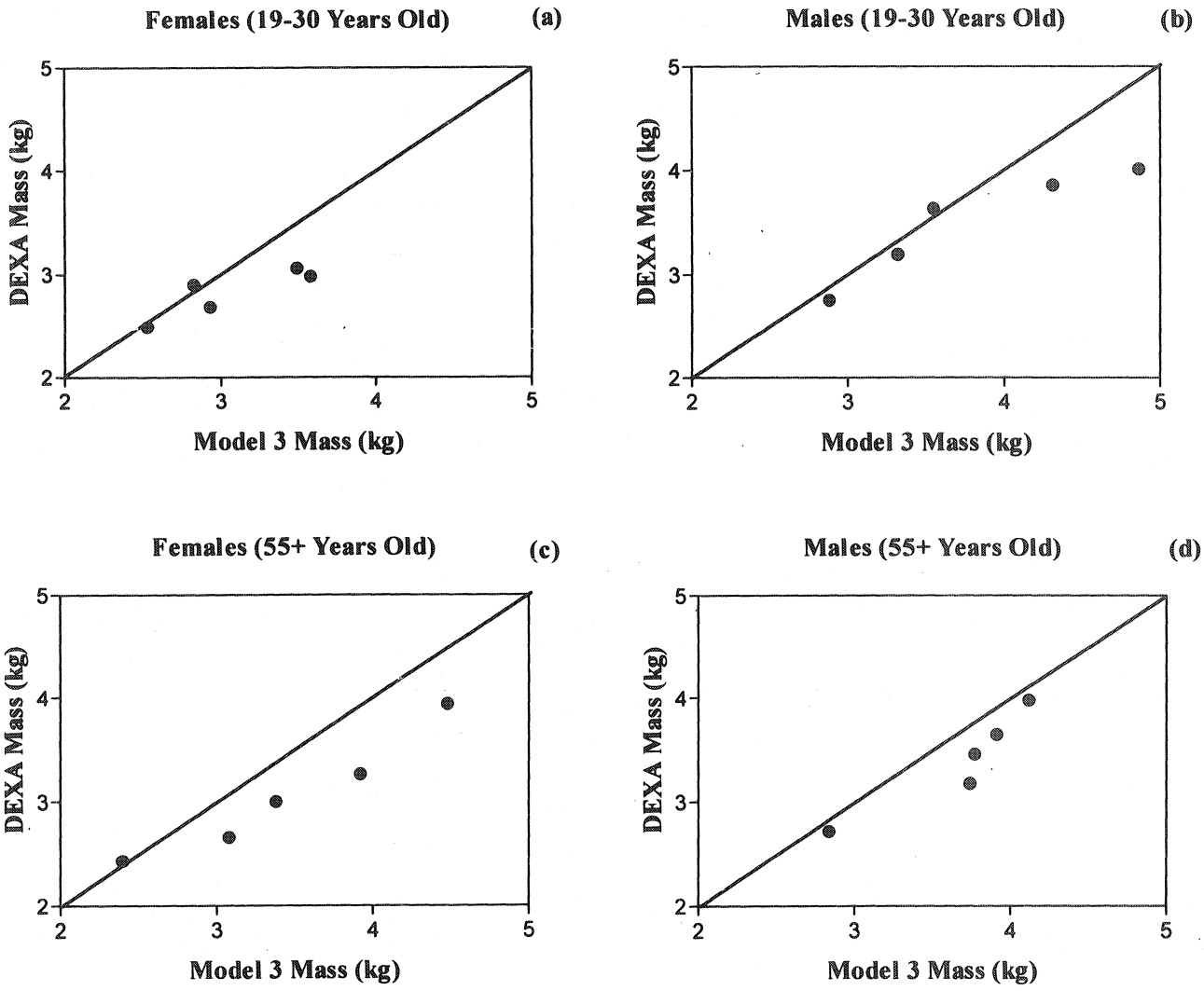

6.1.12 Scatterplots of leg Model 1 I_{CMz} estimates vs. DEXA I_{CMz} estimates.

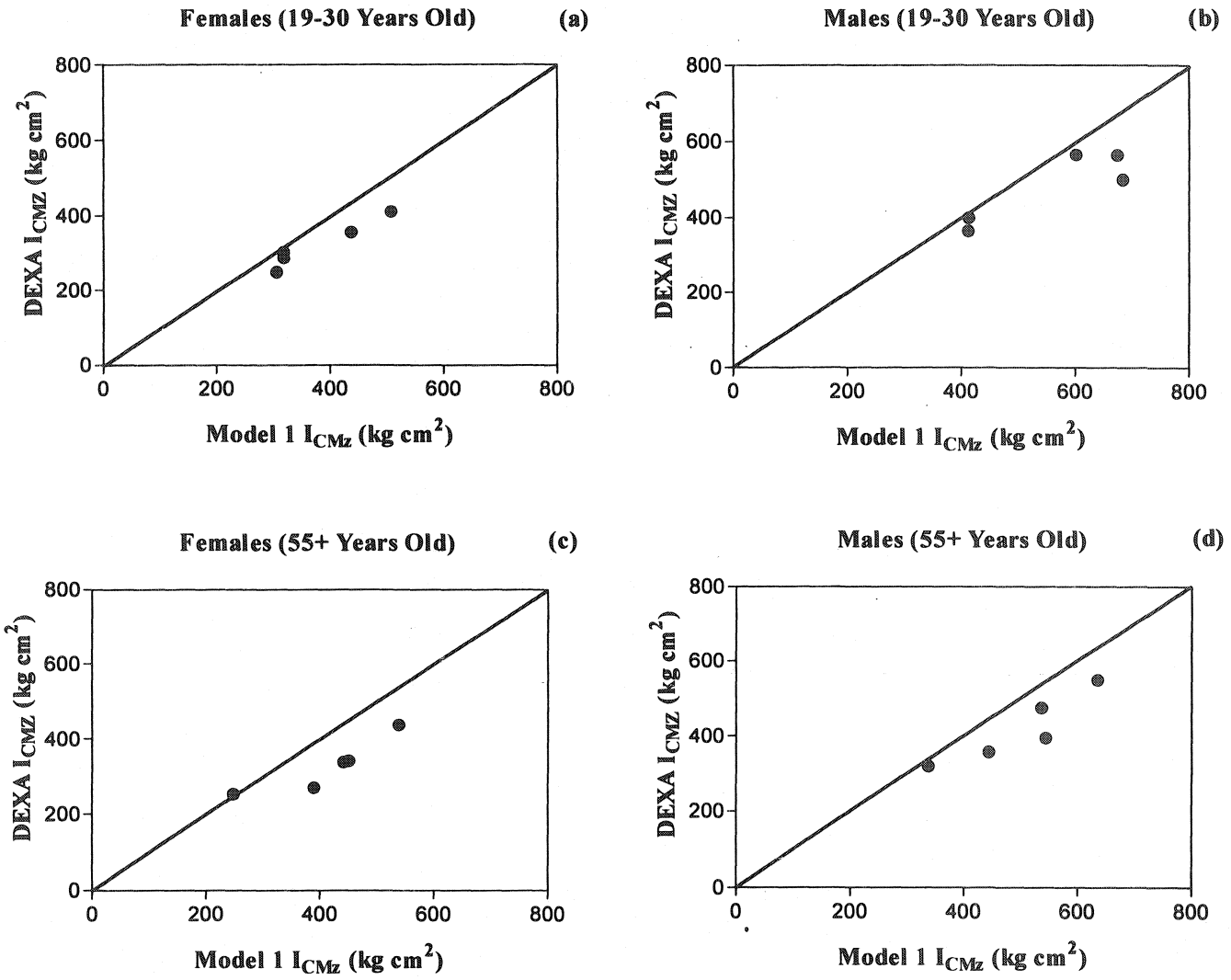

6.1.13 Scatterplots of leg Model 2 I_{CMz} estimates vs. DEXA I_{CMz} estimates.

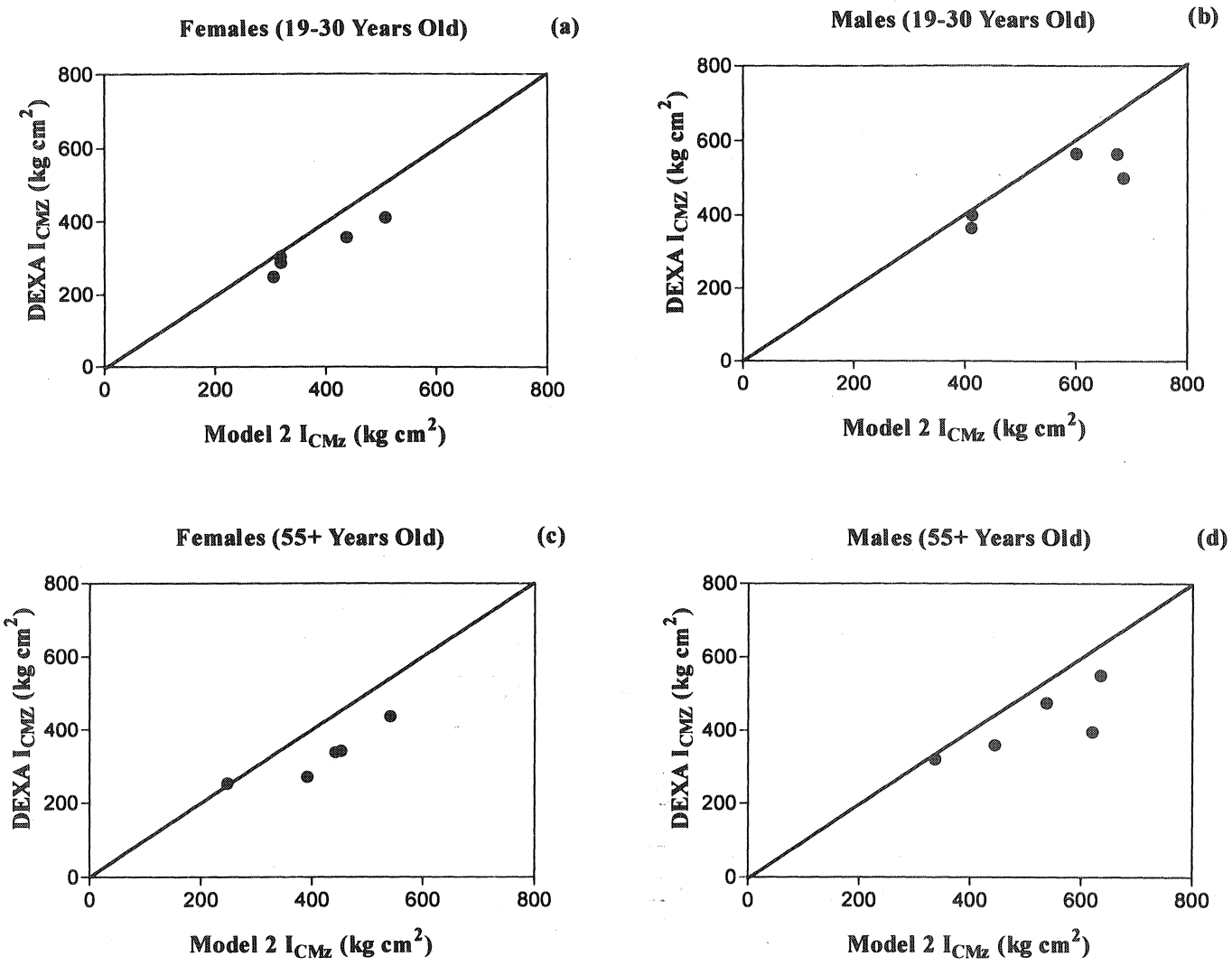

6.1.14 Scatterplots of leg Model 3 I_{CMz} estimates vs. DEXA I_{CMz} estimates.

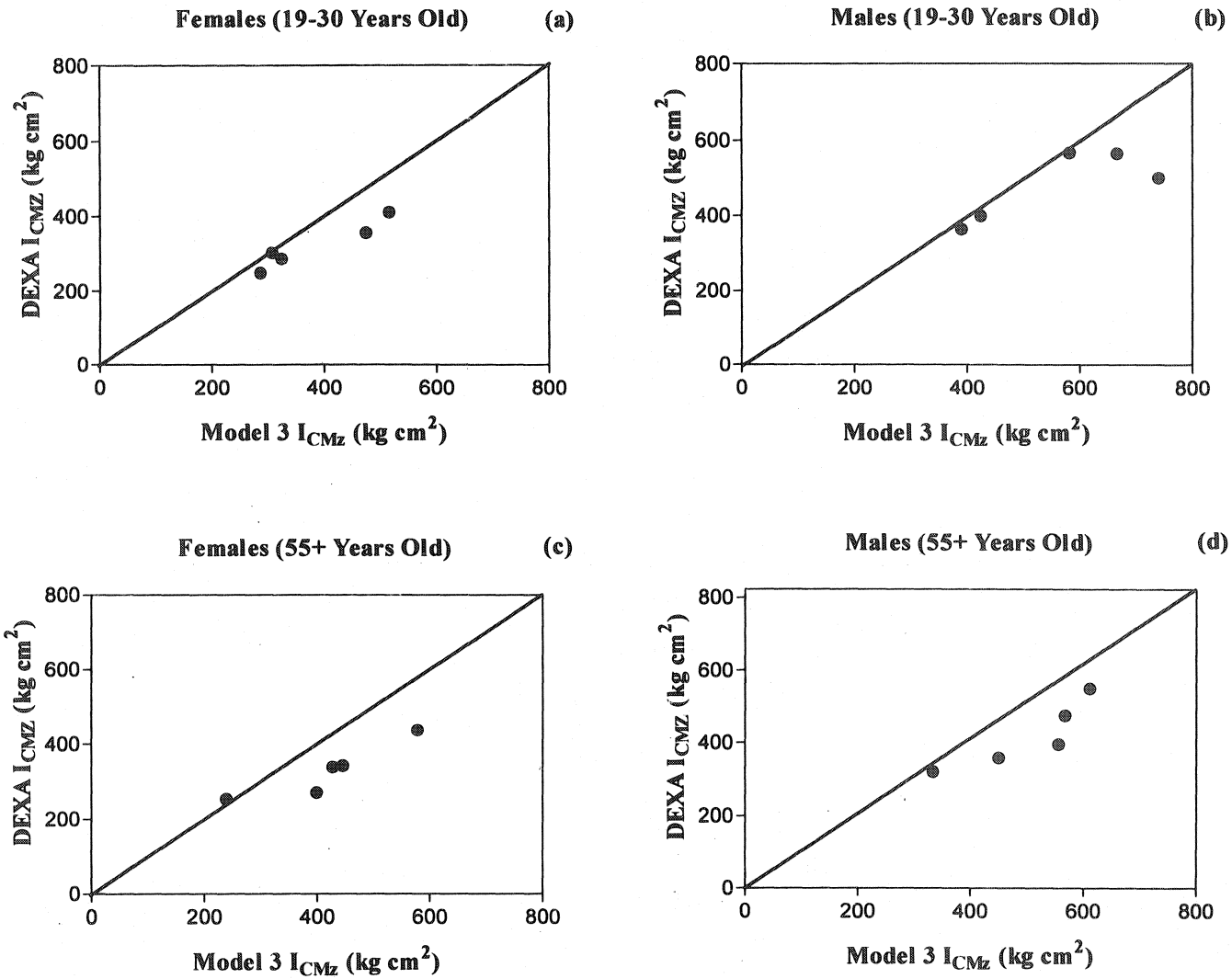

6.1.15 Scatterplots of leg Model 1 I_{CMy} estimates vs. DEXA I_{CMy} estimates.

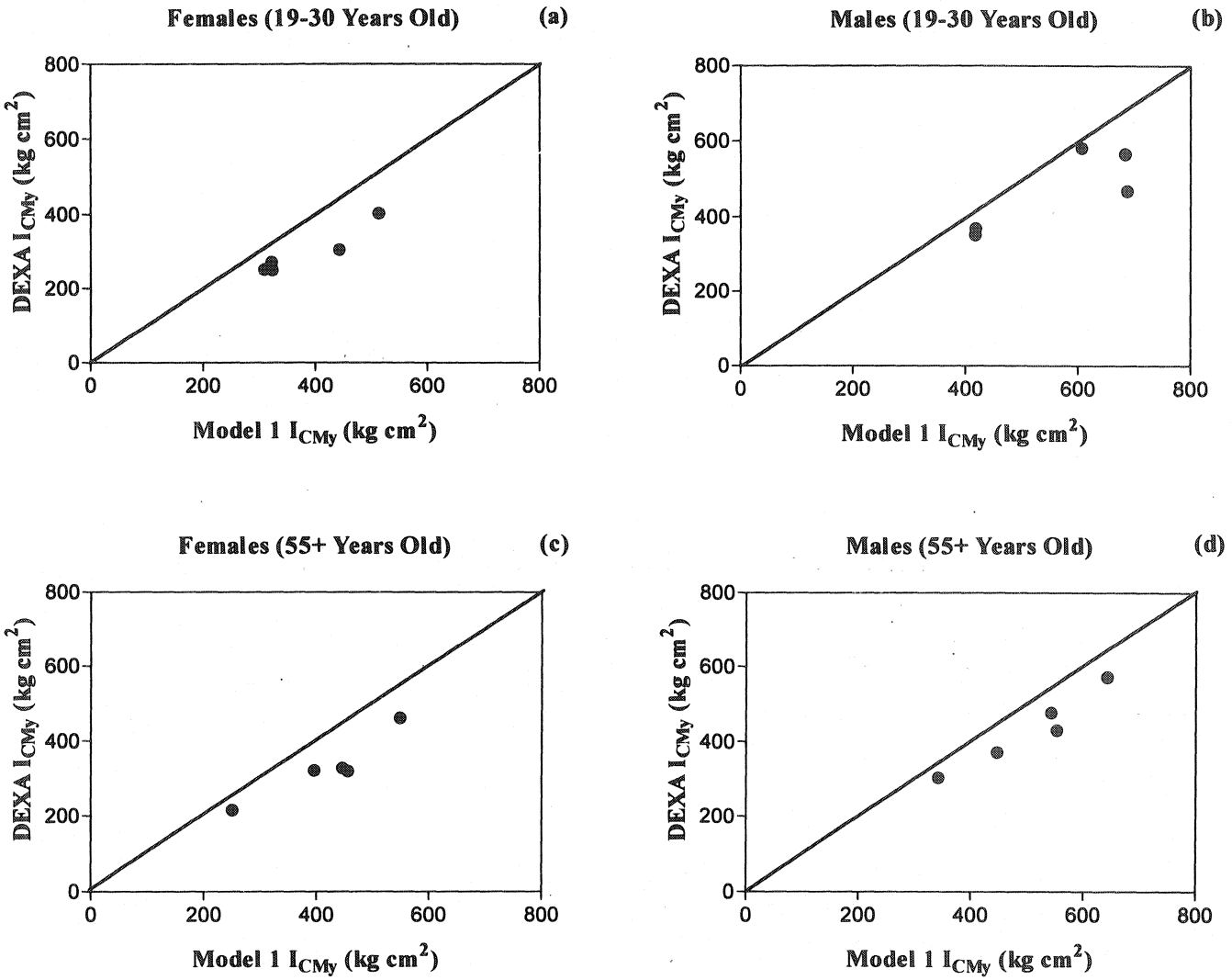

6.1.16 Scatterplots of leg Model 2 I_{CMy} estimates vs. DEXA I_{CMy} estimates.

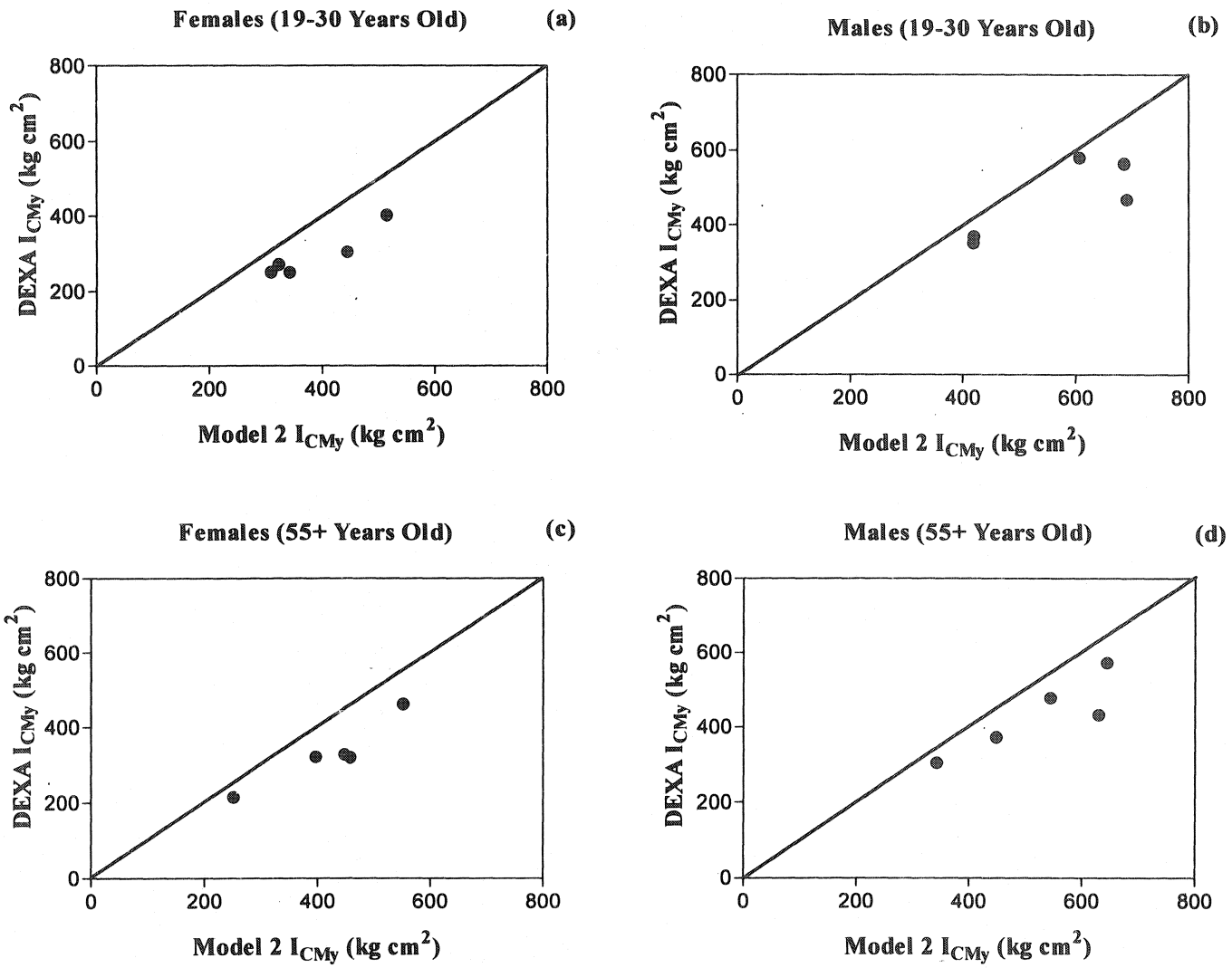

6.1.17 Scatterplots of leg Model 3 I_{CMy} estimates vs. DEXA I_{CMy} estimates.

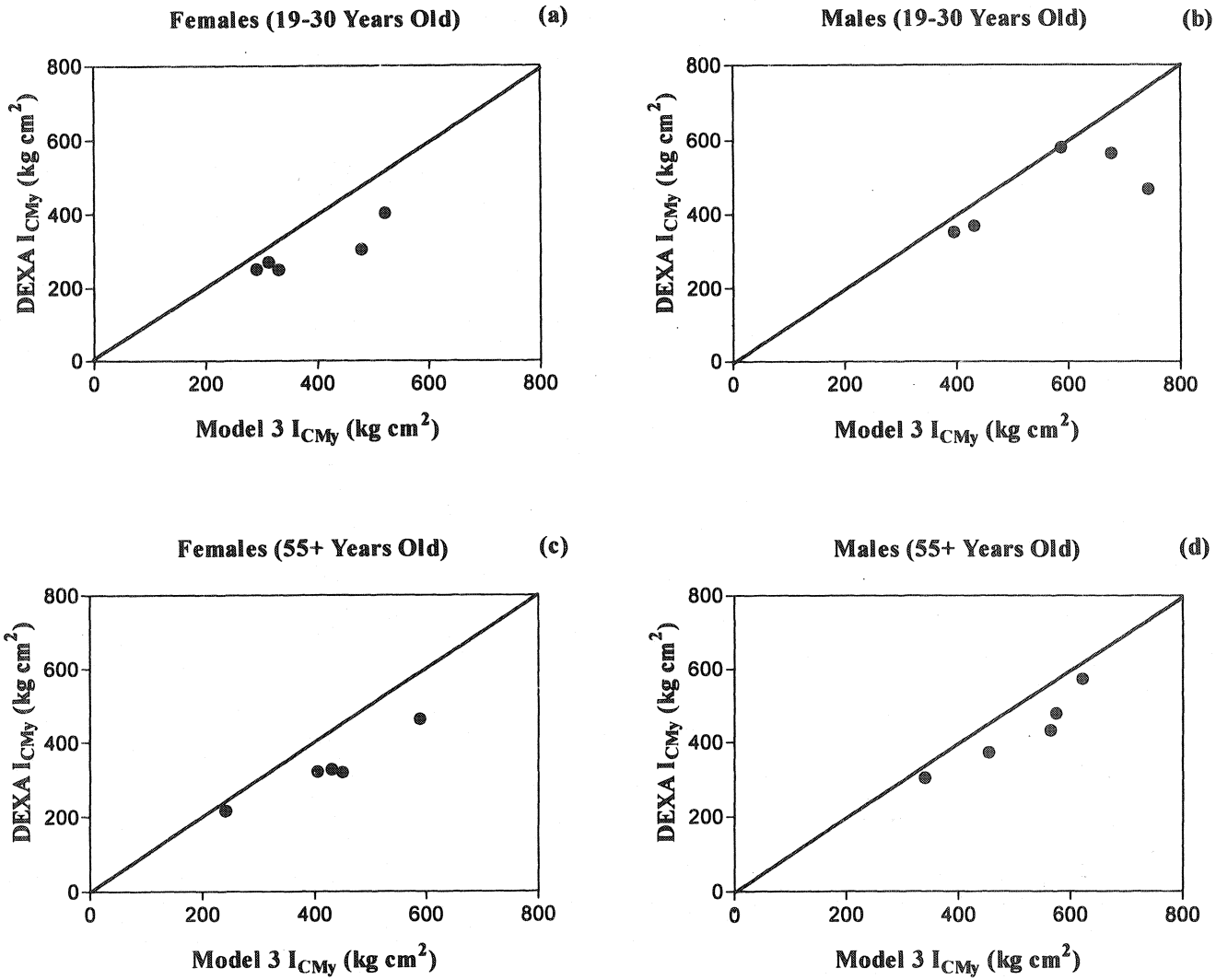

6.2 Mass distribution plots of thigh model vs. DEXA

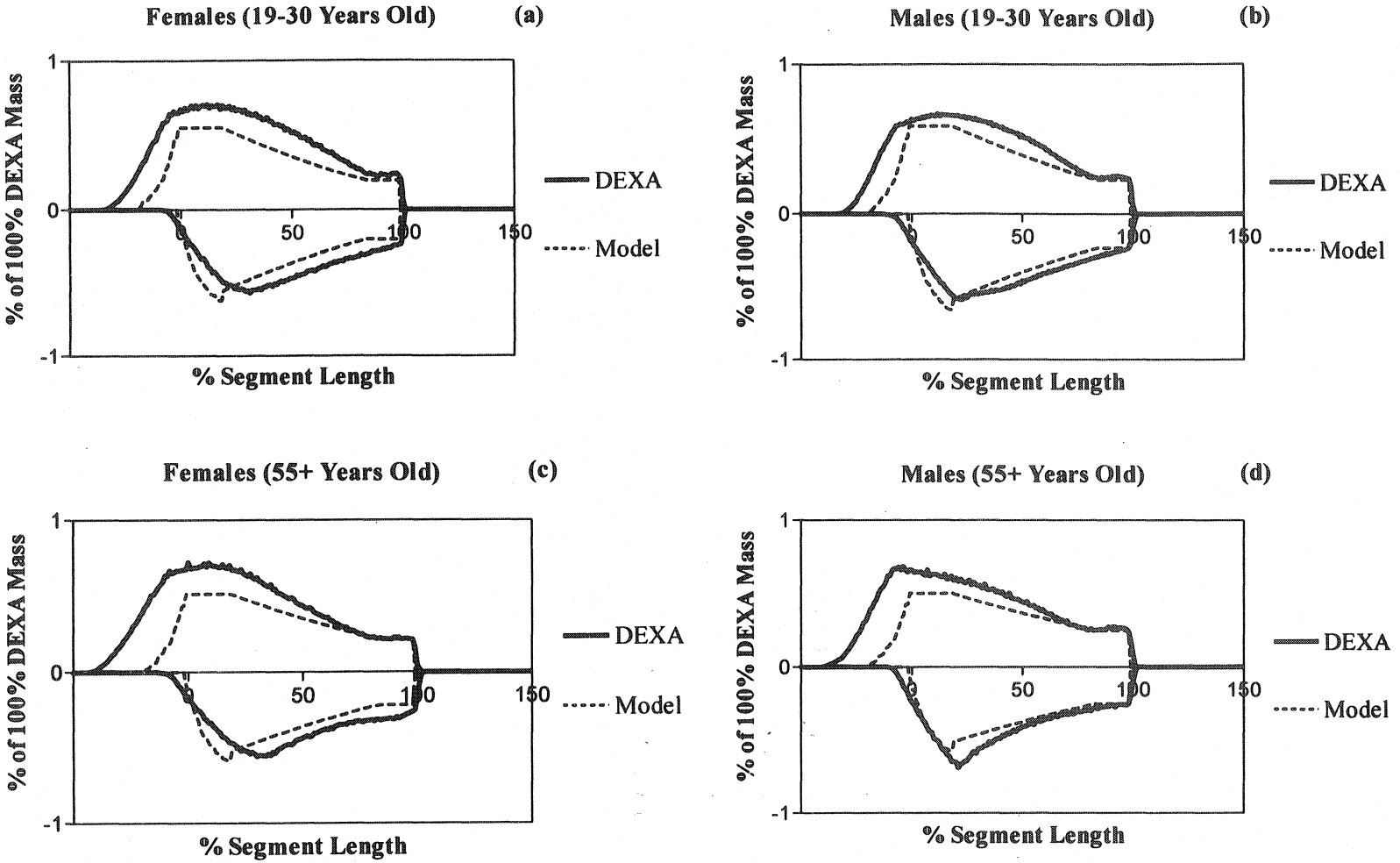

6.2.2 I_{CM} distribution plots of thigh model vs. DEXA

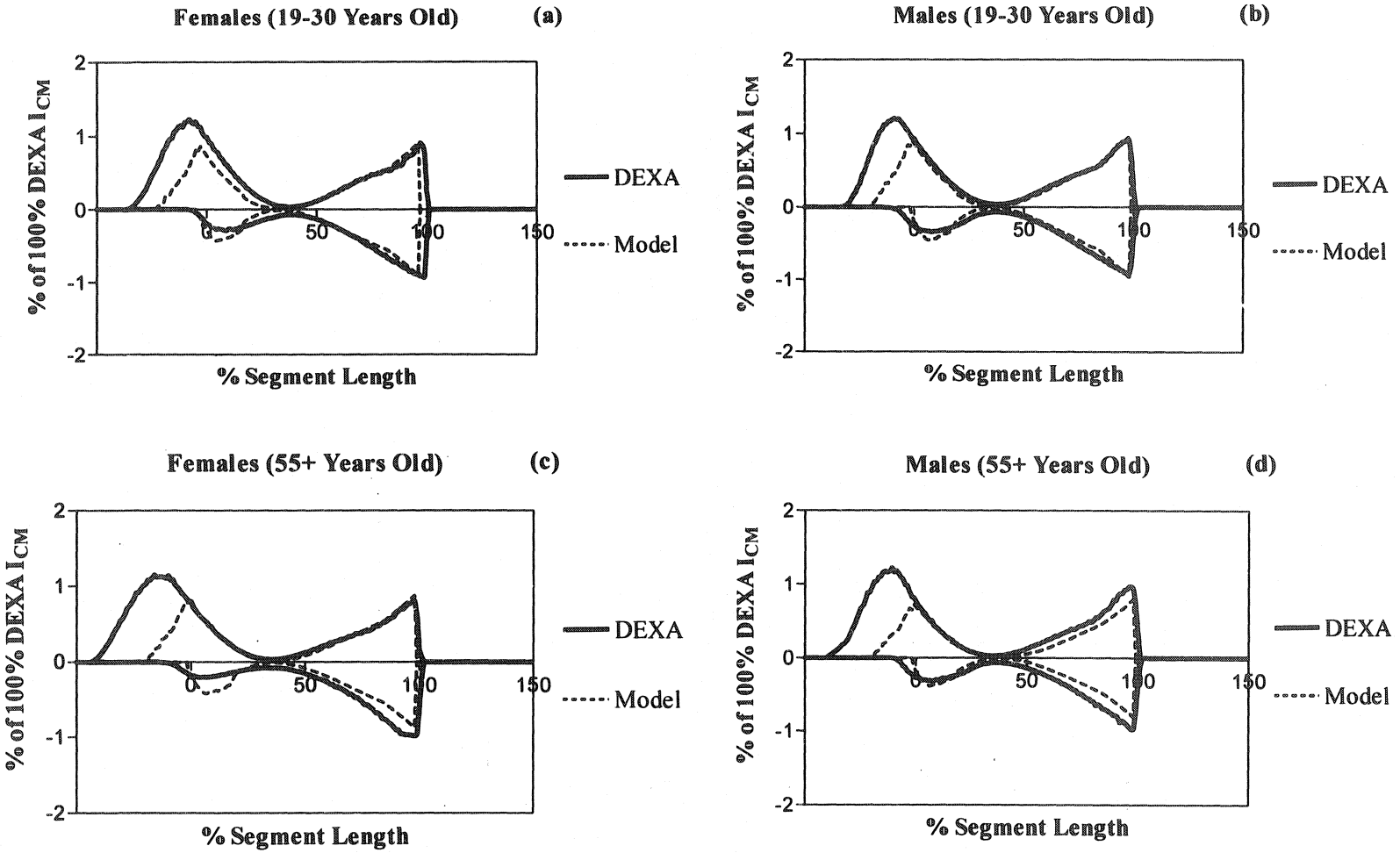

6.2.3 Mass distribution plots of forearm models vs. DEXA

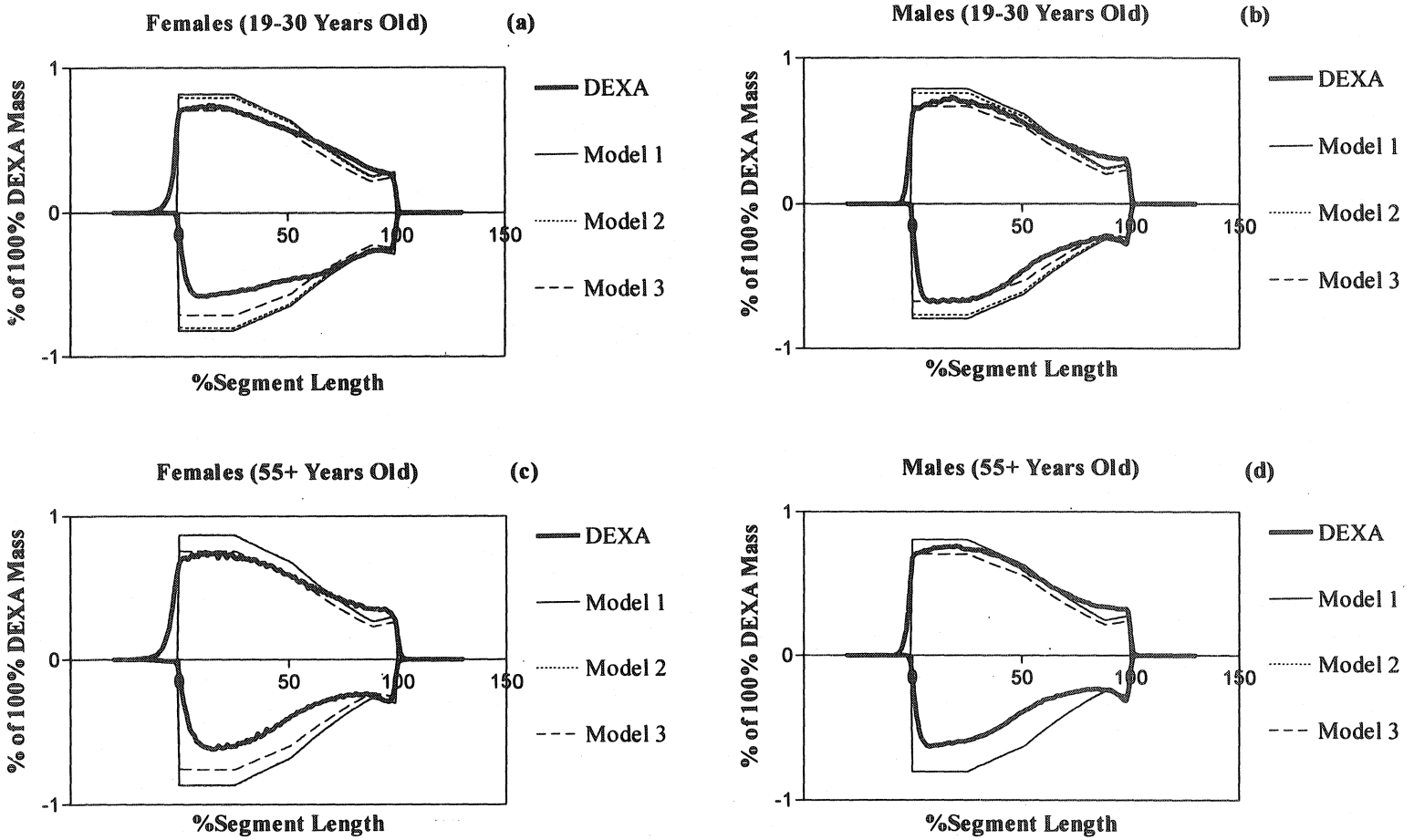

6.2.4 I_{CM} distribution plots of forearm models vs. DEXA

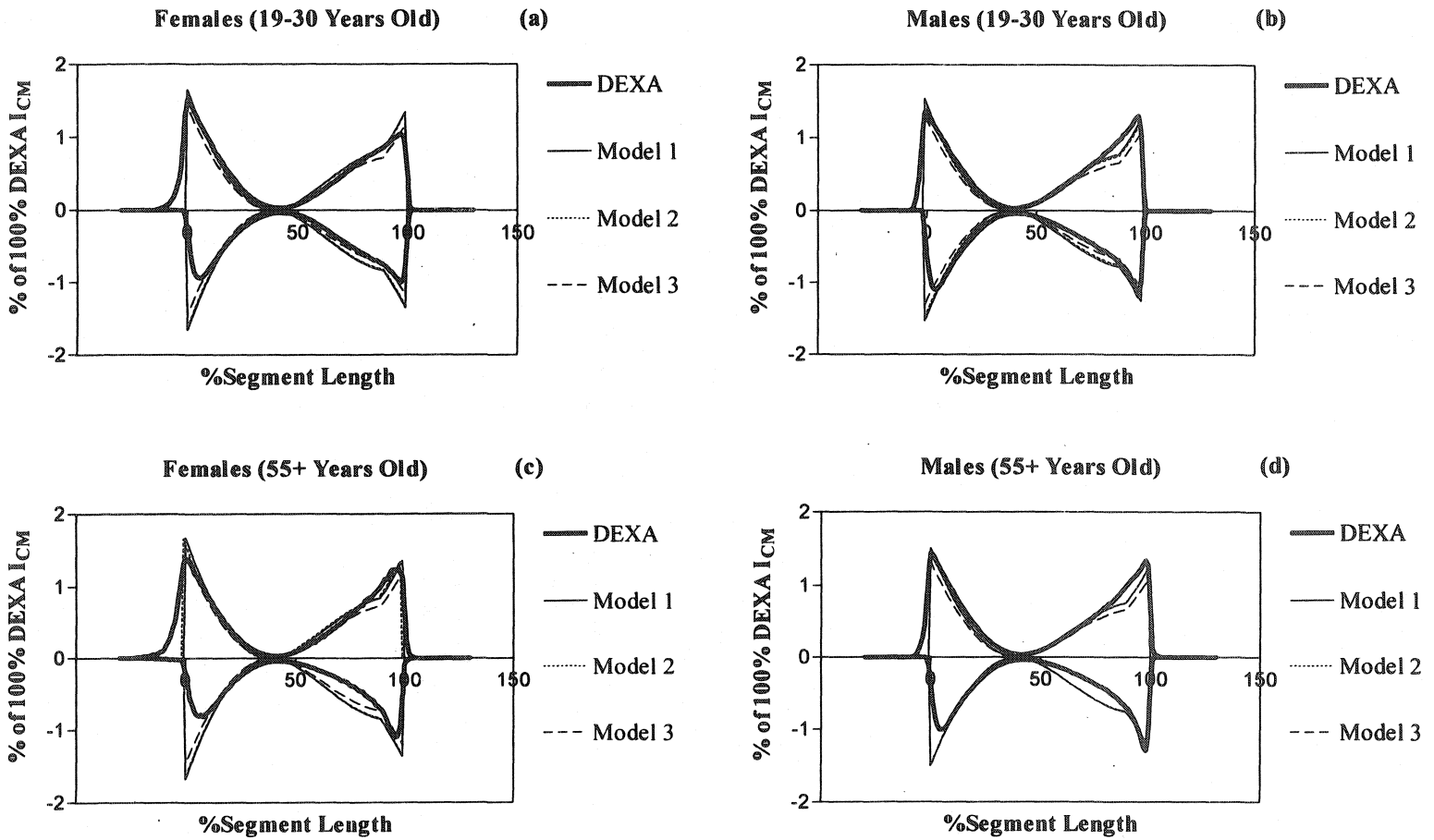

6.2.5 Mass distribution plots of frontal plane leg models vs. DEXA

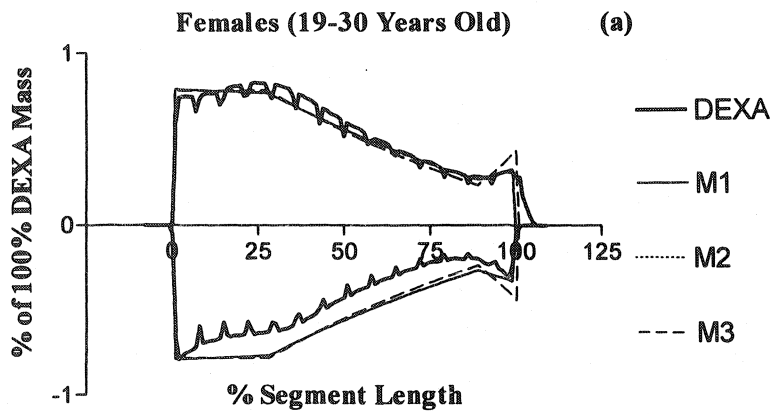

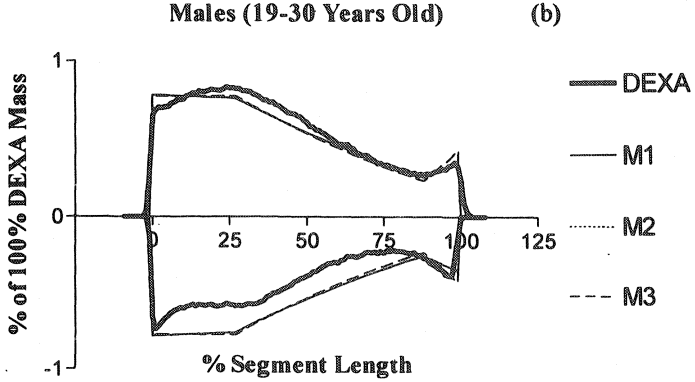

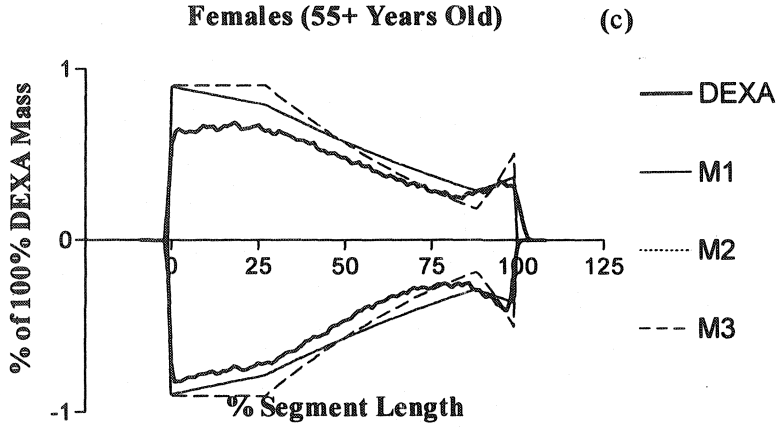

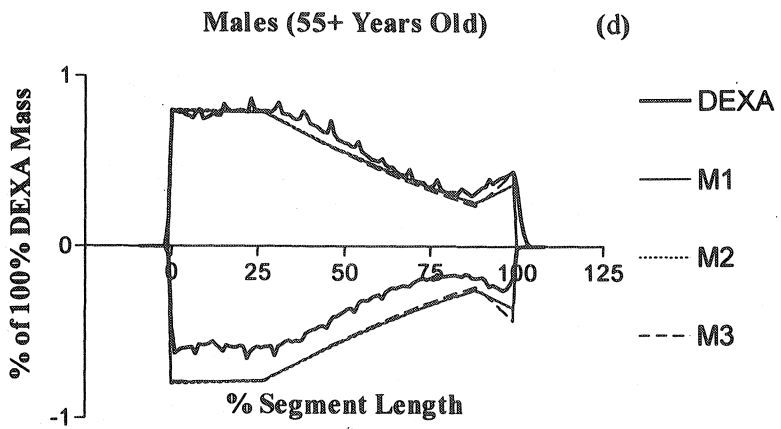

6.2.6 Mass distribution plots of sagittal plane leg models vs. DEXA

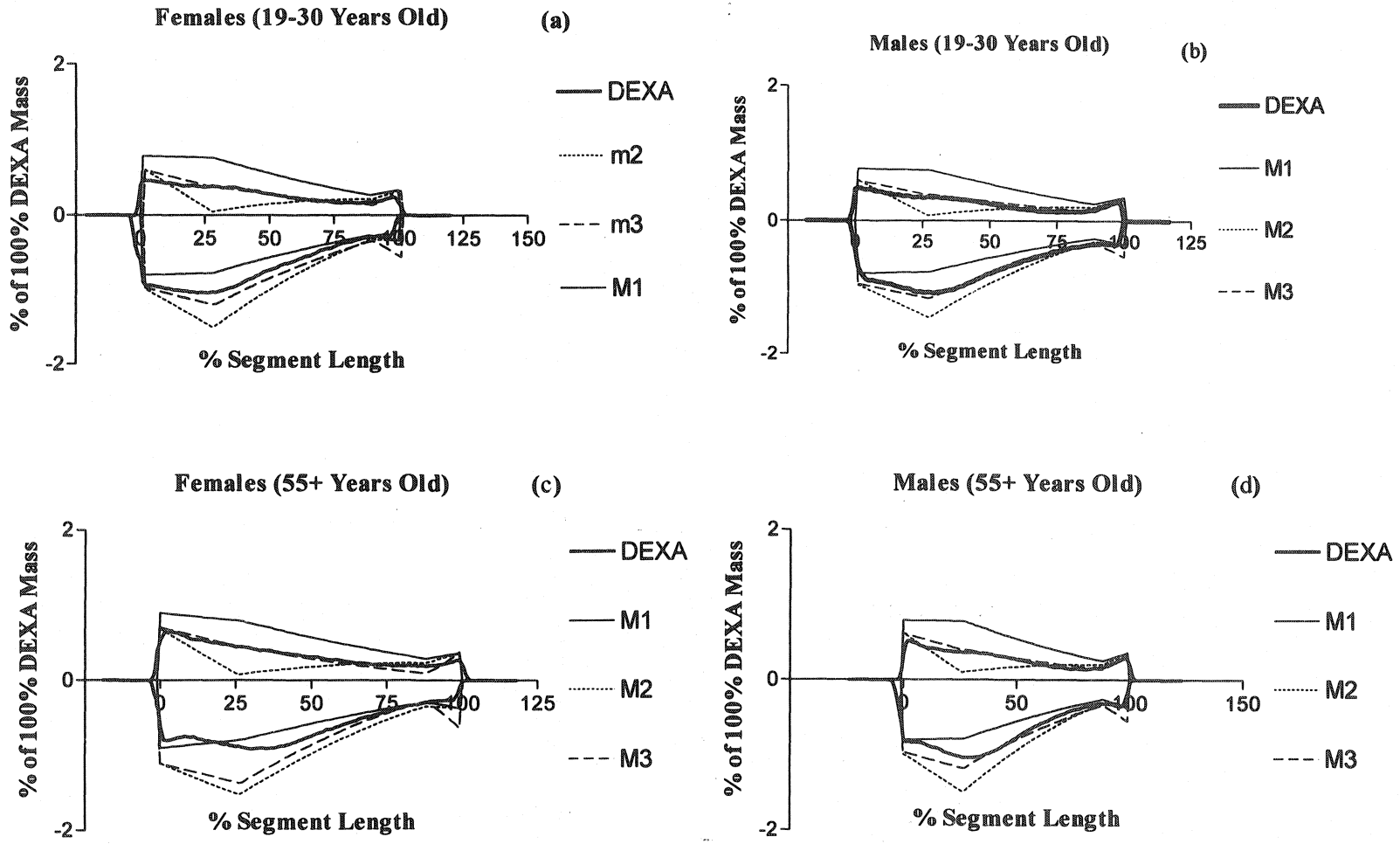

6.2.7 I_{CMz} distribution plots of frontal plane leg models vs. DEXA

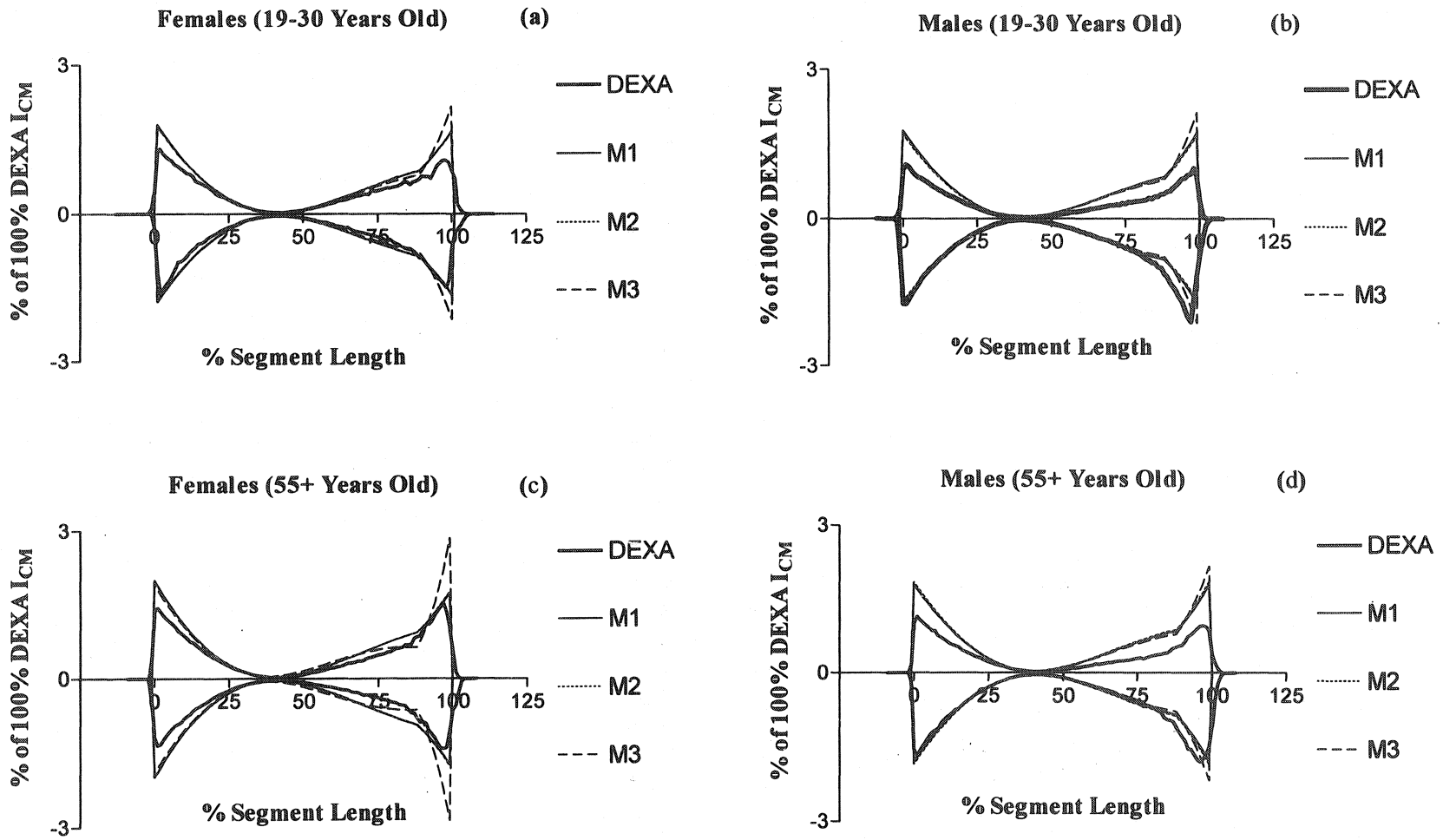

6.2.8 I_{CMy} distribution plots of sagittal plane leg models vs. DEXA